DETERMINATION OF DYNAMIC LOADS CAUSED BY AEOLIAN VIBRATION ON COMPOSITE INSULATOR: EXPERIMENTAL APPROACH

By

Kabwit Alain Ntambwe

(Student number: 212562424)

Submitted in partial* fulfilment of the academic requirements for the degree of Master of Science in Mechanical Engineering

School of engineering
Discipline of Mechanical Engineering,
Supervisor: **Dr. Richard C. Loubser**
Co-supervisor: **Dr Konstantin O. Papailiou**
University of KwaZulu-Natal
February 2015

Declaration 1 - Plagiarism

I, **Kabwit Alain Ntambwe** declare that

1. The research reported in this thesis, except where otherwise indicated, is my original research.

2. This thesis has not been submitted for any degree or examination at any other university.

3. This thesis does not contain other persons' data, pictures, graphs or other information, unless specifically acknowledged as being sourced from other persons.

4. This thesis does not contain other persons' writing, unless specifically acknowledged as being sourced from other researchers. Where other written sources have been quoted, then:

a. Their words have been re-written but the general information attributed to them has been referenced

b. Where their exact words have been used, then their writing has been placed in italics and inside quotation marks, and referenced.

5. This thesis does not contain text, graphics or tables copied and pasted from the Internet, unless specifically acknowledged, and the source being detailed in the thesis and in the References sections.

Signed: …….. Date: …….

Kabwit Alain Ntambwe (Candidate)

As, the candidate's supervisor I have/have not approved this thesis/dissertation for submission

Signed: …… Date: …….

Dr **Richard C. Loubser** (Supervisor)

Declaration 2 - Publications

DETAILS OF CONTRIBUTION TO PUBLICATIONS that form part and/or include research presented in this thesis (include publications in preparation, submitted, *in press* and published and give details of the contributions of each author to the experimental work and writing of each publication)

Publication 1

K.A. Ntambwe, R.C. Loubser, P. Moodley and K.O. Papailiou, Experimental investigation of Aeolian-vibrational loads on composite insulators, Proceedings of the 23rd Southern African Universities Power Engineering Conference (SAUPEC), pp. 19-24, Johannesburg, January 2015

Publication 2

K.A. Ntambwe, R.C. Loubser, P. Moodley and K.O. Papailiou, Composite insulators subjected to Aeolian vibrational loads of overhead conductors, Cigre Cape Town 2015 (In preparation)

Signed ……

Acknowledgements

Glory and Praise to YHWH, the Almighty God who let me finish my degree. I will keep on trusting You for my future. Thank you, Lord. AMEN !

First of all, I wish to express my gratitude to my supervisor, Dr. Richard C. Loubser for the trust he has placed in me by agreeing to this Master work, for his advice and for all the hours he devoted to direct this research.

I wish to sincerely thank my co-supervisor and mentor Dr. Konstantin O. Papailiou, who has generated this inspiring topic and created in me new avenues for further research. He has continued to inspire me with his papers and book.

I appreciate their availability and their unfailing respect in meeting tight deadlines for the proofreading documents I sent to them. Finally, they were extremely sensitive and supportive in listening and understanding my needs throughout this master's work.

My thanks also go to Mr. Pravesh Moodley for his administration and technical support who has supported me and helped me to be motivated, light-hearted and gave me peace of mind since the beginning of my thesis. Very humbly, I would like to thank you for your support during my periods of doubt and for your repeated encouragement.

I gratefully acknowledge the financial support from the VRTC, NRF/THRIP during the course of my study. I wish to thank Eskom, Pfisterer and Babcok for their donations. I express my sincerest gratitude to Prof. Ijumba, Dr Innocent Davidson, Mrs Leena Rajpal, Mrs Charlene King, Mr Thabani Nene, and Mr Joseph Kapuku, Mrs Lydia Weight, Michele H. Mardones (GTKEC).

I had the pleasure of working together with Mr Daniel Kubelwa, Mr Remy Badibanga, Mr Evans Ojo. My sincere thanks go to my all my colleagues and friends for their moral support.

I dedicate this dissertation to my father and mother Mr. Tshiyuk M. Tambwe and Mrs. Pombo Nyota and to the entire Tambwe's family, for their emotional support and constant source of inspiration, and if it was not for them it would have not been possible for me to complete my studies.

Finally, and most importantly, I would like to thank my wife Suzanne Ngeleka for her support, encouragement, quiet patience and unwavering love during this research.

Abstract

High voltage insulators have to fulfil high reliability criteria by being one of the main components for the operational safety and operating efficiency of the transmission system of electrical power. Various advantages and the attractive price of composite insulators have made them the most frequently used insulators in the power industry and have generally proven to be extremely reliable. Nevertheless, there are certain variable loads which occur on the overhead conductor in the field, such as mechanical loads caused by wind-induced vibrations, so-called Aeolian vibration, which might affect the insulators. It should be noted, that standardized tests of composite insulators are providing information only on their static mechanical strength

This thesis describes the experimental investigation of a realistic model to determine the dynamic mechanical loads of the overhead line conductor undergoing Aeolian vibrations. In addition, the dynamic behaviour of the composite insulator was investigated. The tests were performed using a test span in an indoor laboratory. The test procedures used are the swept sine and the steady frequency tests. A shaker connected to a single conductor has simulated Aeolian vibration. Two types of ACSR (Aluminium Conductor Steel-Reinforced) conductor (Tern 45Al. /7St. and Pelican 18Al. /1St.) were tested on two different types of support configurations (suspension and line post), placed at mid-span at four different ranges of static tensile loads (15-30% Ultimate Tensile Strength – UTS with 5% of increment). For both types of support configurations, the suspension clamp was blocked or articulated in order to know the influence of the oscillation motions on vibrational loads of the vibrating conductors. The measurements were done using the bending amplitude range of 0.1 to 1.0 mm on the conductor at 89 mm away from the last point of contact between the suspension clamp and the conductor.

In accordance with the stick-slip bending model of overhead conductors, which predicts a certain degree of non-linearity at low vibration amplitudes, the results obtained were statistically analysed by graphing the vibrational loads versus the bending amplitude. It was found that the magnitude of dynamic mechanical loads on a composite insulator caused by Aeolian vibration is relatively low (10% less) compared to its mechanical strength and can thus most probably not induce fatigue failures on the insulator.

Contents

List of figures

List of tables

Abbreviations

ACSR	: Aluminium conductor steel-reinforced
ANSI	: American National Standards Institute
ASD	: Allowable stress design
ATH	: Alumina Trihydrate (ATH)
cDAQ	: Compact data acquisition
CE	: Clamp edge
CFL	: Cantilever failing load
CIGRÉ	: Conseil International des Grands Réseaux Électriques (International Council on Large Electric Systems)
DAQ	: Data acquisition
ECR	: Electrical / chemical resistance
EDS	: Everyday stress
EN	: European Standard
EP	: Ethylene-propylene
EPDM	: Ethylene-propylene diene monomer
EPRI	: Electric Power Research Institute
ESKOM	: South African electricity public utility
HTV	: High Temperature Vulcanization
IEC	: International Electrotechnical Commission standards
IEEE	: Institute of Electrical and Electronics Engineers
ISO	: International Organization for Standardization
FRP	: Fiberglass reinforced plastic
LPC	: Last point of contact
MDCL	: Maximum design cantilever load
MP55	: HBM instrumentation module
NI	: National Instrument
NRF	: National Research Foundation
PME	: Power Monitoring Expert
RTL	: Routine test load
RTS	: Rated tensile strength
SCC	: Stress corrosion cracking
SCL	: Specified cantilever load
SML	: Specified mechanical load
STD	: Standard
STL	: Specified tension load
THRIP	: Technology and Human Resources for Industry Programme
UTS	: Ultimate tensile strength
UKZN	: University of KwaZulu-Natal
VRTC	: Vibration Research &Testing Centre

List of symbols

Symbol	Description	Unit
A	Cross-sectional area	m^2
A_{al}	cross-section of aluminium	m^2
A_{st}	cross-section of steel	m^2
C_i	Integration constants	
D	Diameter of the conductor	m
d	Diameter of the outer-layer wire (mm)	m
d_{al}	Diameter of aluminium strands	m
d_i	Diameter of the strands	m
d_{st}	Diameter of steel strands	m
D_a	Outer diameter of the end fitting	m
D_i	Inner diameter of the end fitting	m
d_r	Diameter of the rod	m
E_L	Modulus of elasticity (Young's modulus) in axial direction of the FRP rod	GPa
E_T	Modulus of elasticity (Young's modulus) in transverse direction of the FRP rod	GPa
E	Young's modulus	N/m^2
E_{al}	Modulus of elasticity of aluminium strands	N/m^2
E_{st}	Modulus of elasticity of steel strands	N/m^2
f	Vibration frequency	Hz
f_i	Deflection of the FRP rod under bending loads	m
F_b	External load (bending) of the insulator rod	N
H	Constant horizontal tensile force	N
i	Number of signal	i
G_{TT}	Shear modulus ''transverse–transverse'' of the FRP rod	GPa
G_{LT}	Shear modulus ''axial-transverse'' of the FRP rod	GPa
I	Moment of inertia	m^4
k_s	Strouhal number	
L_{cr}	Crimped length of the FRP rod	m
l	Bending length of the rod	m
m	Mass uniform per unit length across the conductor span	kg/m
M	Bending moment of the conductor element	N.m
N_{al}	Number of aluminium strands	
N_{st}	Number of steel strands	
N_i	Number of the strands per layer	
pp_{mean}	Peak-to-peak amplitude value	
p_{max}	Maximum positive amplitude value	
p_{min}	Minimum positive amplitude value	

R	Layer radius	m
t	Time	s
T	Tension of the conductor	N
v	Wind-speed	m/s
$\bar{v}$	Average of the vibrational loads of the vibrating conductor	N
v_i	Peak-to-peak vibrational loads measured	N
V	Shear force	N
V_{LT}	Poisson number ‘‘axial-transverse’’ to the FRP rod	
V_{TT}	Poisson number ‘‘transverse–transverse’’ to the FRP rod	
V, H & Z	Vertical, compression, and tensile loads applied to the free end of the insulator.	N
V', H' & Z'	Vertical, compression, and tensile loads applied to the free end of the insulator inclined at α	N
W	Linear mass of the conductor	kg/m
y_o	Free-span amplitude	m
Y_t	Deflection	m
Y_v	Anti-node displacement	m
σ_b	Dynamic bending stress	MPa
ε	Dynamic bending strain.	
$\bar{\varepsilon}$	Average of strain of the suspension composite insulator	N
$\overline{\varepsilon_b}$	Average of bending strain of line post composite insulator	N
$\varepsilon_{b\,i}$	Peak-to-peak of bending strain measured	
ε_i	Peak-to-peak of strain measured	
σ_{b1}& σ_{b2}	Dynamic bending stresses of span 1 and span 2	MPa
σ_{shear}^{max}	Maximum shear stress of the FRP rod	N/m^2
σ_Z	Tensile stress in the cross-sectional area of the fitting	N/m^2
σ_{zul}	Tensile strength of the fitting	N/m^2
σ_n	Nominal bending stress	N/m^2
τ_{zul}	Maximum shear stress	N/m^2
ρ	Density of the conductor	kg/m
ω	Circular frequency of the considered vibration mode	Hz
Ω	Resistance	Ohm

CHAPTER 1
INTRODUCTION

1.1 Problem definition

High voltage transmission lines are used to transport electric power from the generation plant to the end users. Mounted on the towers and held by insulators, the overhead transmission-line conductors are exposed to pollution and weather (rain, wind, and ice). In particular, wind, ice loadings, temperature variations, and the conductor tension, impose mechanical loads on the overhead-line conductors. When a smooth, steady crosswind blows over an overhead-line conductor, a mechanical phenomenon called Aeolian vibration occurs at a wind speed from 1 to 7m/s, characterized by low amplitudes (approximately one conductor diameter), and relative high frequency (5-120Hz) [1, 2]. This is an undesirable phenomenon because of its dynamic character. If proper countermeasures, such as external damping, are not undertaken, this vibration may cause fatigue failure of the conductor strands. In addition, fittings and insulators can be endangered, whereby insulators are subjected to dynamic and static loads resulting from the conductors [3-5].

The mechanical behaviour of conductors supported by composite insulators, whether in suspension or cantilever position under Aeolian vibrations, has not yet been studied in detail. The primary purpose of this project is to experimentally measure the dynamic loads of a single, vibrating conductor acting on the composite insulators. Secondly, this thesis examines whether those mechanical loads produced can promote fatigue failure of the insulators.

Two types of composite insulators were investigated: the suspension composite insulator and the line post composite insulator, each mounted respectively on a support structure specifically designed for this project. In addition, it was considered necessary to assess the effect of the suspension clamp, i.e. whether blocked or not and, either with or without the insulator (more realistic). To summarize, the Aeolian vibrational loads of

conductors were examined across several clamp configurations at the mid-span tower (suspension or line post insulator), at different tension levels for different conductors, by applying the maximum allowable bending amplitude for each different conductors.

1.2 Background

This thesis focuses on Aeolian vibration of transmission lines. The wind, which depends on the weather conditions, imposed cyclic mechanical loading, not only to conductors but also to the supports, fittings, accessories, and ground lines of the overhead transmission line. The effects may be visible and interpreted by the swinging of the conductors at field observations. It is not only Aeolian vibration that makes conductors swing. All cyclic motions (such the galloping and the wake-induced oscillation) create this effect. When the natural frequencies of the conductor coincide with the Strouhal frequency, this situation is called resonance; which occurs when the conductor reaches the maximum amplitude of vibration. The mechanical behaviour of overhead-line conductors under vibration is quite complex, the conductor being an assembly of various twisted strands from different materials. The Aeolian vibration imposes stresses on the strands of the conductors by repetitive and alternating movements. As a result of this scenario, fatigue failure will occur and there will be signs of cracks on the strands of the conductor. After some time, broken strands in the outer layer will be noticed. Over the long-term, this will lead to the rupture of the conductors, which can cause serious accidents and economic loss. The highest alternating bending stresses and tensile stresses caused by the vibration of the conductor are located and concentrated in the area close to the clamps as shown in Figure 1-1 (LPC – Last point of contact).

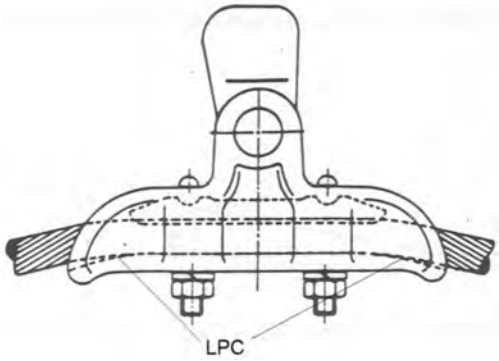

Figure 1-1: Suspension clamp/cable schematic [6]

This is owed to the intention for the clamp in its vicinity to restrict the movement of the conductor. The vibration stresses of the conductor will be transferred to the insulator (suspension or line post), the suspension clamp being obviously held by the insulator.

Nowadays, the composite insulators have become more commonly used and have been accepted by several electrical utilities worldwide. These insulators are in many cases replacing the traditional ceramic and glass insulators which had been used on transmission and distribution lines (69 kV to 735 kV). This replacement has been justified by their significant advantages over other insulators, as their low weight, high resistance against vandalism, excellent anti-pollution performance in highly contaminated areas, their easy transportation and installation, and maintenance. Also, with regard to mechanical considerations, composite insulators present significant merits, such as high flexibility, and mechanical strength-to-weight ratio [2, 5, 7]. As a new product, its design, manufacturing, and life expectancy has attracted much attention. Both users and manufacturers have shown great interest in these insulators. Composite insulators must withstand, not only long-term static loads, but also cyclic loads, as well as, occasionally, sudden loads. Composite insulators have been tested according to international standards and recommendations expressed by the manufacturers [8, 9]. Based on static tests, the manufacturers have developed mechanical loading curves or combined loading charts which can assist the user in the selection of the most appropriate insulator for their purpose. During dynamic conditions, the test results of the composite insulator are very different from static test results. Because they cannot be linked to static loads, the results can only be estimated. De Toureil concluded that, owing to cyclic loads, the mechanical strength of the composite insulators is 22 to 75% less than their static strength [4].

International standards and recommendations require that the “static” Routine Test Load (RTL) should be 50 % of the specified mechanical load (SML) for suspension insulators, and 50% of the specified cantilever load (SCL), or specified tension load (STL) [8-10]. These loads have been indicated by the manufacturers, although often the manufacturers do not provide the ultimate load of their product.

1.3 Research question

As mentioned before, this study aimed to determine the dynamic loads acting on composite insulators whether suspension (Figure 1-2) or line post (Figure 1-3) when the

related conductor was undergoing Aeolian vibration. It also sets out to examine and analyse the impact of those loads on the composite insulator. The main set-up of this research required the placing of a support in the middle of the 84.6 m long vibration laboratory span in which the composite insulator was fixed. The major question raised in this study is on how the dynamic mechanical loads should be determined and which bending amplitude should be used in order to determine these loads. Do these loads impact greatly on the insulator? And if so, when will the signs of fatigue failure begin to appear on the composite insulator?

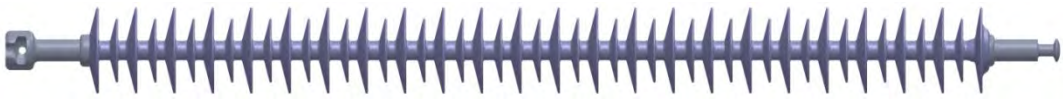

Figure 1-2: Suspension composite insulator

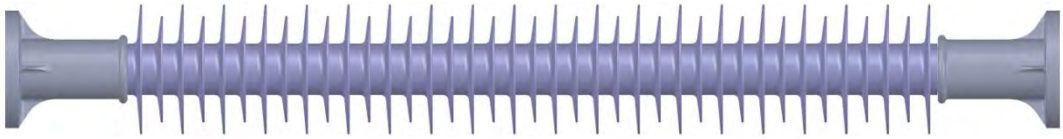

Figure 1-3: Line post composite insulator

By using experimental and analytical methods and techniques, mainly the bending amplitude method, the answers to these main questions were established and revealed. Graphs for the mechanical loading of the vibrating conductor have been plotted, and the mechanical behaviour of the composite insulators interpreted. Vibrational loads versus bending strain are presented and discussed.

Various conductors at different static tensions, and the types of composite insulators most commonly used in South Africa, were tested. The outcome of this study will benefit ESKOM and the insulator manufacturers, as well as the Overhead Lines industry.

1.4 Project aims and objectives

This project required a comprehensive study of the mechanical behaviour of the conductor, an in-depth investigation of the stress mechanism created by the clamp-conductor system, knowledge of the dynamic behaviour of the composite insulator

under dynamic loads, and of the strength of the composite material (Fiberglass Reinforced Plastic/FRP – rods).

This project proposed to determine the vibrational loads generated by the conductor under Aeolian vibration which may impact on the composite insulators (suspension or line post). The objectives of this thesis are:

- to produce graphs or curves for each conductor tensioned at different static tensions for a typical post and a typical suspension point, showing the dynamic force acting on the insulator in relation to the bending amplitude (up and above to the safe-vibration level as given in the EPRI transmission line reference book [1].
- to determine for each typical post insulator and each typical suspension insulator at the maximum bending amplitude of the conductor and at the safe-vibration level range, whether any signs of fatigue have appeared, and at which number of cycles any particular failure may have resulted. The fatigue behaviour of the composite material FRP-rods should also be examined.

The experimental work of this project has been performed at the Vibration Research and Testing Centre (VRTC) which was designed according to IEEE standards. This study focuses on the measurement at the mid-span support structure of the following parameters, while the conductors were under Aeolian vibration:

- vibrational loads of the conductor;
- bending amplitude of the conductor at 89 mm away from the clamp edge (CE) of the suspension clamp;
- strain of the FRP rod of the suspension insulator; and,
- bending strain of the composite insulator.

1.5 Dissertation outline

The introduction of this dissertation has been elaborated in this chapter. Chapter Two presents a literature review comprising a brief overview of the mechanical behaviour of the vibration conductor under Aeolian vibration. The composite insulators and their mechanical stresses have been also described, and their testing of standard procedures has been detailed. Chapter Three is an experimental description of this project. The

utilities of the laboratory, the test procedures, and the methodologies used during the test, are presented. Chapter Four focuses on the presentation and discussion of the laboratory data. In this section, graphs of vibrational loads and strains are shown and explained. Chapter Five will conclude with a summary of the output of the project comparing this with the main objectives described previously. Recommendations for future research will be discussed.

CHAPTER 2
LITERATURE REVIEW

2.1 Introduction

Overhead transmission lines, while transferring electric power from generation plants to the users, are evidently subjected to weather conditions, especially the wind. Exposed to wind-induced vibrations, the conductors, which are composed of many twisted layers of strands and are suspended to the line towers via non-ceramic or ceramic insulators, develop a complex dynamic behaviour [11, 12], which influences the insulators, the fittings and the towers [1, 2, 13, 14].

The main aim of this thesis is to determine the influence of the above mentioned loads to the insulators, which have the primary function of mechanically supporting the high-voltage line, while also providing electrical insulation between the tower and conductors. It is thus helpful to determine the cyclic conductor motion of the conductor in order to predict the mechanical behaviour of the insulators [15]. In order to achieve this, a dynamic mathematical model was developed for Aeolian vibrations of single conductors without dampers [16]. This can also be used to estimate the aerodynamic coefficients and the damping characteristics of the conductor. Several tests were conducted in order to understand the mechanical behaviour of the vibration conductor under Aeolian vibrations [17]. A mathematical analysis of transmission line vibration data is required, based on the measurement of bending amplitude and conductor strain or bending stress of the conductor [18]. Three methods are presented by Davall [19, 20] which are powerful predictors of fatigue failure of the conductor.

1. Cross-over frequency/amplitude analysis method recommended by the IEEE committee. In which for a given sample interval, the analysis consisted to vibrate the overhead line sinusoidally at peak-to-peak constant amplitude. Over the complete test duration at any given frequency, the number of the cycles of the overhead line vibration and the amplitude would be measured.
2. Peak-trough analysis of line vibration method considered that the line vibrations are narrowband random in nature with several frequency modes superimposed

comparing to the cross-over frequency method. These analyses are based on the peak-trough probability distribution estimated by sampling the vibration data and recording the amplitudes of successive significant peak-trough pairs in the signal.

3. The power spectral analysis of line vibrations method is known to be most significant and useful.

A good evaluation of the severity of the predicted conductor response was achieved by calculating and comparing the bending stress amplitudes at each side of the suspension clamps to the internationally acceptable levels [21, 22]. Numerical simulation of a single vibrating conductor presented a good correlation between the tension and the damping equivalent of the conductor [16]. The analysis of the conductor-clamp system is important because slippage can occur when the conductor is subjected to alternating motion, owing to the wind-induced vibration [22]. This has confirmed the suitability of the bending amplitude method as the standard method of assessing overhead line conductor vibration. This method was adopted by international institutions (IEEE, CIGRE, and IEC). The vibrations of the conductor are transferred to the support structures via the insulators. Composite insulators which are tested only statically by the manufacturers, are subjected also to additional dynamic loads caused by the wind-induced vibration in service [8-10, 23].

Mechanically composite insulators have to withstand everyday loads, such as wind and ice loading, while supporting the conductors attached to grounded structures. The FRP rod of the insulator has a high resistance to the axial tensile loads; however, it is rather weak when torsion loads as well as bending loads are applied.

This chapter describes the background and theories of dynamic behaviours of a single conductor without dampers. An analytical model of the vibrating conductor and an analysis of its bending are discussed. The standard called bending amplitude method is presented. Composite insulators (suspension and line post) are presented. Their ratings are discussed and the mechanical behaviour is analysed. A brief presentation of their failure mode is important because the origin of their different failure modes being as yet unknown.

2.2 Power line motion

2.2.1 Cyclic conductor motion

There are three types of overhead line motion caused by winds. The differences are related to vibration frequency, amplitude of vibration, energy transfer, and motion patterns. Wind-induced conductor motion which was observed from the early 1900s has caused damage and failure on overhead conductors, insulators, and several overhead line fittings, even extended to the towers [1, 2, 24]:

- Aeolian vibration;
- Galloping conductor; and
- Wake-induced vibration.

The weather is the differentiating factor between power line motions.

2.2.1.1 Aeolian Vibration

Aeolian vibration is a most unwelcome phenomenon. It is caused by steady laminar winds which produce a stream of vortices alternating from the top and bottom of the conductor, as illustrated in Figure 2-1. The winds in the frequency range of 3 to 120 Hz cause the conductors to vibrate in a transverse direction at the same frequency of the vortex shedding, producing a vertical pulsating force.

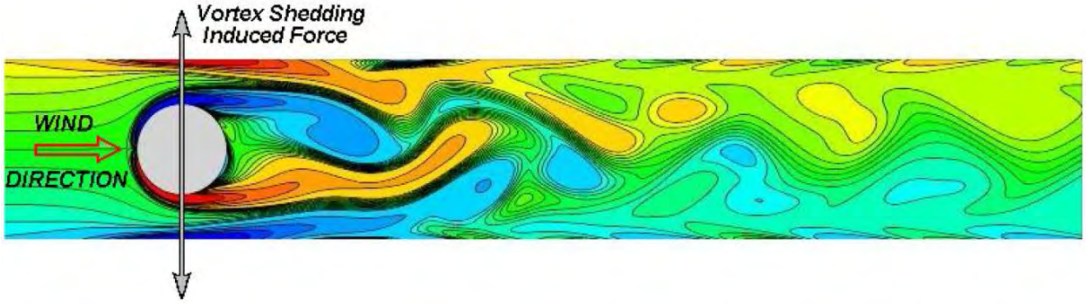

Figure 2-1: Vortex Shedding phenomenon induced by wind flowing over a cylinder [25]

Not only are the overhead line conductors affected, but all fittings, dampers, insulators including the grounded towers of overhead transmission lines are subjected to Aeolian vibration [1, 2].

The vibration amplitude of the conductor can reach a peak-to-peak value equal to the conductor diameter. This vibration frequency can be approximately calculated using a non-dimensional number k_s, called "Strouhal number" ($0.18 < k_s < 0.22$) [1]:

$$f = k_s \frac{v}{D} \tag{2.1}$$

The equation (2.1) is called Strouhal formula with: f frequency, v wind-speed and D: diameter of the conductor.

2.2.1.2 Galloping

The phenomenon of galloping is the most spectacular form of conductor motion. It was observed early in the 1900s and it occurred on asymmetrically-iced conductors. Both single and bundle conductors are affected by this phenomenon which is result of the action of wind on ice-coated conductors to areas that experience snow. This is caused by the aerodynamic instability of the deposit of ice accretion on the conductor which modifies the cross-sectional circular shape of the conductor to an asymmetrically-iced conductor surface. The vibration is at low frequencies in the range of 0.1 to 1 Hz with one to three standing waves within the span. The vertical motions can be twice the sag of the conductor span, the maximum peak-to-peak motions reliably observed being 10 m. With winds approximately normal to the line with a speed above 7 m/s usually considered, it cannot be assumed that there is necessarily an upper-speed limit [1, 26-29].

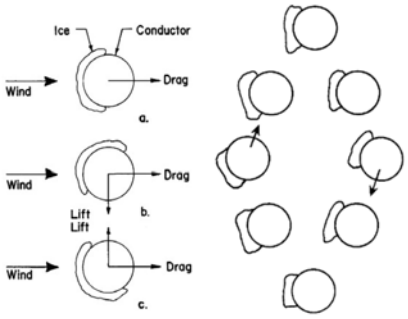

Figure 2-2: Lift and drag on iced conductor (a) and its combination of vertical and torsional motion (b) [1]

2.2.1.3 Wake-induced oscillation or sub-span oscillations

As the third major wind-induced motion, the wake-induced oscillation which concerns only the bundle conductors, is also recognized as a significant problem in transmission lines. The vibration amplitudes can reach up to 20 times the conductor diameter at frequencies in the 5 to 30 Hz range. This is caused by the wake from the upstream sub-conductors acting on the leeward sub-conductors. The motions occur in moderate to strong winds, usually in the range of 7 to 18 m/s.

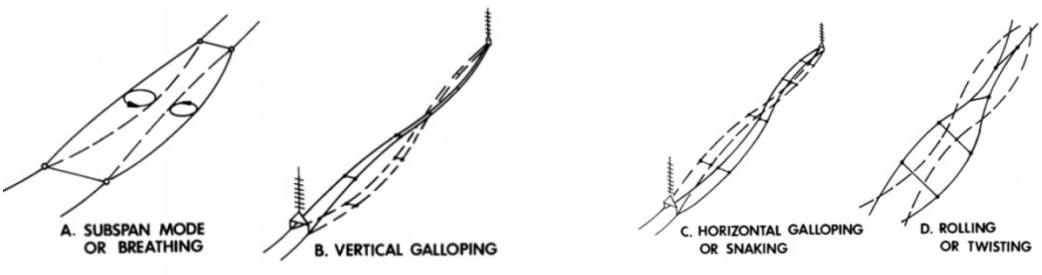

Figure 2-3: Type of wake-induced oscillations [1]

2.3 Modelling of a single conductor

2.3.1 General mathematical model of the conductor

To establish the motion equation of the conductor, many assumptions have been adopted in building up a mathematical model of a single conductor under load-induced vibration. [16, 30]: The conductor has been considered as a simple inextensible beam stressed by a constant horizontal tensile force H with the mass uniform per unit length m across the conductor span attached at both ends (Figure 2-4).

- The bending stiffness EI of the conductor is disregarded.
- The effect of the wind along the span conductor is constant and continuous.

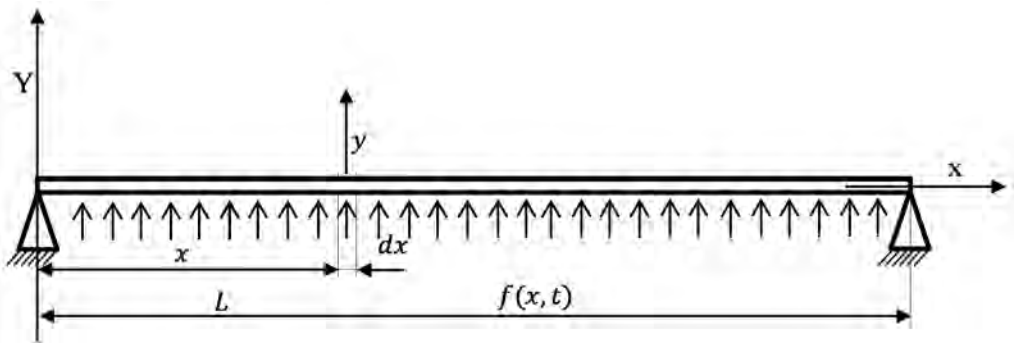

Figure 2-4: Simply-supported beam

Figure 2-5 describes the free-body diagram of an infinitesimal distribution of the force of a conductor excited with dx, the initial length, y displacement of conductor under vibration, t the time and probably x conductor's coordinate, $V(x,t)$ the shear force, $M(x,t)$ the bending moment and $T\ (x,t)$ the tension at the left-end of the conductor element. At the right-end of the conductor element the conductor will be $(x + dx)$.

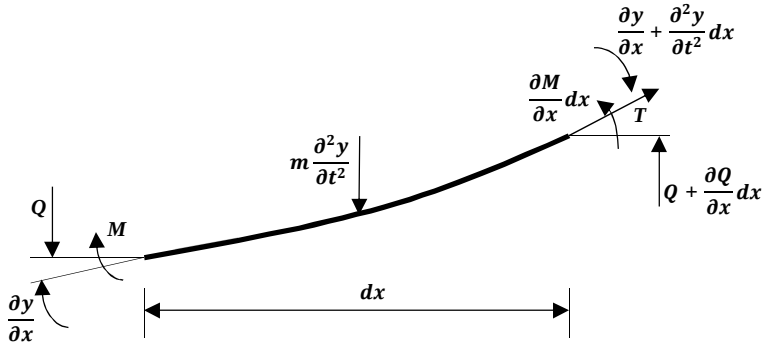

Figure 2-5: Infinitesimal distribution of the force of a conductor excited [31]

By applying the Euler-Bernoulli beam theory,

$$V(x,t) = -EI\frac{\partial^3 y}{\partial x^3} \qquad M(x,t) = EI\frac{\partial^2 y}{\partial x^2} \qquad \theta = \frac{\partial y}{\partial x} \tag{2.2}$$

Whereby, E is the Young's modulus, and I is the moment of inertia. EI is known as the flexural rigidity.

The following equation is found after applying Newton's law of motion $\sum F = ma$ and Taylor series to (2.2):

The equation (2.2) can be written as:

$$\frac{dV(x,t)}{dx} + \frac{d(T(x,t)sin\theta)}{dx} + f(x,t) = \rho A\frac{\partial^2 y}{\partial t^2} \tag{2.3}$$

By substituting the following expression:

$\rho A = m$, which is the mass-per-unit of length, and where A is the cross-sectional area, and ρ is the density of the conductor.

$\sin\theta \cong \theta$ as the θ is small; it may be ignored, the deflection being smaller.

For a constant tension in the beam, the equation (2.3) may now be expressed as:

$$\frac{dV(x,t)}{dx} + T\frac{d\theta}{dx} + f(x,t) = m\frac{\partial^2 y}{\partial t^2} \tag{2.4}$$

By replacing (2.2) with (2.4) and multiplying (2.4) by (-1), a fourth-order differential equation is achieved, which is considered the mathematical model of the conductor under Aeolian vibration.

$$EI\frac{\partial^4 y}{\partial x^4} + T\frac{\partial^2 y}{\partial x^2} - f(x,t) = -m\frac{\partial^2 y}{\partial t^2} \tag{2.5}$$

This equation illustrates the equation of the conductor when the self-damping force of the conductor and the conductor bending stiffness are not considered. $f(x,t)$ is defined as the aerodynamic force due to wind flow which is applied transversally on the conductor, and $y\,(x,t)$ is the transverse deflection of the conductor located at x.

2.3.2 Theoretical natural frequency

By considering the natural mode of the conductor, the transverse deformation $y\,(x,t)$ may be expressed as:

$$Y(t) = X(A\sin\,\omega t + B\sin\omega t) \tag{2.6}$$

Here, ω is the circular frequency of the considered vibration mode. By using the set solutions

$$Y(x) = Ke^{ax} \tag{2.7}$$

inserted into the bending-moment equation (2.2), the solutions obtained lead to four roots: two real $n_{1,2} = \pm\alpha$ and two imaginary $n_{3,4} = \pm\beta$ which are (2.8):

$$\alpha = \sqrt{\frac{T}{2EI} + \sqrt{\frac{m\omega^2}{EI} + \left(\frac{T}{2EI}\right)^2}} \qquad \beta = \sqrt{-\frac{T}{2EI} + \sqrt{\frac{m\omega^2}{EI} + \left(\frac{T}{2EI}\right)^2}} \tag{2.8}$$

Finally, the boundary conditions are considered. Should there be no displacements and no moments at both ends, the parabolic functions may be used:

$$Y(x) = C_1\cosh\alpha x + C_2\sinh\alpha x + C_3\cosh\beta x + C_4\sinh\beta x \tag{2.9}$$

where C_1, C_2, C_3, C_4 are the integration constants.

These constants are called the characteristic equation and roots of the equation of the natural frequencies.

However, from equation (2.9), in considering the boundary conditions and good approximation of C_4, the following equation results from (2.14):

$$y(x) = y_o \sin \beta x \tag{2.10}$$

This is the transverse displacement of a conductor with y_o the free-span amplitude. By taking into account the boundary conditions at both sides of the span, and assuming that the conductor-bending stiffness is not negligible, the following equation may be produced:

$$\omega_n = \frac{n\pi}{L}\sqrt{\frac{T}{m} + \left(\frac{n\pi}{L}\right)^2 \frac{EI}{m}} \tag{2.11}$$

The following relationship gives the frequencies of a conductor span as a function of its average bending stiffness *EI* [1, 2]. This relationship is realistic as the bending stiffness and its tension are included. All resonant frequencies are an integer multiple of the resonant frequency corresponding to the first mode shape.

2.3.3 Bending method

Actually, there are several pieces of equipment and many methods which allow for measurement of the Aeolian vibration of conductors. In 1966, The IEEE Transmission and Distribution committee established a standard method called the bending amplitude method which is promoted by many organizations such as CIGRE and IEC. This method is recommended mainly for the determination of the fatigue risk that can occur on overhead line conductors. This assumes direct measurements of the displacement relative to the supporting clamp, at 89 mm from the last point of contact between the conductor and clamp, as initiated by Tebo [32, 33].

The Bernoulli-Euler theory is considered in the bending amplitude method [2]. The conductor-clamp system is modelled as a cantilever beam with one force acting on the

free end. The equation of the bending moment may be expressed as a function of the tension (T), due to the weight of the conductor and deflection Y_t :

$$M = T.Y_t \tag{2.12}$$

By including (2.2) in (2.12), the deflection may be expressed as follows:

$$\frac{d^2Y_t}{dx^2} = \frac{TY_t}{EI} \tag{2.13}$$

The solution to this equation (2.13) leads directly to the measurement of bending amplitude (2.14), The motion of the conductors (bending back and forth) in the vicinity of the clamp imposes alternatives stresses to the conductor's strands. This causes the strands to slip relative to one another, causing shear stresses and fretting of the strand surface. Poffenberger and Swart used the equation (2.10), to establish a formula which interpreted the zero-to-peak dynamic bending stress σ_a at 89 mm from the last point of contact between the clamp and conductor [34].

$$\sigma_a = KY_b \tag{2.14}$$

Y_b is the vertical displacement range of the conductor, and K is the Poffenberger parameter, which may be expressed as follows:

$$K = \frac{E_a.d.p^2}{4(e^{-px} - 1 + p.x)} \tag{2.15}$$

E_a is the modulus of elasticity of the outer-wire material (N/mm^2), d the diameter of the outer-layer wire (mm). x is 89 mm, the distance on the conductor between the last point of contact between conductor and clamp. Therefore:

$$p = \sqrt{\frac{T}{EI}} \tag{2.16}$$

This formula established the relationship between the bending amplitude and bending dynamic stress at 89 mm away from the LPC (last point of contact) between the conductor and clamp. Calculations and laboratory measurements often shown a good correlation for many samples of several conductors tested.

2.3.4 Dynamic stress

The relationship between strain and stress in a strand of vibrating conductor based on Hooke's law may be expressed thus [2]:

$$\sigma_a = \varepsilon E_a \tag{2.17}$$

With ε : dynamic bending strain.

Using the Poffenberger-Swart formula (2.15) and (2.16), the dynamic bending stress in the conductor at the suspension clamp may be found, assuming that each single wire flexes autonomously. The bending alternatives stress in the overhead lines at the vicinity of the suspension clamp may be expressed [21]:

$$\sigma_b = \pi d E_a \sqrt{\frac{m}{EI_{min}}} f Y_v \tag{2.18}$$

with σ_b the dynamic bending stress, and Y_v the anti-node displacement, and EI_{min} the flexural rigidity minimum.

The suspension clamp is always positioned between two spans and when the conductor is vibrating, a rocking movement is imposed on the suspension clamp.

$$\sigma_{b-susp} = \sqrt{\frac{\sigma_{b1}^2 + \sigma_2^2}{2}} \tag{2.19}$$

Where σ_{b1} and σ_{b2} are the dynamic bending stress of span 1 and span 2 found with (2.18) at each side of the clamp.

2.3.5 Conductor stiffness

The bending stiffness of the conductor during its alternative bending motion lies between its minimum and its maximum value, but since the conductor is composed of twisted wires of aluminum and steel, the calculation of the bending stiffness is quite complex. For high bending amplitude values, the strands of the conductor are considered to be moving independently and without any friction around their own axes [2, 35].

$$EI_{min} = \frac{\pi}{64}\left(N_{al} d_{al}^4 E_{al} + N_{St} d_{St}^4 E_{St}\right) \tag{2.20}$$

where N_{al} and N_{st} are the number of aluminum strands and steel strands, d_{al} and d_{st} the diameter of aluminum and steel strands, respectively, E_{al} and E_{st} the modulus of elasticity of aluminum and steel strands, respectively.

For the upper bending stiffness limit, it has been assumed that the strands form a homogenous body.

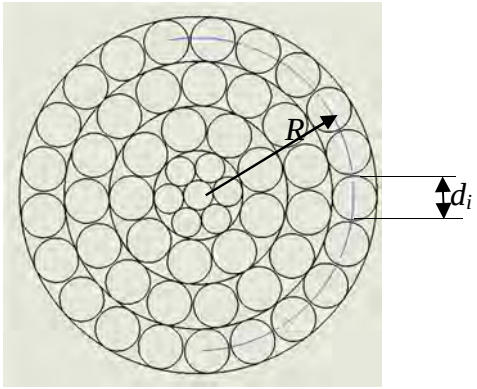

Figure 2-6: Conductor cross-section (multi-layer conductor)

$$EI_{max} = \sum_{i=1}^{n} \frac{N_i \pi d_i^2}{8} \left(\frac{d_i^2}{8} + R_i^2 \right) \tag{2.21}$$

with N_i the number of the strands per layer, d_i the diameter of the strands, and R the layer radius.

2.3.6 Stress distribution in the conductor wires

The dynamic behaviour of the individual wires of the conductor subjected to the tensile loads and tensile stresses must be defined in order to understand the entire dynamic character of the conductor under motion. The following formula gives the stress distribution for the aluminum wires σ_{Al} [1]:

$$\sigma_{Al} = \frac{E_{al} T}{E_{al} A_{al} + E_{st} A_{st}} \tag{2.22}$$

and for the steel wire stress σ_{st} :

$$\sigma_{st} = \frac{E_{st} T}{E_{al} A_{al} + E_{st} A_{st}} \tag{2.23}$$

with A_{al} and A_{st} the cross-sections of aluminum and steel, respectively.

2.4 Composite insulator

The function of the insulator is to mechanically support the overhead-line conductor, and to ensure a good electrical insulation between the conductor and the tower. Traditionally, insulators were made of ceramic material (porcelain or tempered glass) and such insulators are still in service in most countries. Composite materials, and especially the fibre reinforced plastic (FRP) provide improved performance benefits over ceramics due to their inherent properties [36, 37].

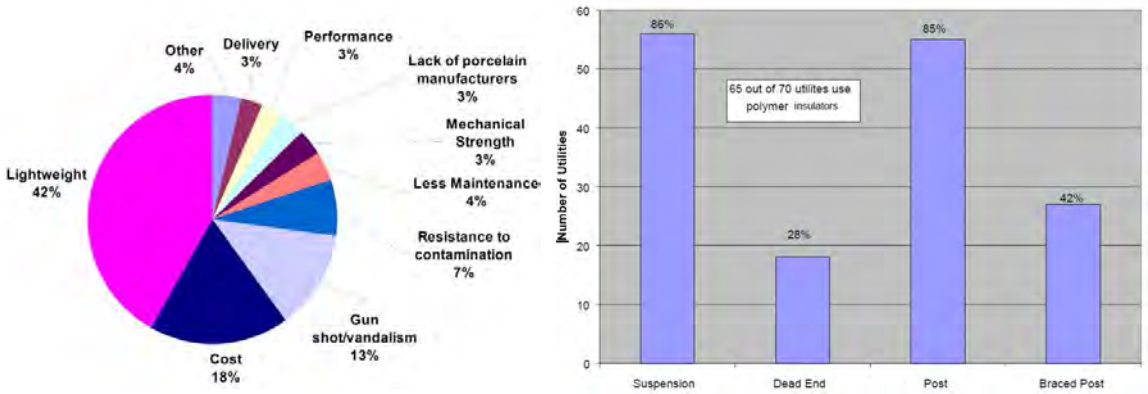

Figure 2-7: Reasons for applying polymer insulators; and number of utilities utilizing polymer insulators in different configurations [38]

The most significant reason for using composites is the strength-to-weight and stiffness-to-weight ratios. Composite insulators, also known as polymer insulators or non-ceramic insulators, represent 2 to 5 per cent of the cost of a transmission line. They are frequently found on transmission systems owing to their lightweight nature, ease of handling, resistance to vandalism, and relatively attractive cost. Long-term behaviour of the composite insulator and their failure occurring, is not well defined. Operationally, the insulators should have high mechanical resistance (MDCL or SML) which carries the load with enough operational security [39]. Previous experimental studies have admitted that the composite insulators which are exposed to accelerated mechanical cyclic loads might possibly display and even accelerate signs of fatigue failure. Composite suspension or dead-end insulators are practically exposed to axial tensile forces; their failure modes might be well-known and defined. For the line post towers, which allow an overall dimension and the height of the tower reduced in monopole

structures over the traditional tower lattice and H-frame construction, the situation is more complex. The line post towers reduce the visual impact of the line, as well as the cost, enhancing construction efficiency and reliability, providing urban aesthetics and a low environmental impact in Distribution and Transmission lines. The post insulators may be subject to bending as well as tension or compression loads; their failure mode is more complicated [5, 39].

2.4.1 Composite insulator components

2.4.1.1 Core

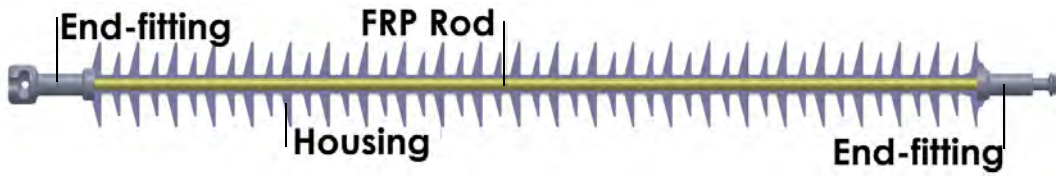

Figure 2-8: Construction of a composite long rod insulator [5]

The core is made up of 60 to 70 per cent of its volume of unidirectional fibre reinforced plastic, positioned parallel to the insulator rod axis. This is the principal mechanical load-bearing component of the insulator. Epoxy resins, polyester or modified vinyl-ester reinforced with E-glass or ECR-glass fibres may be used as constituents in the pultrusion-manufacturing process.

2.4.1.2 Metal End Fittings

The end fittings of the insulator which are crimped to the extremities of the FRP rod, providing a mechanical link used to transmit mechanical loading from the overhead conductor to the FRP rod (at the line-end), and from the FRP rod to the tower (at the tower-end). These are either made of galvanized cast iron, forged steel, stainless steel, or aluminium (Figure 2-9).

Figure 2-9: Typical end fittings for composite long rod insulators [5]

Six types of end fittings of suspension insulator may be used, depending on the method of attachment to posts and conductor clamps.

2.4.1.3 Silicone housing

To protect the FRP rod from the external environment (moisture ingress) and electrical leakage, a layer of rubber sheath housing covers the rod with several disc-shaped weather sheds. These are made of either silicone rubber compounds, ethylene-propylene (EP), or ethylene-propylene diene monomer (EPDM), with silicone rubber being nowadays the material of choice for the majority of insulator manufacturers. In order to withstand more high voltage on the transmission line, the insulators have to be provided with more weather sheds and greater overall length to maintain adequate leakage distance. Properties such as hydrophobicity and corona-cutting resistance may be added to the housing under certain working conditions.

2.4.2 Insulator types and their loading criteria

According to the load criteria and their intended applications, the composite insulator may be classified as suspension, substation, or line post insulators. The Table 2-1 and Figure 2-10 give description of different types and configurations of insulators.

Table 2-1: Types and configurations of insulators

Type of insulator	**Configuration**	**Options**
Suspension insulator	I-string	
	V-string	
	Dead-end insulator	
	Suspended line post insulator	
Line Post insulator	Unbraced	Horizontal
		With an angle
	Insulated cross-arm (braced)	Rigid
		Pivoted

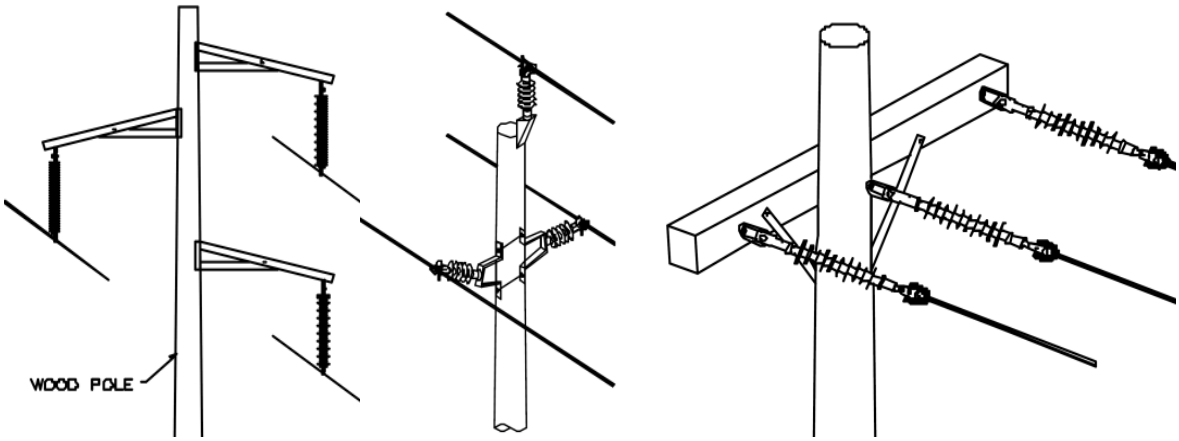

Suspension insulator Line post insulator Dead-end or suspension insulator

Figure 2-10: Insulator types [7]

In this project, only two types of composite insulator: suspension and line post insulators were considered. Many options of insulator arrangements may be used to sustain more mechanical loads on compact transmission lines.

2.4.3 Suspension insulator

These insulators are mainly subjected to axial tensile loads. The suspension insulators are mostly loaded in I-string configuration (vertically), while the dead-end insulators support the power line horizontally. Both experience tensile and torsional loads. V-string configurations have the advantage of supporting bigger loads. However, this is a costly choice. The suspension insulator may be used for the transmission line voltage range of 69 to 735 kV. Mechanical strength may be varied from 40 kN to 600 kN [5, 39]**.** The following types of end fittings are used in the suspension insulator: oval eye, y-clevis, socket, ball, clevis, and tongue (Figure 2-9).

2.4.3.1 Ratings

The ratings explain which maximum load may safely be applied to the insulator in service. The rating methods of testing insulators are clearly described by organizations such as the International Electro-technical Commission (IEC), the American National Standards Institute (ANSI) or the Institute Electrical and Electronics Engineers (IEEE) [8-10, 23]. It has been noted that these tests are mostly static axial tensile test for the

suspension and the post insulator, while the static bending tests are only conducted on the post insulator. In service, the testing approach is quite different from that of the insulator loading in the field where axial tension/compression, bending, and torsion are raised, and have therefore to be considered. Three types of mechanical ratings of composite insulators are [10]:

a) Specified mechanical load tests

Only one insulator from any given manufacturing schedule is tested. The standard ANSI C29.11 explains that the term SML (specified mechanical load) as the loading that should the insulator be able withstand 75% of this load for 90 seconds without failure. At 100% of the load, the insulator should fail instantly. The IEC standard test increases the number of insulators tested at four units; it is the most-used standard.

b) Time-loads tests

In this test, the importance is given to the factor “time” as the strength of the composite insulator decreases after a certain period while the insulator is loaded. A period of 50 years is considered optimal by users. It has been estimated that composite insulators can fail at 50% of their SML rating if this loading only is constant for several years and at 10% of their SML if in operation, the insulators are exposed to a high electrical pollution area (acid), to rain, or to electrical partial discharge. The ANSI C29.11 standard states that the three insulators should be continuously loaded at 60% of their SML for a period of 96 hours. The IEC specification is considered to load at 70% of SML for the same length of time and number of insulators tested as ANSI C29.11 [9, 10].

c) Routine tests

This test is carried out on every composite insulator manufactured. 50% of SML should be reached for a period of three seconds.

2.4.4 Line post insulator

The line post insulators have a great diameter but a shorter length than the suspension insulator. They are principally loaded in cantilever (bending) mode. These insulators may be mounted perpendicularly to the tower or they may have an angle of approximately 15 degrees up from the horizontal. This requires special end fittings.

The station posts which are used in electrical substations are mainly loaded in axial compressive loads. For both insulators, axial tensile loads may be considered. Flange end fittings are mostly used for the station post. The following forces may be considered, while the line post insulators are in service (Figure 2-11):

- Vertical loads: These loads are principally associated with the conductor weight. The vertical loads produce the bending force of the line post insulator.
- Longitudinal load, perpendicular to the vertical loads. This load corresponds with an unbalanced load on the two spans. The longitudinal loads are particularly high in dead-ends.
- Transverse loads act perpendicularly away or towards the post (tower). Tension or compression on the line post has loading transverse to the direction of the line.

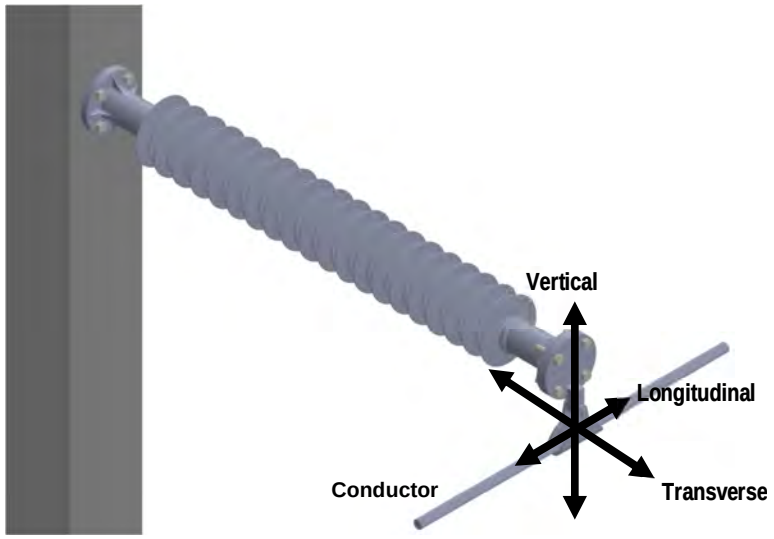

Figure 2-11: Geometry and loading of a line post insulator with angle

2.4.4.1 Ratings

Many tests are conducted in order to establish the “limit load” on the line post insulator. This is described in the international standard as IEC 61952. The test is generally conducted by the manufacturer. The following tests are performed to establish whether the insulators are faultless [5, 23] :

a) The specified cantilever load (SCL)

Specified by the manufacturer, this is characterized by the bending load applied at the conductor side of the insulator, which an insulator can withstand during a test.

b) The cantilever failing load (CFL)

Greater than the SCL, the CFL is the maximum load reached during the post insulator test. It is normally 15-20% higher than the SCL.

c) The maximum design cantilever load (MDCL)

The MDCL expresses the loads over which damage of the FRP rod is initiated. This represents the "limit load" which can arise during an operation. Normally this would be approximately half of the SCL. This test focuses on three insulators with standard end fittings tested at 20 ± 10°C by the manufacturer. The duration of the test is four days. The insulators are gradually loaded up to 1.1 times the MDCL at the conductor side. Once the MDCL has been reached, the loads are maintained for 96 hours, as for the suspension insulator. The deflection is recorded after a certain interval of time before reaching 96 hours. A visual inspection has to be carried out during the interval period in order to check any deformation or cracks initiated. A close investigation is undertaken in order to inspect for fine cracks and delamination. This is achieved by cutting the insulator close to the end fittings at which the loads were previously applied. Thus, the bottom of the end fitting is cut longitudinally, dividing it in two as shown in Figure 2-12.

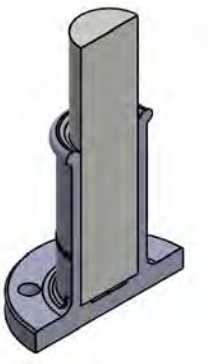

Figure 2-12: Section of the bottom of the end fitting

2.5 Mechanical behaviour of flexural stressed composite insulators

As mentioned before regarding the loads that insulators are facing, torsional forces may be added even though the FRP rod reacts badly to torsion. These forces occur while in service or during installation or maintenance. The mechanical strength of the insulators depends strictly on the FRP rod characteristics and the technique of crimping the metal end fitting. It has been observed that the first sign of failure was shown where the rod was no longer in contact with the end fitting. Generally speaking, this is caused by the shear stress which is perpendicular to the fibre direction. Compression brings about the first crack on the rod. For high compression loads, delamination may be detected for both the tension and the compression load sides of the rod, and, at times, even in the middle plane [5, 39]. When loads generate small deflections, analytical formulas (2.28) and (2.29) may be used for the line post case, which is the unbraced case contrary to the line post braced case. This is valid only for percentage less than 10% of the length of the insulator. Above 10 %, the use of a computer may be required [40].

In order to simplify analytical calculus of the composite insulator structure, some assumptions must be considered:

- There is a perfect rigid liaison between both the metal end fittings and the FRP rod of the post insulator.
- Loads are applied at the point located on the axis of the insulator, at the tip of the insulator.
- The composite insulator is rigidly fixed and there is no movement of the pole or tower.
- The effect of the elastomeric housing of the insulator is negligible.

The composite material, being a unidirectional FRP reinforced composite material, has a Young's modulus and a Poisson's ratio.

2.5.1 Suspension insulator

As described previously in Section 2.4.3, the suspension is subjected to tensile loads, while the line post insulator is a pure cantilever, as described in the international standards [9]. The mechanical behaviour of the suspension composite insulator depends on the quality and the application process of the end fittings. It has been noticed that the influence of the temperature is important. A cold environment will be beneficial as

ultimate tensile stresses of insulators increase with d_r the diameter of the rod, L_{cr} being the crimped length. The analytical model of the suspension insulator gives an overview mainly on the strength of the FRP rod and the end fittings which have to withstand to the minimum requirement of the specified mechanical loads (SML) and limit load (2.13).

The maximum shear stress σ_{shear}^{max} of the FRP rod must be approximately 40 N/mm^2; the SML may be found by this formula:

$$SML = \pi d_r L_{cr} \sigma_{shear}^{max} \tag{2.24}$$

In order to establish whether the end fitting will withstand the SML specified, the transition zone between the connection part of the fitting and the crimped part, and the cross-sectional area of the end fitting are identified as the critical zone in which the failure may occur.

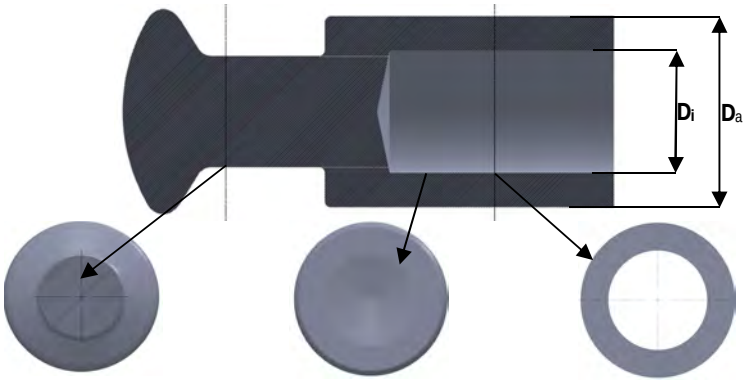

Figure 2-13: Critical cross-sections when dimensioning an end fitting [5]

The tensile stress in the cross-sectional area of the fitting σ_Z as shown in Figure 2-13 is:

$$\sigma_Z = \frac{SML}{\pi(D_a^2 - D_i^2)/4} < \sigma_{zul} \tag{2.25}$$

with σ_{zul} the tensile strength of the fitting, $D_a$the outer diameter, and D_i the inner diameter of the end fitting.

The transition areas are subjected to shear stress τ which should withstand the SML

$$\tau = \frac{SML}{\pi D_i \, l} < \tau_{zul} \tag{2.26}$$

with τ_{zul} the maximum shear stress.

2.5.2 Line post insulator

2.5.2.1 Damage limit load

An evolution of deflection is observed when a constant stress is applied to the material. It has been observed that deflection is formed from a family of the straight linear equation $\Delta f = A.log\ t$ in a semi-logarithm diagram. This is illustrated by Figure 2-14.

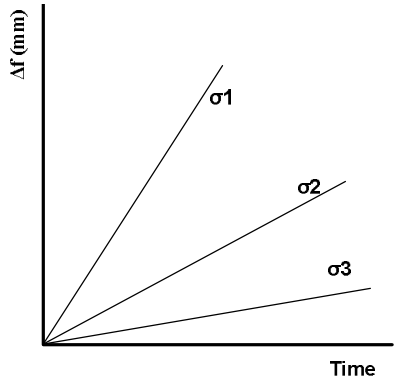

Figure 2-14: Deflection variation versus time and variation of the creepage rate coefficient A versus the stress in the embedded cross-section

The creepage rate at the given moment t is equal to A/t. t is the time (moment) and A is a coefficient found experimentally. In the case of a line post insulator there is a ductile behaviour similar to metallic materials, with an elastic deformation at low stress levels and a quasi-plastic deformation at high stress levels. During the strain behaviour, there is an intermediate area separating both phases, called the "damage limit" [40].

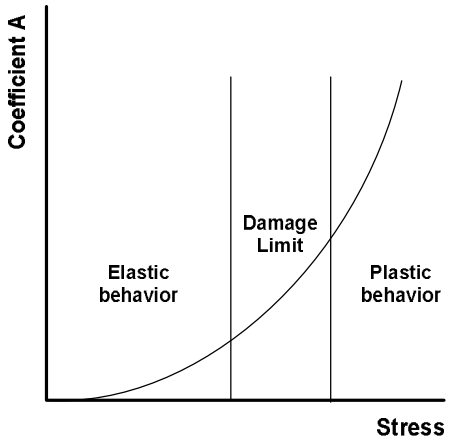

Figure 2-15: Damage limit

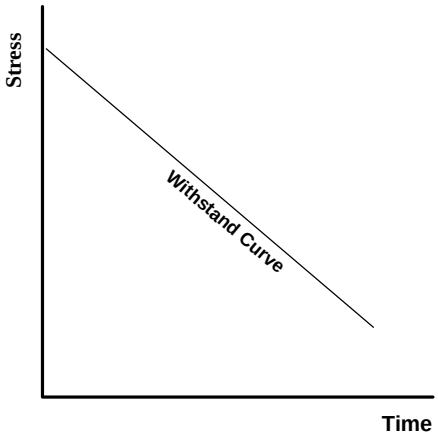

Figure 2-16: Load-time curve for composite insulators stressed under cantilever load.

2.5.2.2 Long-term mechanical behaviour

Figure (2-15) shows that the stresses applied to a composite line post insulator must be maintained below the "damage-limit" stress. The first sign of failure or fatigue depends on the loading time and the load applied.

The "damage limit" was established by the CIGRE Working Group 22.3 after many series of tests of the insulator without weather sheds. This was inspired by the variation of deflection over time, with a visual inspection for cracks of the surface of the rod. The conclusion of these tests was that the damage limit of short insulators is smaller (between 325 and 425 MPa for a 45mm rod diameter), while for longer insulators with the same insulator diameter, the damage limit is greater (between 475 and 600 MPa). The nominal bending stress σ_n may be determined by [5]:

$$\sigma_n = \frac{F_b l}{d^3/32} \tag{2.27}$$

with F_b the external load (bending), l the bending length, and d the diameter of the rod.

The damage limit load is approximately 25% higher than the MDCL, and 20-40% smaller than the SCL.

2.5.2.3 Load application curves obtained with the analytical formula

In order to plot the loading curves, some analytical formulas are used for small deflections (10% of the insulator length). The general formula of the moment comes from the "Theory of Elasticity of Timoshenko" [40]. For compression loads:

$$M_c = \sqrt{\frac{(V^2 + T^2)EI}{H}} \tanh\left(s\sqrt{\frac{H}{EI}}\right) \tag{2.28}$$

and tension loads :

$$M_t = \sqrt{\frac{(V^2 + T^2)EI}{Z}} \tanh\left(s\sqrt{\frac{Z}{EI}}\right) \tag{2.29}$$

with V the vertical load, T the longitudinal load, H and Z the compression and tensile loads, E:Young's Modulus, I: Moment of Inertia of the FRP rod, with $I = \pi\frac{D^4}{64}$; D the diameter of the FRP rod; finally the stress on the FRP rod may be calculated by :

$$\sigma = \frac{M_{H/Z}}{W} \tag{2.30}$$

with $W = {D^2}/{32}$

Figure (2-17) shows the load curves which may be produced by the analytical formula for a horizontal line post insulator.

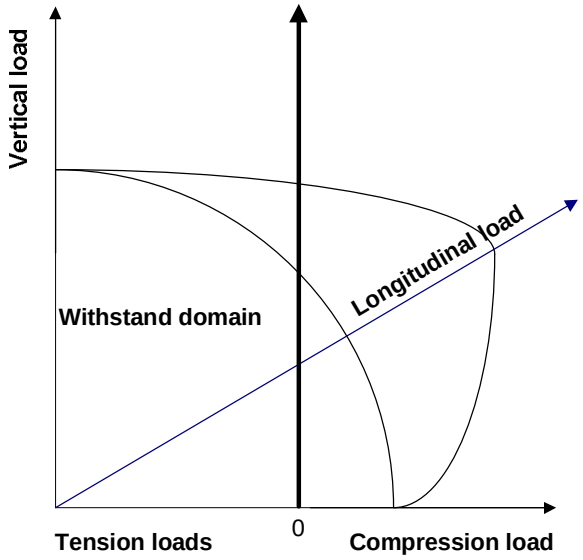

Figure 2-17: Model of combined load curves for the line post composite insulator [40]

2.5.2.4 Line post insulators with an angle to the horizontal

By considering α=15° the angle to the horizontal, the following modification is considered [5]:

$$\begin{aligned} V &= H' \sin(\alpha) + V' \cos(\alpha) \\ H &= H' \sin(\alpha) + V' \cos(\alpha) \\ Z &= Z' \sin(\alpha) + V' \cos(\alpha) \end{aligned} \tag{2.31}$$

V', H' and $Z'$are the loads applied to the free end of the insulator inclined at α.

The deflection f_i may be calculated by the following formula:

$$f_i = \frac{F_b l^3}{3EI} \tag{2.32}$$

with $I = \frac{\pi D^4}{64}$

It is not easy to predict the life expectancy of composite material because failure modes and mechanisms are complex and react differently according to the fatigue behaviour and the environment in which the material will be used. Because the composite insulators for transmission and distribution lines have been designed for a long service life, the materials required for the insulators should be free from damage which is a consequence of the degradation of material during operation. The durability criterion of the composite materials shows the relationship between the material strength and the loading time. The long-term loading of the composite material will accumulate damage which is induced by accelerated stress. The material damaged will be intensified by the environment service condition such as temperature, moisture etc. This will lead to the studying of endurance limits. Figures 2-15 and 2-16 present different curves to give an interpretation of the long-term strength behaviour of the composite material. The material strength is intensely affected by the time of loading. Once the composite material is unloaded, the material should recover its initial static strength that was before the long-term loading.

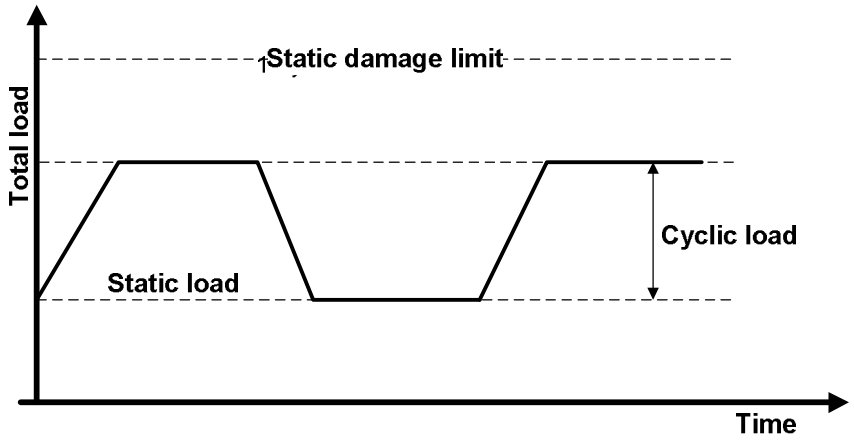

Figure 2-18: Cyclic loading of the dynamic tests [5]

2.6 Failure of composite insulators

In this section, only mechanical failure will be discussed. In service, a -very remote- possibility exists for a series of cascading failures occurring along many kilometres of the power line owing to the instability created by the mechanical failure of a single insulator. Survey results on the failure mode of composite insulators have indicated that the FRP rods are the components of the insulator most exposed to mechanical failure [5,

7, 37-39]. The mechanical failure modes of the composite insulator may be summarized as follows:

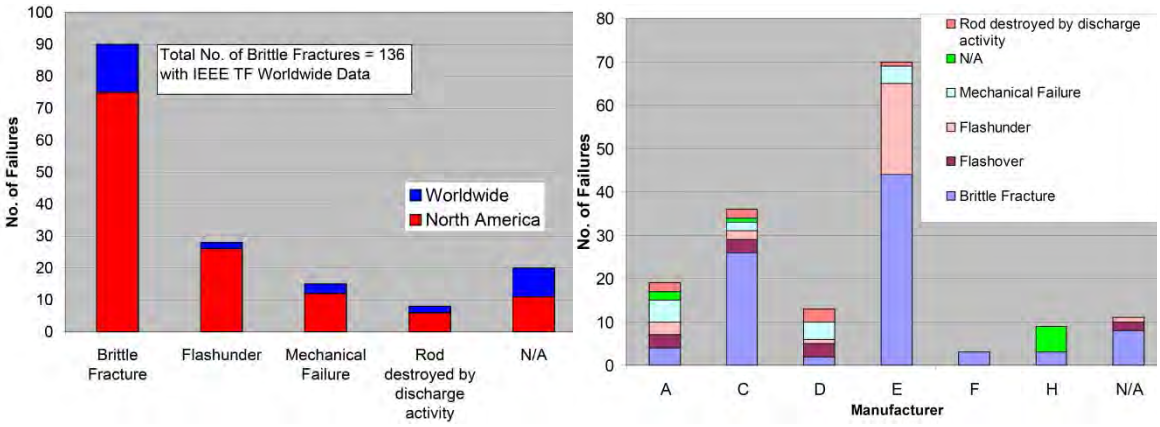

Figure 2-19: Insulator failure modes and their failures sustained by different manufacturers subcategorized by failure [38]

2.6.1 Brittle fracture

This affects the FRP rod of the composite insulator; it is the so-called “stress corrosion cracking” (SCC) mechanism. It is principally caused by the moisture (acid or rain) in the end fittings of the insulators. Individual fibre failures are observed as the cracks spread perpendicularly to the fibres. This reduces the cross-sectional area of the FRP rod resulting in brittle fracture.

2.6.2 Intra-laminar failure of the FRP rod

This failure occurs principally in post insulators subjected to excessive bending loads. Based on the beam theory (Euler-Bernoulli bending theory), axial compressive and tensile stresses develop in the direction of the FRP rod axis under bending loads. The tensile stress is found at the uppermost edge of the FRP rod, while the compressive stress is located at the lower edge. The neutral (central) axial of the FRP rod has to resist shear stress, or so-called intra-laminar failure. This type of failure is very difficult to detect.

2.6.3 Crimping damage

Failure is caused by a high radial compression load applied to the FRP rod via the end fittings during the crimping process.

2.6.4 End fitting slippage

Owing to insufficient radial compression of the end fittings during the crimping process, an internal sliding of the FRP rod of the insulator from the end fitting can happen during operation. This applies mostly to the suspension insulators, and describes a complete separation of the FRP rod from the end fittings.

2.7 Previous laboratory work

Various laboratories around the world are focusing on the studying mechanical behaviour of the overhead-line conductors and composite insulators. Additionally, it is deemed necessary to consider the dynamic behaviour of composite insulators under Aeolian vibrations, in order to estimate their life expectancy.

However, certain questions have been raised from the analysis of laboratory work completed by previous researchers. In 1983, R. Mier-Maza, J. Lanteigne, and C. De Tourreil [41] were interested in the mechanical performance of the end fittings of the suspension synthetic insulators. They calculated the internal stresses of synthetic insulator rods inside the end fitting by developing an analytical model. At different temperatures, they observed fractures after tensile and creep tests. Two years later, C. de Tourreil, R. Roberge, & P. Bourdon [3] investigated mechanically composite insulators with various end fitting designs, concluding that the ultimate tensile strength measured (UTS) at -25 to 100°C represents 60 to 70% of the potential material properties of the fibreglass rod.

In 1990, C.H. De Tourreil [4] concluded that, during loading, failure does not occur when the dynamic loads are low - from 22% to 75% of the static load. It was suggested that only the dynamic, not a static load performance should lead to the selection of a composite insulator. D. Dumora, D. Feldmann, and M. Gaudry [40] found two approaches to solve the mechanical behaviour problem of the insulator by time-load characteristics and combined loading. They showed that the permanent deformation remains low provided the cantilever moment stress does not exceed a certain value. The researchers developed a mathematical model which determines the maximum stressed area.

Frank Schmuck & C. De Tourreil [42] investigated the brittle phenomenon which appears when the glass fibre is in contact with an acid. This affected a small number of

insulators. B. Mobasher, D. Kingsbury, J. Montesinos, & R. S. Gorur [43] focused on the manufacturing procedures of composite insulators, developing a procedure for crimping the assembly of the insulator rod. In 2006 J. Wańkowicz, J. Bielecki, and E. Strużewska [44] concluded that the model of the mechanical resistance of the composite insulator subjected to the cyclic loads should be based on experimental testing**.** A. Prenleloup, T. Gmür, J. Botsis, K. O. Papailiou, and Kurt Obrist [45] investigated the silicon composite insulator numerically and experimentally, finding that the stress concentration appeared mainly in the end fitting area (including the rod in the end fitting). Finally, they observed that the damage initiated to the composite insulator may occur as result of this. They established a relationship between the bending load and the acoustic emission during a load-displacement test.

In 2009, J. Wankowicz and J. Bielecki [4] revealed that the time for a certain maximum mechanical load, the vibration amplitude, does not influence the fatigue strength of the composite insulator. Nevertheless, the length of time that can cause failure is strongly dependent not only on the vibration amplitude, but also on the maximum mechanical load, as declared by C. Toureil. One year later, these researchers concluded that standard tested insulators with the same mechanical parameters could show a different status of fatigue characteristics. They differed significantly in resistance to cyclic loads which is maintained until the composite insulator fails (for low-range to extraordinarily high load values) [46].

2.8 Summary

This chapter had reviewed all necessary theories and consideration on the dynamic character of the conductors under wind effects especially the Aeolian vibration by producing an analytical model. A particular attention was given to the contact conductor-clamp system as the bending amplitude method is based on. A brief presentation of the bending stiffness of the conductor at the vicinity of the clamp was presented. The composite insulator which has same significant advantages on the traditional insulators (ceramic) was presented and their standard testing discussed. Based on industrial survey, the mode failure of the composite insulator was explained briefly. Many published studies, standard recommendations and laboratory works have been published mechanical behaviour of the composite insulator static and cyclic loads but few published have examined the mechanical behaviour under Aeolian vibration. In

order to find the mechanical behaviour, many parameters and considerations have been taken into account and some researches have been focused on the internal stress of end fittings; others considered the crimping operation and some studied the behaviour of the composite material used for manufacturing of the insulators.

CHAPTER 3
EXPERIMENTAL EQUIPMENT & SET-UP

3.1 Introduction

The objective of the test is to establish experimentally the vibrational loads which are generated when the overhead lines are under Aeolian vibration conditions and to assess the mechanical behaviour of the composite insulators (suspension or line post) which are held by the vibrating conductors. In order to evaluate the vibrational loads of the vibrating conductor, an experimental test rig was required. The Vibration Research and Testing Centre (VRTC) is an indoor laboratory facility equipped with an 84.6 m test span. Two support insulator structures which were designed, manufactured and placed at the mid-span. The instrumentation which included force and displacement sensors was connected to a data-logging system: Puma vibration control system, or NI data-acquisition system. LabView software and Matlab software were used for the analysis of the measurement results. By using the bending amplitude range of 0.1 to 1.0 mm, two support configurations were used (suspension and line post insulator) and two aluminum conductors, steel-reinforced ACSR (Pelican and Tern) were used at four different static tensions (% ultimate tensile strength -UTS-). For each support configuration, the clamp could either be rocking (articulated) or blocked.

3.2 Background & Vibration Research and Testing Centre (VRTC)

3.2.1 General

The tests were performed at the University of KwaZulu-Natal (UKZN) - Westville Campus at the Vibration Research and Testing Centre (VRTC), Durban, South Africa. This indoor facility laboratory was built in 2004 in partnership with Eskom and NRF/THRIP for the investigation of mechanical vibration, most especially Aeolian vibration testing of conductors and for pursuing research on overhead line components according to IEEE, IEC, and CIGRE recommendations. The laboratory test for this research was carried out according to the IEEE and IEC standards (IEEE 563 STD-

1978 for span tests and IEEE 664 STD & IEC 61897 STD for vibration dampers) [33]. The main characteristics of the testing facility are:

- A single span of 84.6 m conductor ;
- 2 concrete blocks on which there are fixed dead-end clamps supported by rigid clamps (Figures 3-1 and 3-16) ;
- 6 air-conditioners with temperature control, which allow the testing to be performed at a constant temperature (±21ºC);
- a constant tension loading device with a monitoring system (Figure 3-16c);
- An electrodynamic shaker used to simulate the input of the wind power in the conductor (Figure 3-3) and;
- A control system to control, measure, and analyse the excitation of the conductor.

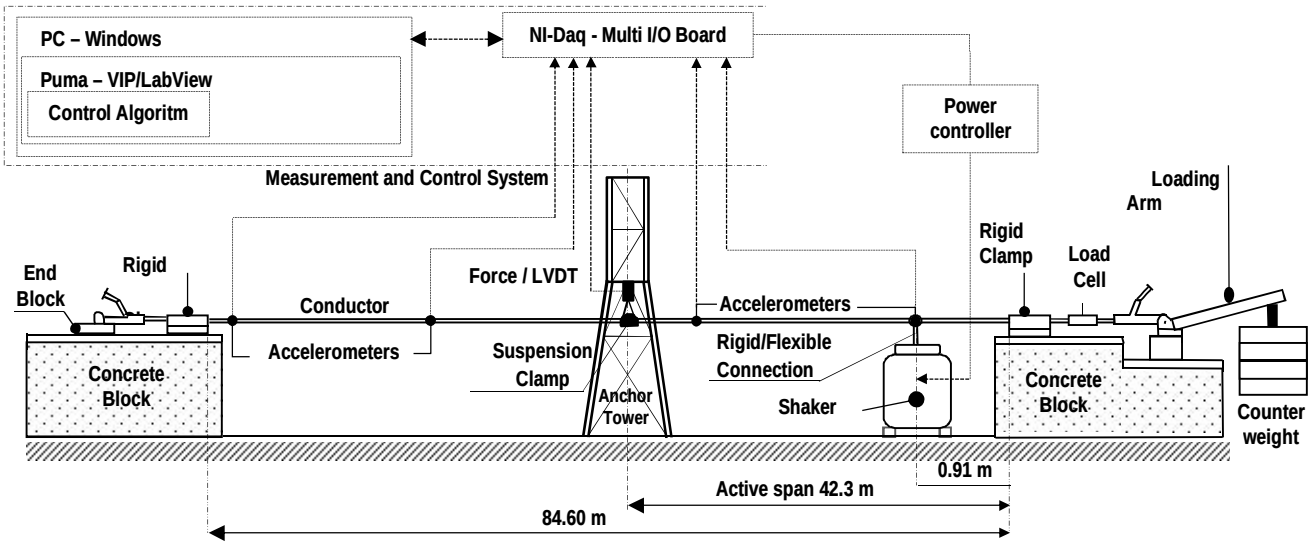

Figure 3-1: Schematic view of the laboratory set-up for load measurement

An anchor tower and a line post support were placed and bolted at mid-span of the laboratory. The suspension clamp (Figure 3-2a), suspension insulator (Figure 3-2a) or line post insulator was fixed (figure 3-2b) to the tower.

3.2.2 Insulator supports

3.2.2.1 Anchor tower

The anchor tower which was placed at mid-span of the laboratory was modified from an old existing fretting fatigue stand at the VRTC (Figure 3-2a). The height was increased and at the legs the anchor tower were reinforced. The CAD – SolidWorks software was used to design and to perform the FEA of the anchor tower.

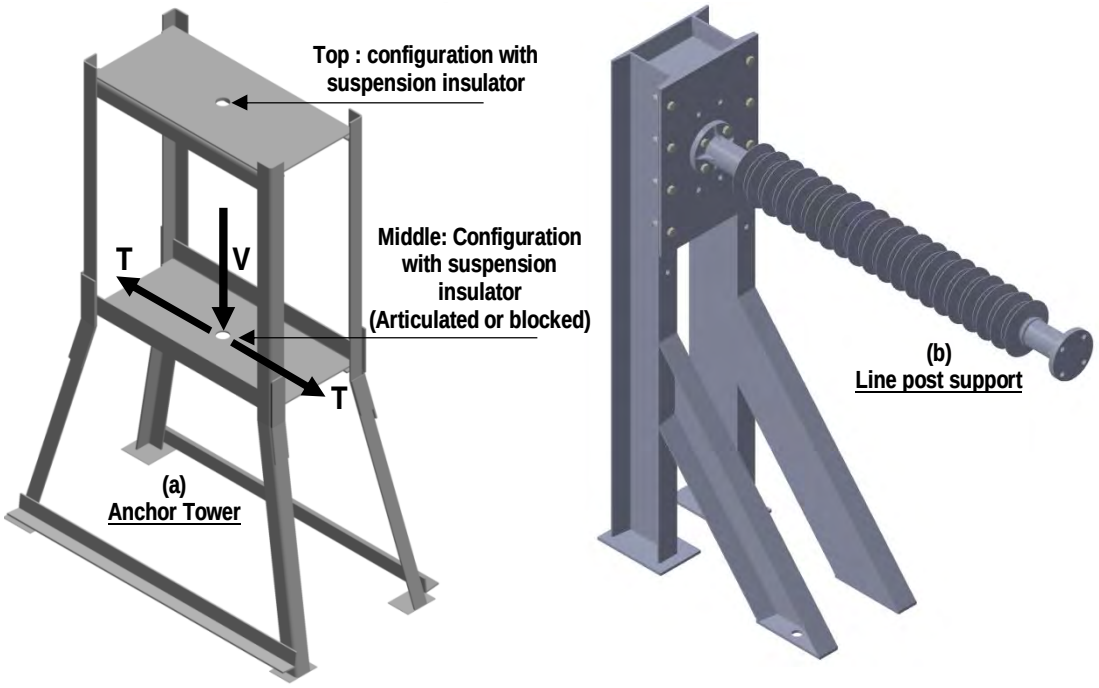

Figure 3-2: Anchor tower: for suspension clamp and suspension insulator (a) & the line post insulator support (b)

The anchor tower was designed for vertical loads up to 30 kN, and to withstand high static tension of up to 50% UTS for the Tern conductor (the biggest conductor tested, with an overall diameter of 27mm). This anchor tower not only offered flexibility due to its various clamp configurations, but also due to the variation of the height of the suspension point. The top of the anchor tower was used for a suspension insulator with no plate at the middle as shown in Figure 3-2a, while at the middle only the suspension clamp (blocked or articulated) could be mounted.

This constituted three suspension support points (including the end span) of the conductor which were at the same height from the ground (Figure 3-1).

3.2.2.2 Line post support

For the scenario in which a line post insulator would be tested, a line post support was also designed (Figure 3-2b). As previously, the commercial package SolidWorks was used for the design. The line post support could mechanically withstand a cantilever load up to 5kN.

3.3 Laboratory configuration and equipment

3.3.1 Equipment & instrumentation

3.3.1.1 Electrodynamic shaker

The electrodynamic shaker TIRA Model, Type TV 56263/LS, which has a frequency range of 5-3000Hz, with a displacement of up to 50.8 mm peak-to-peak, is used to simulate the action of the wind on the conductors and dampers (Figure 3-3). The electrodynamic shaker which operates like a loudspeaker but is more robust, acts on electromagnetic forces which have been created by two interacting magnetic fields. The coils are the source of the magnetic field. One of the coils has its own magnetic field which is proportional to the voltage applied, while the other has a static magnetic field.

Figure 3-3: Electrodynamic shaker (TIRA Model, Type TV 56263/LS) at the Vibration Research and Testing Centre.

The conductor was connected to the mobile armature by either a flexible or rigid connection, while the other armature was fixed as a coil. This causes the armature to move forwards and backwards in the magnetic field, causing the conductor to vibrate in

response to a certain input signal. Vibration generated by the shaker may be used for several types of vibration tests, such as sine, random, shock, sine-on-random, random-on-random, or diverse complex waveforms, as well as replicating data collected from real-world conditions. The excitation of the conductor may be achieved in either a vertical or horizontal position. The shaker has a cooling system composed of a compressor used to cool down the field- and the armature-coils. The control system of the shaker piloted by an amplifier, shuts down the entire system in case of an abnormal behaviour of the shaker.

3.3.1.2 Piezoelectric Accelerometers

Accelerometers of Brüel & Kjær type 4508-002 and 4507 B which rely on the piezoelectric effect of quartz or ceramic crystals, were used during the vibration testing to control the conduction motion. These accelerometers were selected for their high-sensitivity (100mV/g), wide-range frequency of measurement, and low inertia (mass). The sine-wave signals of the accelerometers which were interpreting the sinusoidal behaviour of the conductor during the test, were collected by the Puma Vibration Control and Analysis System. The data from the accelerometers provided valuable information (amplitude, velocity, acceleration, and frequency) regarding the system integrity of the overhead-line span and operating mode shapes. The accelerometer cables were securely fastened to their connectors in order to avoid any potential noise passing into the vibration measurement (Figure 3-4) [47].

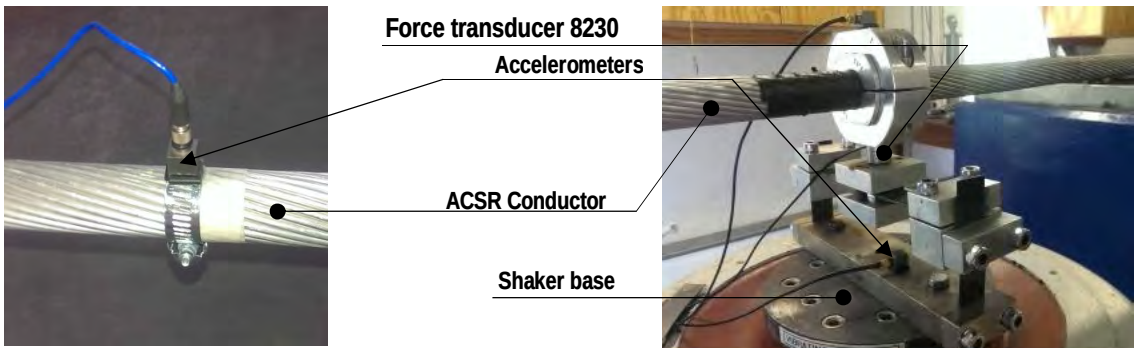

Figure 3-4: Accelerometers: on the conductor (a) and on the flexible connection (b)

3.3.1.3 Force transducer

The vibrational loads of the vibrating conductor at the suspension point (mid-span) were measured with a dynamic force transducer which is made of strain gauges (Figure

3-5). The direction of these forces may be provided by either traction or compression. An HBM S9M-10kN force transducer with 2 mV/V as the nominal sensitivity was used, and mounted to the anchor tower at the top and the middle according to the measurement desired (Figures 3-2a, 3-5, and 3-21). Its signal was collected by a MP55 Module before sending it on to the NI-DAQ module.

The MP55 module made by HBM is a carrier frequency amplified which allows connections of different transducers (force, pressure, torque and displacement). The input parameters can be assigned with a keyboard visible by a display panel. It is a PME product line (Power Monitoring Expert). The NI-DAQ (data acquisition) module is made by National Instrument (NI) and allows the connection of different sensors (force, pressure, torque and displacement) to a cDAQ module (Compact Data acquisition) which is an interface between the data acquisition system and the PC (personal computer) with programmable software (LabView).

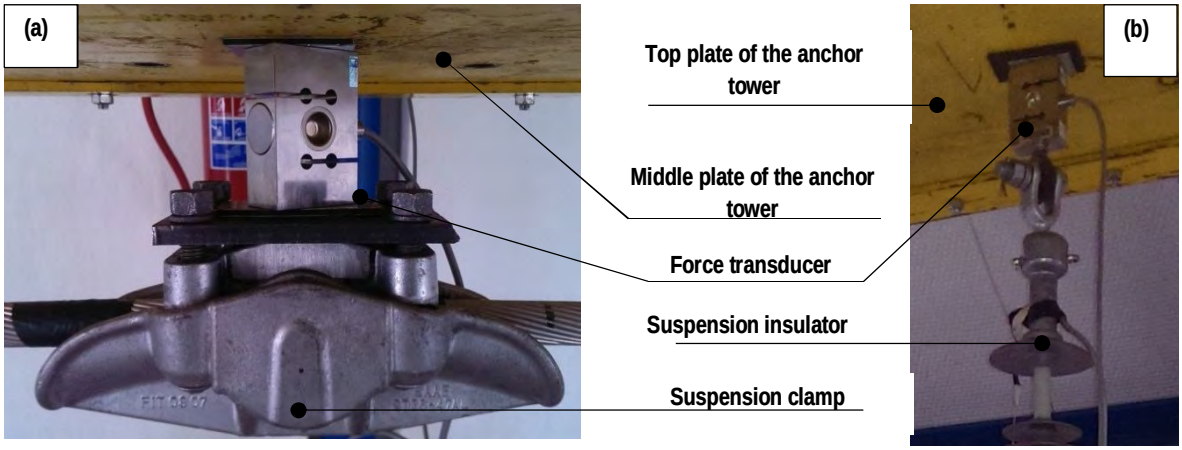

Figure 3-5: Force transducer in the blocked clamp (a) and the suspension insulator configuration (b)

3.3.1.4 Linear variable differential transformer (LVDT)

The bending amplitude measurements are usually taken in the field by vibration recorders at 89 mm from the clamp edge (CE). For this indoor vibration testing an LVDT, which operates as a linear variable differential transformer, was used to measure the peak-to-peak bending amplitude of the vibrating conductor at 89 mm on the conductor from the last point of contact between the conductor and the clamp. The LVDT HBM WA/10mm-T with a maximum displacement of 10 mm and a sensitivity of 80 mV/V was chosen. A plunger (magnetic core) provided a path for magnetic flux

linkage between the coils by moving through a bobbin. Any variation of plunger position creates a variation of flux which is then converted into voltage and interpreted in units of length (mm). This displacement transducer was mounted on a stand independently of the anchor tower or the line post tower (support). The signal of the LVDT was also connected to the MP55 (Figures 3-6. 3-21 and 3-22).

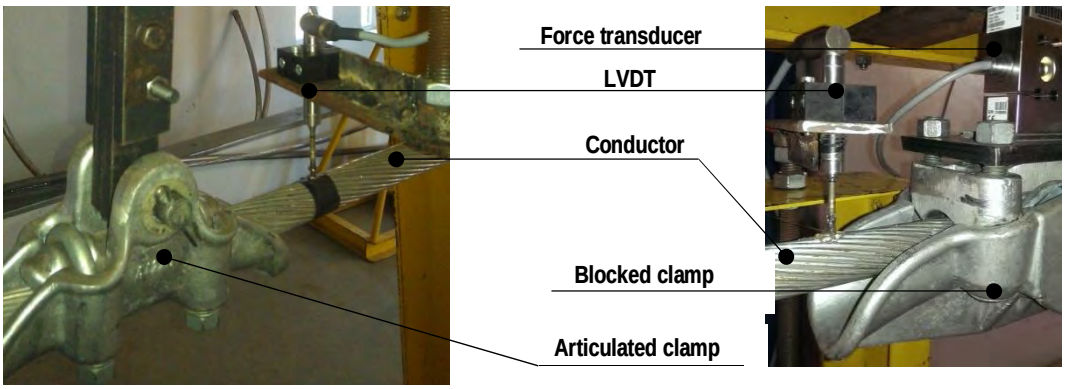

Figure 3-6: LVDT Transducer on the conductor

3.3.1.5 Strain gauges

The metallic strain gauges are fine metallic foils arranged in a grid pattern to measure the strain either statically or dynamically (Figure 3-7). The strain gauges change their electrical resistance linearly and proportionally to the force applied on the test specimen (FRP rod of the composite insulator) to which they are attached. All strain gauges used in this project have a resistance of 350 ± 5% Ω and a gauge factor of 2.07 ± 0.5 % at 24°C.

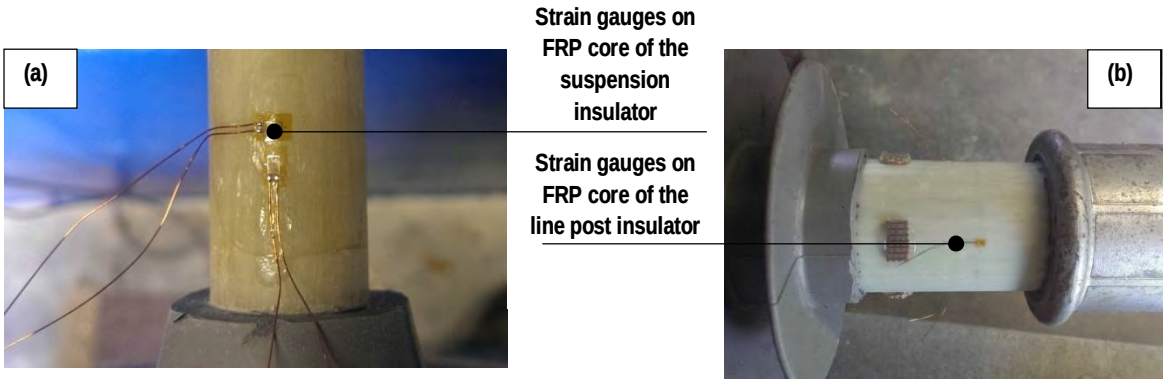

Figure 3-7: Strain gauges stuck on the FRP rod of the suspension insulator (a) and line post insulator (b)

Strains on the core of the suspension insulator were measured at three different places on the insulator (in the middle and at each end on the FRP core, and close to the end

fittings - Figure 3.14) while the bending strain of the line post insulator was measured on the FRP core at the end close to the end fittings of the insulator, using four strain gauges separated by an angle of 90 degrees (Figure 3-15). Strain gauges connected as Wheatstone bridges were necessary for measuring the small changes of resistance caused by the mechanical loads of the vibrating conductor on the composite insulators (suspension or line post) [48, 49]. The strain gauges system for the line post insulator used temperature compensation systems (dummy gauges: Figure 3-9).

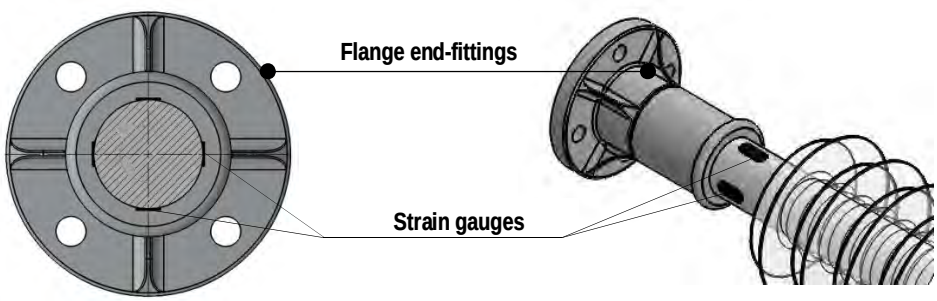

Figure 3-8: Strain gauges on the line post insulator.

Strain gauges which were attached to the FRP of the rod of suspension insulator in four half-bridge configurations, assisted in measuring the strain (Figure 3-7a and 3-14). For the line post insulator four couples of strain gauges were used (Figure 3-15). For each couple of strain gauges system: an active gauge was attached on the FRP core of the line post insulator to measure the bending stresses (Figure 3-7b and 3-8), and the other strain gauge was stuck on a non-active FRP rod (an FRP rod separated mounted – Figure 3-9). Both the active strain gauge and the non-active strain gauge were connected in the quarter-bridge configuration.

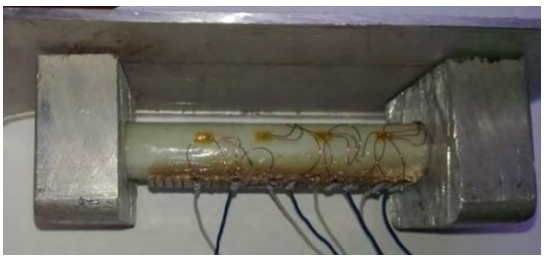

Figure 3-9: Temperature compensating gauges for the line post insulator

3.3.2 Signal conditioner, Data acquisition & Monitoring

All signals from the sensors were collected at the mid-span of the laboratory on the support tower (Figure 3-1). It was necessary to use amplifiers, data acquisition (DAQ) and suitable wiring to collect the signal, in order to avoid noise during the vibration.

The LVDT and force transducer were connected to two separate MP55 modules (carrier-frequency amplifier). These are single-channel signal conditioners (4.8 kHz carrier frequency amplifier with built-in filters between the ranges of 0.05 to 500Hz) with amplification up to 5000 to boost the signal's strength. This improved the performance and the reliability of the transducer measurements (Figure 3-10). The signals from the strain gauges and transducers (LVDT and force transducer) were directed into two data-acquisition (DAQ) modules (50 ksample/sec sampling rate and 24 bit-resolution).

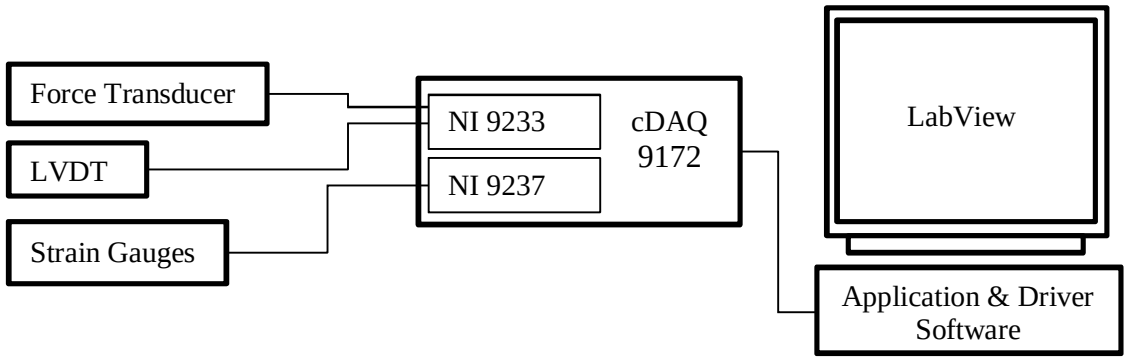

Figure 3-10: Data-acquisition scheme of the measurement

The NI 9237 (four analogue inputs), is a bridge module able to simultaneously connect via RJ-50 cable (or wires) the three (suspension insulators) or four bridge-based strain-gauges (line post insulators).The MP55 module signals (LVDT and force transducer) were transmitted through RG-058 cable (BNC coaxial cables) to the NI 9233 which is also a four-channel dynamic signal acquisition module. The two modules described previously were connected to the NI cDAQ 9172, which was connected to a PC by a USB cable. The NI-cDAQ was the interface between the computer and signals from sensors. For a better interpretation and understanding, the LabView SignalExpress software (no programming required) was used to acquire and analyse data speedily in order to control and check whether all transducers were working properly. The NI LabView system-design software provided a virtual comprehensive interface to the computer for all transducers and strain-gauge measurements. A LabView programme was designed for recording the data measurements needed, while Matlab and Excel were also used to analyse and plot the graphs.

3.3.3 Puma Spectral Dynamics

The Puma Spectral Dynamics' controller, which is a vibration and analysis system, was used during the sweep method. The accelerometers, the force transducers, and the LVDT were directly connected via RG-058 to the data-acquisition hardware of the Puma, while the Computer-Aided Test Suite performed the testing, data-analysis and production of reports.

3.3.4 LabView programme

The five signals which included the transducers and the strain-gauges of both support-configurations were collected (Table 3-1), using the cDAQ 9172 via NI 9233 and NI 9237 modules as shown in Figure 3-10. These signals were managed by a NI LabView programme which was designed and adapted according to a support configuration and mainly by the tower configuration by using three pairs of strain-gauges for the suspension insulator.

Table 3-1: Classification of five signals collected per support-configuration.

Types of support structure	**Sensors used**	**Output measurement**
Anchor tower	LDVT	Bending amplitude
	Force Transducer	Vibrational load
	Three couples of strain-gauges	Strain
Line post insulator	LDVT	Bending amplitude
	Four couples of strain-gauges	Bending strain

Both insulator-support structures used the LVDT, but the force transducer was only used on the anchor tower. The scheme of the LabView programme as shown in Figure 3-11 is created with a DAQ assistant.

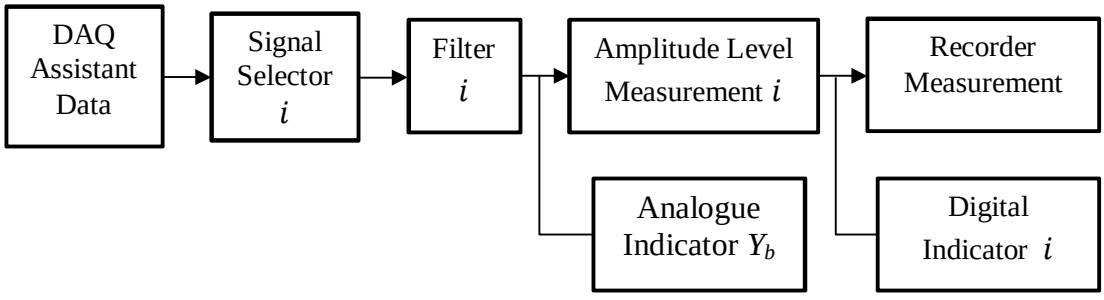

Figure 3-11: Flowchart of the data-collection with NI LabView

Five signal selectors, five filter applications, and five “amplitude-level” modules were used which allowed the choice to be made either positive or negative peak, or peak-to-peak value. All measurement data were stored using a “write-to-measurement-file” application in LabView. The behaviour of all signals could be monitored and controlled with analogue and digital indicators (Figure 3-12).

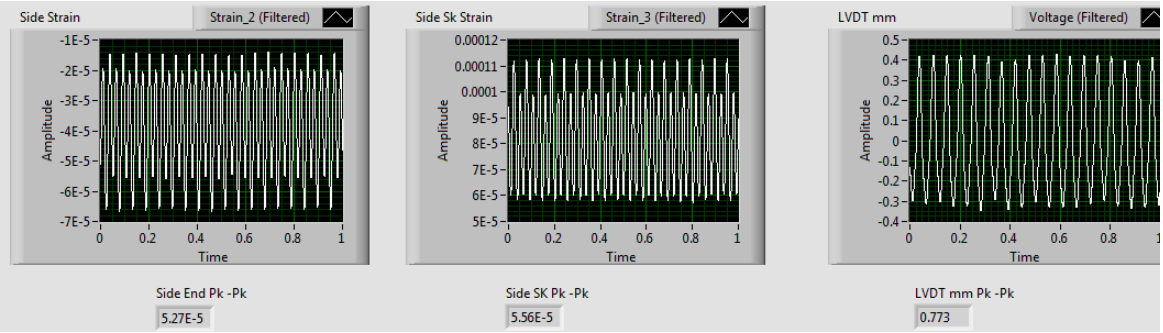

Figure 3-12: Analogue and digital indicator of the LVDT and the strain gauges

3.3.5 Material

3.3.5.1 ACSR Conductors

For better assessment of the evaluation of the mechanical loads, it was preferable to use some old conductors already used in previous tests, rather than new conductors, as the former were more flexible. Conductors are usually composed of twisted strands from different materials, meaning that conductors have a transverse section with either single or multi-layer strands (Figure 3-13). The ACSR conductors (aluminum conductor steel-reinforced) are most commonly used in South Africa.

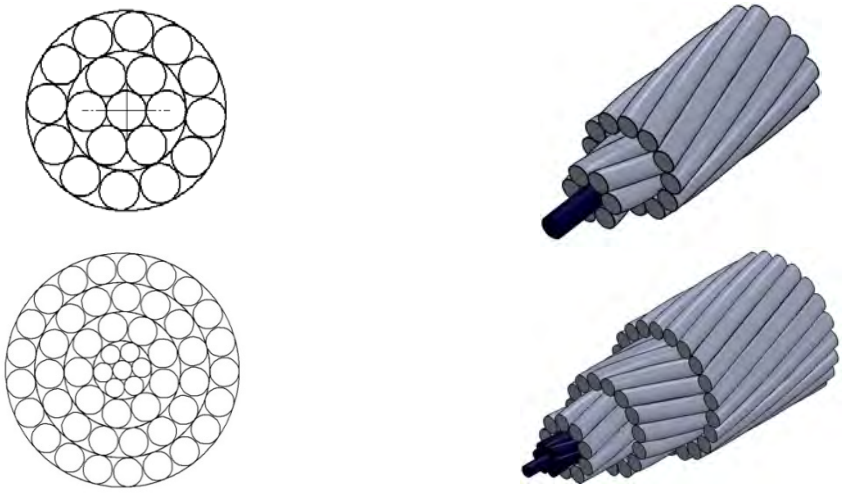

Figure 3-13: Stranding configuration of the ACSR Pelican and Tern conductors

The mechanical characteristics and the geometric configurations of the conductors used are shown in Table 3-2 and in Figure 3-13.

Table 3-2: Mechanical characteristics and cross-section of the ACSR Pelican &Tern

Mechanical characteristics		Unit	ACSR Conductor	
			Pelican	Tern
Overall Diameter (mm)		mm	20.70	27
Number of Strands	Aluminum (Al.)	-	18	45
	Steel (St.)	-	1	7
Diameter of Wire	Aluminum (Al.)	mm	4.14	3.38
	Steel (St.)	mm	4.14	2.25
Linear Mass		kg/m	0.775	1.34
Rated Tensile Strength		N	53.8	98.7
Minimum Stiffness		Nm^2	20.78	21.60

The aluminum wires of these conductors are made of type 1350 H19, while the steel wires are made of high-strength galvanised steel core. Two types of ACSR conductors were used: Pelican (18 Al. /1St.) and Tern (45Al. /7St.). This choice was motivated by the fact that these are conductors that ESKOM uses in low, medium, high, and extra-high voltage, and they are being manufactured in South Africa. Used singly or in bundles (twin, triple, quad, etc.), Tern conductors are the most commonly used conductors in South Africa. The Pelican conductor is also widely used, however, the Tern conductor covers many kilometres of transmission line in high Voltage and Extra-High Voltage (EHV) between 400 and 765 kV. This is shown in Table 3-3.

Table 3-3: Illustration of km coverage of the ASCR conductors in South Africa selected for the testing.

Conductor type	Distance (km)	Start Station	End Station	Voltage
4 Pelican	17.19	Grassridge	Poseidon	220kV
4 Pelican	115.13	Dedisa	Poseidon	400 kV
1 Tern	93.80	Aggeneis	Paulputs	220 kV
2 Tern	19.51	Durban South	Klaarwater	275 kV
3 Tern	406.80	Beta	Delphi	400 kV
3 Tern	285.05	Arnot	Maputo	400 kV
6 Tern	234.77	Mercury	Perseus	765 kV
6 Tern	429.48	Gamma	Perseus	765 kV

3.3.5.2 Suspension clamp

The suspension clamp was made of a non-magnetic mould-cast 356-T6 aluminum alloy with a 70 kN-rated tensile strength (RTS) and consisting of an upper (keeper) and lower

(body) clamp with a U-type carbon galvanised steel bolt and nut. The cotter pins are made of stainless steel. The test required two configurations of the clamp (articulated or non-articulated). In order to restrict the suspension clamp to any movement, a modification was made for this purpose. For the test, the suspension clamp, articulated or not, was directly mounted on the force transducer without an insulator, and later mounted to the suspension insulator and line post insulator (Figure 3-1, 3-5, 3-6, 3-21 & 3-22). The clamps were attached to the conductor by 50 Nm torque applied to the nuts of the U-bolts of the suspension clamp.

3.3.5.3 Composite insulator

The tests were carried out on two types of insulators (suspension and line post) which used the same basic materials. Material parameters are in Tables 3-4 and 3-5. The FRP rods of the insulator are made of the pultruded ECR-Glass Fibre and epoxy resin. The end fittings of the insulators were made of drop-forged steel according to EN ISO 1461, while the cotter pins were made of stainless steel. The FRP rod of the insulator was covered by 3 mm thickness of grey housing or sheds made of injection-moulded HTV silicone rubber with an ATH Filler. The rod resists mechanical loads, while the housing resists electrical loads.

Table 3-4: Mechanical parameters of FRP rod of composite insulators [5].

Modulus of elasticity		**Shear Modulus**		**Poisson number**	
E_L (GPA)	E_T (GPA)	G_{TT} (GPA)	G_{LT} (GPA)	V_{TT}	V_{LT}
44	10.3	4.3	5.1	0.5	0.32

Whereby :

V_{LT} Poisson number ‘‘axial-transverse’’ to the FRP rod

V_{TT} Poisson number ‘‘transverse–transverse’’ to the FRP rod

E_L Modulus of elasticity (Young’s modulus) in axial direction of the FRP rod

E_T Modulus of elasticity (Young’s modulus) in transverse direction of the FRP rod

G_{TT} Shear modulus ‘‘transverse–transverse’’ of the FRP rod

G_{LT} Shear modulus ‘‘axial-transverse’’ of the FRP rod

In this study, the composite insulators chosen are normally used on 132 kV transmission lines. The delicate operation of removing the housing and cleansing the

place designated on the composite insulator for strain measurement, was conducted carefully in order to attach the strain gauges on the core of the insulator.

Table 3-5: Strengths of the FRP Rod of the composite insulator (suspension and line post) [5]

Strength value	**(MPa)**
Longitudinal (tension)	1 038
Longitudinal (compression)	-794
Transverse (tension)	32
Transverse (compression)	-141
Longitudinal-transverse (shear)	54

a) Suspension insulator

The model of the suspension insulator is a silicone long-rod insulator HASDI 725/4500 c/w 16 mm ball & socket. The specified mechanical load (SML) is 120kN. The rating of the ball is in accordance with IEC 60120 (16), while that of the socket is IEC 60120 (16A). The diameter of the FRP rod is 16 mm and the height is 1464 mm. The diameters of the big shed are 120mm and 24, respectively, while the small-shed diameters are 90mm, and 23mm, respectively. According to the specification provided by the manufacturer the mass of the composite insulator is 5.29 kg. The mechanical and electrical rating was conducted according to IEC 61109. The strain-gauges were stuck on the core of the insulator at three different places as shown by Figure 3-14:

- at the middle of the FRP rod of the insulator and,
- at 60 mm from each end fitting.

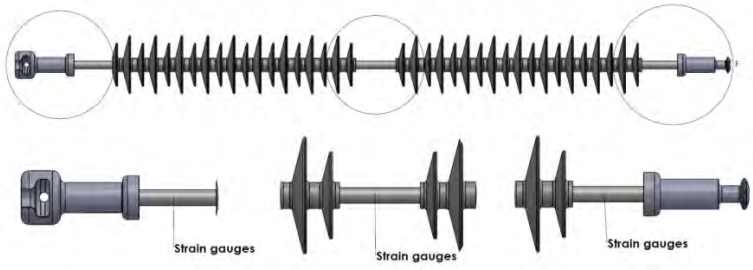

Figure 3-14: Suspension insulator

b) Line post insulator

The line post insulator “silicone station post insulator 670/4500 c/w twin 4 x Ø17.5 x 127 mm PCD flange fittings-straight” with 13.3 kN specified cantilever loads (SCL) was used (Figure 3-15).

Figure 3-15: Composite line post insulator

The overall height of the insulator including its end fittings is 1.5 m and the diameter of the FRP rod is 63.5 mm. This line post insulator has flanges as end fittings. The electrical and mechanical ratings are in accordance with IEC 61952 and 62231. Four strain-gauges were attached around the FRP rod of the insulator at 12 mm from the last point of contact between the FRP rod and the end fittings bolted to the line post support. The first two strain-gauges were placed on top and bottom of the FRP rod and they were 180 degrees apart. The last two strain-gauges separated by 180 degrees were attached on the neutral axis. Each strain-gauge attached on the FRP rod of the line post insulator was connected to a dummy gauge which was attached to non-active FRP rod apart from the insulator tested (Figure 3-7a and 3-8).

3.3.6 Other test equipment

3.3.6.1 Rigid block (so called square-faced clamp)

The rigid clamp at each end of the Tern conductor permitted the attaching of the conductor on the loading arm and the end-termination block (Figure 3-1 and 3-16). Rigid clamps were bolted in the tee (T) slots of the metal plate of the concrete block. These were rigidly maintained in compression to the conductor at the static tension chosen (Table 3-5) after tensioning the conductor by the arm loaded with dead weights. The Pelican conductors at each end-span used pistol grips as connectors between the end-termination block and the loading arm, owing to its small overall diameter. The Tern conductors used dead-end clamps crimped at each end of the span (See Figure 3-16b and 3-20b).

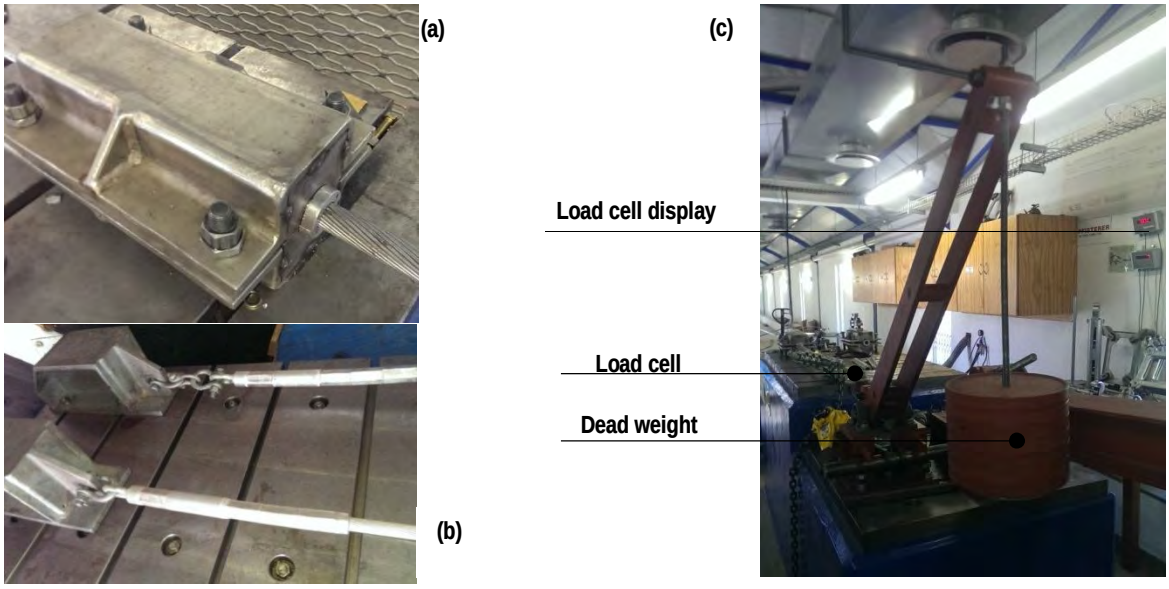

Figure 3-16: Rigid block (a), End-termination block (b) and the loading arm (c)

3.3.6.2 Attachment fittings

The end fittings of the suspension insulator were ball and socket typeand this required the use of a socket tongue to mount the suspension clamp on the insulator. A ball clevis was used to attach the suspension insulator to the force transducer fixed on the anchor tower (Figure 3-17a & 3-17 b).

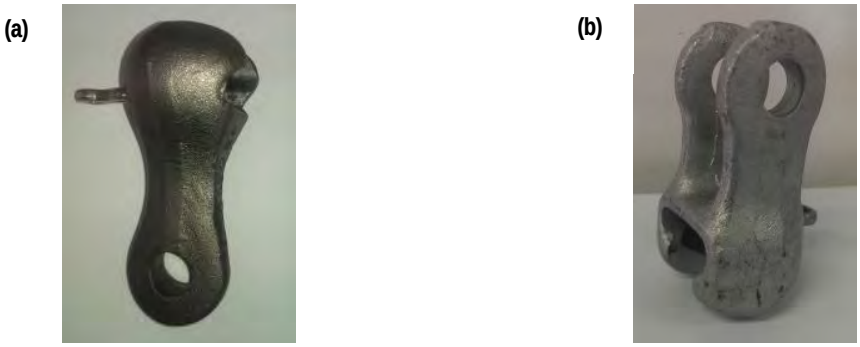

Figure 3-17: Suspension insulator connectors : socket tongue (a) & ball clevis (b)

3.4 Method of testing

3.4.1 Experimental methodology

The standard method called bending amplitude method was used. This method was established by the IEEE Transmission and Distribution Committee, motivated by the Poffenberger-Swart formula, and validated by many authors. This method is considered suitable for assessing conductor vibration**.** Adopted as a standard procedure by IEEE

standards, CIGRE and EPRI, this method assumes direct measurements of the bending amplitude y_b preferably at 89 mm of the last point of contact (LPC) of the suspension clamp [30, 32, 33, 50-56]. This had led to an intense investigation of the stress/strain on the conductor close to the suspension clamp (Figure 1-1, where the first signs of fatigue failures most often occurred**.** The bending amplitude was valuable in establishing a relationship with the bending dynamic strain, and subsequently with the dynamic stress and the fatigue of the power-line conductors. Thus, in this project, the mechanical loads of the vibrating conductor have been firstly evaluated as a function of the bending amplitude and subsequently the mechanical influences of those loads on the tensile strain of the suspension insulator or the bending strain of the line post insulator were assessed.

3.4.2 Test method

As recommended by IEEE, EPRI, IEC and other standard organisations, CIGRE has stipulated the methods of assessment of the vibration conductors [1, 33, 50, 57]. Table 3-6 indicates the method of testing used.

Table 3-6: Method of testing, the instrumentation and DAQ used.

Testing method	**Software used**	**DAQ**	**Sensors used**	**Output measurement**
Swept frequency-shaker-excitation	Puma Spectral Dynamics	Puma Controller	LVDT	Bending amplitude
			Force transducer	Vibrational load
			Accelerometers	Velocity/Acceleration
Steady frequency-shaker-excitation	Labview Programme	NI 9233 NI 9237 cDAQ 9172	LVDT	Bending amplitude
			Force transducer	Vibrational load
			Strain gauges	Strain

These methods provide a better understanding of the dynamic behaviour of the conductors. At VRTC, two types of testing (free- and forced-vibration testing) are conducted with the purpose of giving experimental information on the dynamic characteristics of overhead-line conductors

3.4.2.1 Free-vibration testing

The free-vibration testing evaluates the damping characteristics of the conductor which is a natural response of the conductor. The conductor reacts to that impact or displacement, and the amplitude of vibration decays with time as a result of conductor self-damping [1].

3.4.2.2 Forced-vibration testing

This method requires a shaker which causes a constant and repetitive forced movement to the conductor. This could force the conductor to vibrate at the frequency of the excitation. As the conductor is excited at one specific point, it is assumed that the oscillation of the conductor caused by the effective loading input of the conductor is concentrated on the link point (shaker or exciter/conductor). Two methods are used in the forced vibration: the Swept frequency-shaker-excitation and the Steady frequency-shaker-excitation methods. Importance is given to the linking device between the shaker and the line. (Figure 3-18).

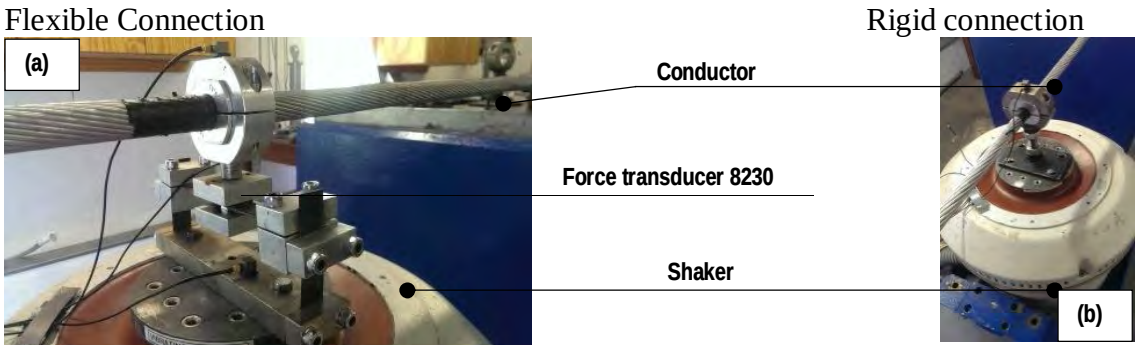

Figure 3-18: Flexible and rigid connection : Accelerometers on top and a force transducer is inserted to the flexible connection

An elastic connection is used for the sweep method while a rigid connection is using for constant vibration at certain amplitude at the resonance frequency.

d) Swept frequency-shaker-excitation method

This method is well known as a search method for the resonance frequency. It may also be called the “swept sine” test. The response of the excited conductor is a sine wave whose frequency changes over time. The amplitude of the signal measured by an accelerometer may be acceleration, velocity, or displacement. The flexible connection

was equipped with a quartz miniature force transducer (Brüel & Kjær, 8230) which measured the exchanged energy between the shaker and the conductor. This sweep method was conducted only with the Puma system (Figure 3-18a).

e) Steady frequency-shaker-excitation method

Here, the power method was used, in which the conductor is excited with constant frequencies. The conductor was forced into resonance by using one of its natural frequencies. These frequencies were kept in the Aeolian vibration range, i.e. matching the Strouhal frequency. Measurements were taken at frequencies close to self-excited frequencies (resonance) of the conductor. This method used a function generator (Agilent 3322A) and the LabView programme (Figure 3-18b). The function generator was used to control the bending amplitude close to the suspension point as described previously (at the mid-span) by modifying the displacement of the shaker.

3.4.3 Test procedure

To conduct a full-scale mechanical load (Figure 3-19**)**,strain or bending strain test on Pelican and Tern conductors, several tests were conducted according to the following (Figures 3-5, 3-6, 3-21 and 3-22):

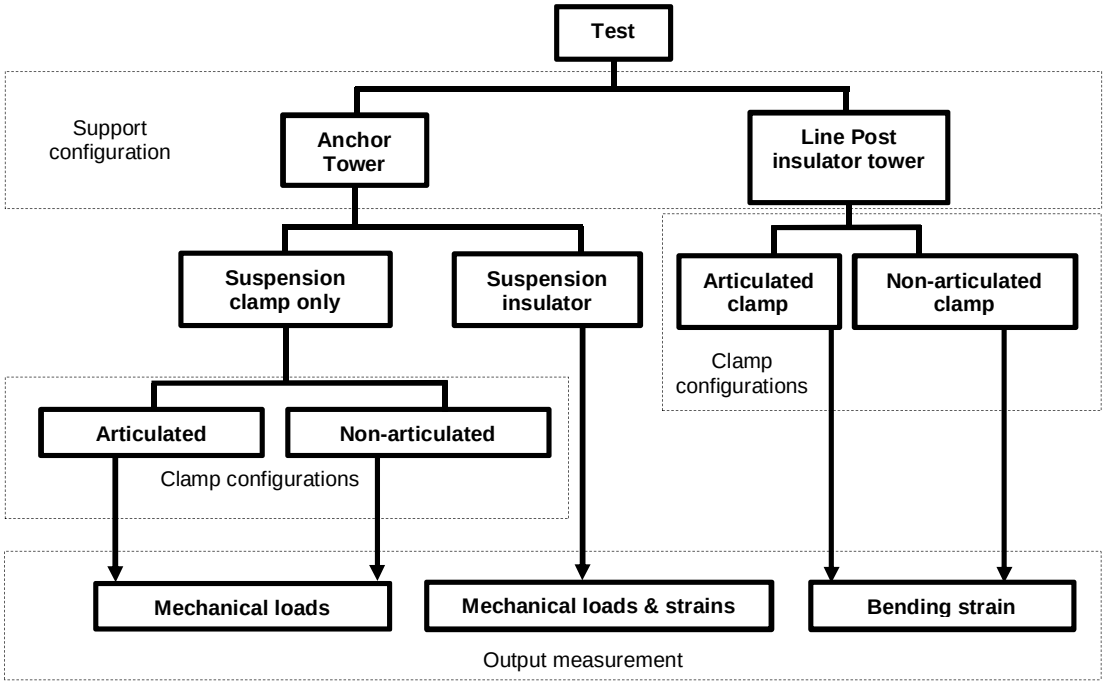

Figure 3-19: Flowchart of the testing

- the static tension of the conductor (Table 3-5);
- the type of support tower at the mid-span tower (suspension and line post) (Figures 3-2, 3-21, 3-22); and
- the type of clamp configurations (non-articulated or articulated shown in Figures 3-5, 3-6, 3-22a and 3-22b).

It took a relatively long time to obtain conclusive results from all tests. Below is the flowchart of the testing at all four different static tensions (% UTS):

3.4.3.1 Installation of the conductors and insulators

The two ACSR conductors (Pelican and Tern) tested were pre-tensioned up to 35% of UTS before being relaxed for three days before the tests. As described previously, the pistol-grip strain-clamp was used on the Pelican conductor for the attachment to the dead-termination block and the loading arm.

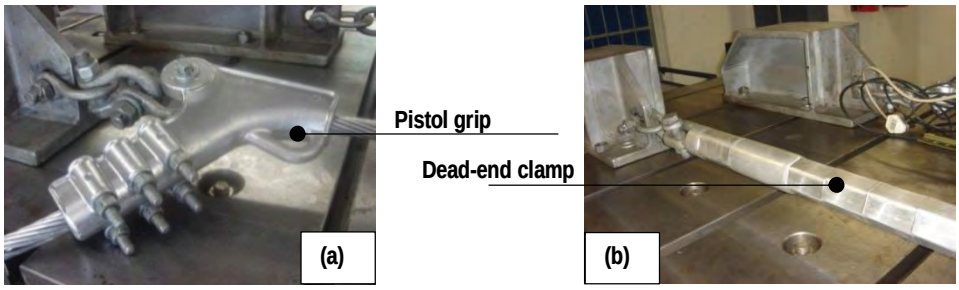

Figure 3-20: End-termination block with pistol-grip strain clamp (a) of the Pelican and the dead-end clamp of the Tern (b)

3.4.3.2 Choice of the static tension of the conductor

Four levels of static tension from 15% of UTS with a 5% increment were applied to conductors (See Table 3-5). The static tension of 15% UTS was added to the range that is commonly used by Eskom in order to further investigate the influence of this tension of the conductor. The choice of these static tensions was motivated by everyday stress (EDS) used by ESKOM in transmission lines recommended by a procedure named allowable stress design (ASD). The following formula is recommended by ESKOM for the choice of the static loading (%UTS) [54]:

$$C = \frac{T}{w} \tag{3.1}$$

where: T (N) represents the everyday tension, while W (N/m) is the conductor weight per unit length, C (m) referring to the catenary equation of the conductor [58]. ESKOM strongly recommends a maximum value of 1800m which results to 26.50 % UTS for ACSR Pelican, and 24.40 % UTS for ACSR Tern.

Table 3-7: Static tensions (kN) of the conductors used in relation to the UTS

ACSR Conductor	**Ultimate Tensile Strength (UTS) (%)**			
	15	20	25	30
Pelican	8.010	10.500	14.450	16.610
Tern	18.405	19.740	24.675	29.610

3.4.3.3 Support configurations

The anchor tower at mid-span allowed the possibility of having different clamp configurations (Figure 3-21). This was achieved by a movable fixation system which allowed maximum flexibility either to block or hold the clamp to/or by the force transducer. The following measurements were taken from the anchor tower:

- Measurement of mechanical loads of the vibrating conductor with an articulated and/or a non-articulated clamp mounted on the tower via a force transducer mounted under the middle plate of the anchor tower.
- Measurement of mechanical loads of the vibrating conductors and their effects on the suspension insulator in the strains were collected. The suspension insulator was mounted to the anchor tower via the force transducer. The middle plate was removed.

For the line post insulator mounted in cantilever, bending strains were only collected while the conductor was vibrating (Figure 3-22). Both tower set-ups used the LVDT (See Figure 3-21 & 3-22).

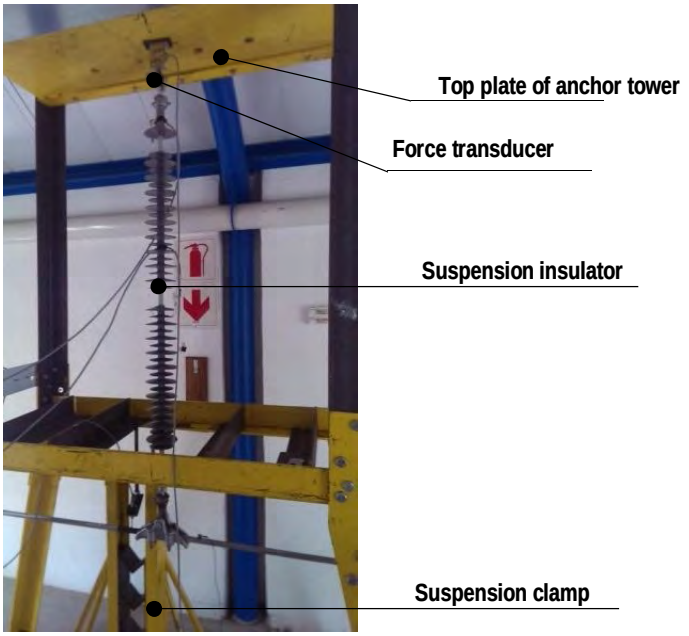

Figure 3-21: Set-up of the anchor tower with composite insulator and suspension clamp (articulated and non-articulated)

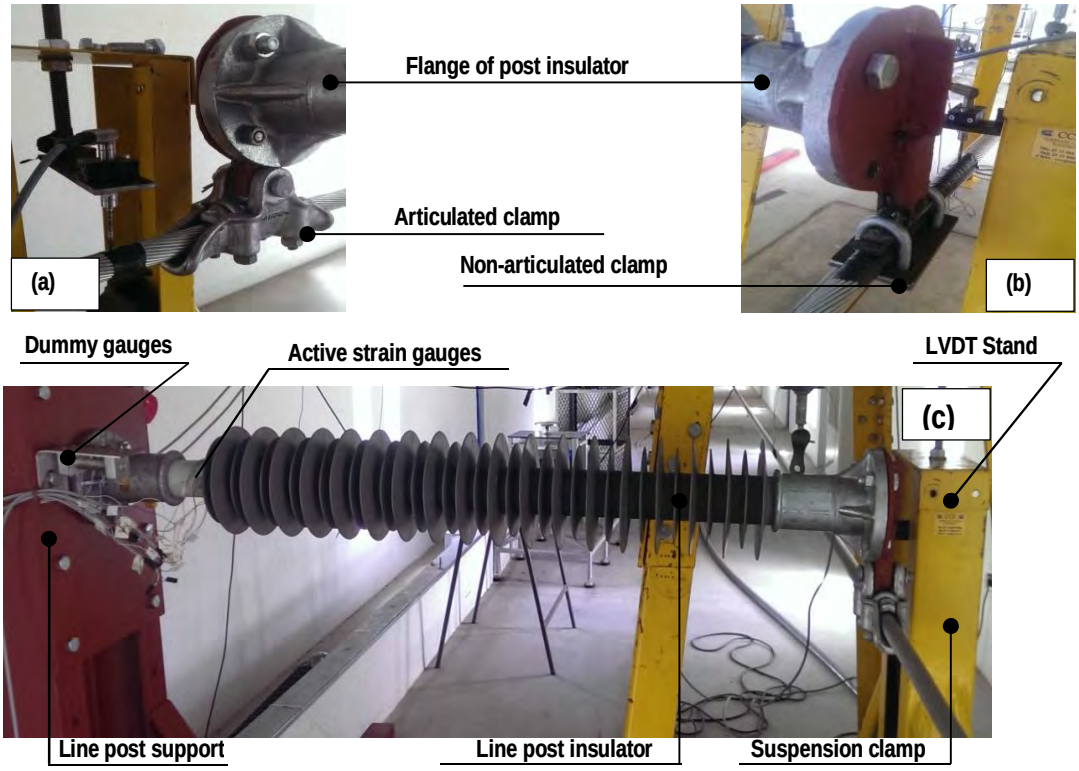

Figure 3-22: Line post insulator tower and the insulator with two clamp configurations.

3.4.3.4 Mechanical loads and strain measurement

As explained previously, the mechanical loads of the conductor, the strain of the suspended insulator, and the bending strain of the line post insulator were measured as

functions of the bending amplitude of the LVDT placed on the conductors at 89 mm away from the last point of contact of the suspension clamp.

a. Choice of the natural frequency

The sweep method (performed at 0.3 m/s), which is an experimental searching resonance frequencies method using an elastic connection, was applied, in order to find and select the stable measurement frequencies near natural frequencies of the conductor which would be used during the steady-frequency method deploying a rigid connection. Thus, this was achieved for each conductor, each static tension, each clamp configuration and for each mid-span support. In accordance with the Strouhal formula, the frequency range was chosen between two limits. The experimental resonance frequencies found were checked by the VIP software, which is a resonance calculator based on the conductor parameters, i.e. linear mass, static tension, and the diameters. Table 3-6 shows the frequency range used for both conductors.

Table 3-8: Frequency range of conductors tested during the sweep method

ACSR Conductor	Frequency (Hz)	
	Minimum	Maximum
Pelican	5	70
Tern	5	50

b. Choice of bending amplitude

The bending amplitude method was used according to the IEEE and IEC standards and CIGRE recommendations [1]**.** The bending amplitude measurement of the conductors measured by the LVDT was taken at 89 mm from the last point of contact (LPC) of the suspension clamp with the conductor (Figure 3-23).

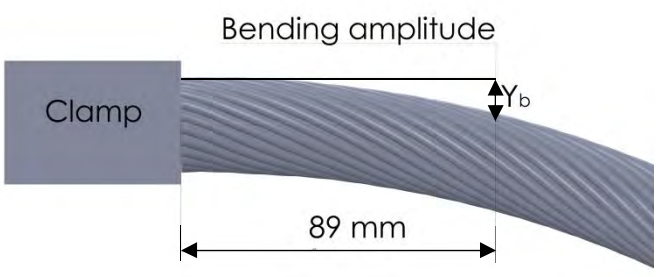

Figure 3-23: Bending Amplitude method

Thus, a range of acceptable limits between 0.1mm and 1.0 mm constant peak-to-peak bending amplitudes was chosen, while the conductor was vibrating at steady frequency.

3.4.4 Static measurement

The static measurements were performed mainly in order to:

- Calibrate the equipment, transducers, and the strain-gauges used during the dynamic measurement. Thus, referring to their specifications, error measurements could be estimated.
- Check and evaluate the bending amplitude and mechanical loads of the conductor. This could further be compared with the dynamic measurement.
- Evaluate the mechanical loads acting on the line post insulator by its bending strain, it being mounted in cantilever and not allowing any direct measurement of the dynamic loads created by the vibrating conductor.

Briefly, the static measurement was compared with the dynamic measurement by verifying the precision of the instruments used (sensors).

3.4.5 Dynamic measurement analysis

All measurements were conducted as functions of the bending amplitude, and were determined by peak-to-peak amplitude, except for the measurement achieved with the sweep method. The peak-to-peak amplitude comprises the peak positive and the peak negative values. This may be interpreted by the motion of the conductor at the suspension point where the forces or loads were acting in compression and traction. As shown in Figure 3-13, all the measurement samples were taken as a function of time (three times 60 seconds) at well-specified peak-to-peak bending amplitude of the vibrating conductor at the suspension point. This was directly obtained by Amplitude Level Measurement application of the LabView programme as described previously (Figure 3-12) when the bending amplitude curve as a function of time was a sinusoidal shape function.

$$pp_{mean} = \frac{p_{max} + p_{min}}{2} \tag{3.2}$$

where pp_{mean} is the peak-to-peak average value, and p_{max} and p_{min} *are* respectively, the maximum and the minimum values measured.

Theoretically, the p_{max} and p_{min} have to be equal which could be verified by these experiences. This shows that there is always a minor difference which may be attributed to the bending stiffness of the conductor.

3.4.5.1 Vibrational loads

As detailed previously, the force transducer had measured peak-to-peak vibrational loads *v* acting on the suspension point, which is composed of the assembly of clamp (articulated or non-articulated) and force transducer, or clamp, suspension insulator and force transducer. At different levels of tension of the vibrating conductor (% UTS), and as a function of the bending amplitude at 89 mm away of the conductor, the loads were recorded.

$$\bar{v} = \frac{\sum_{i=1}^{n} v_i}{n} \tag{3.3}$$

3.4.5.2 Strain measurement

The peak-to-peak strain $\bar{\varepsilon}$ or bending strain $\overline{\varepsilon_b}$ measurement concerned only the FRP rod of the composite insulator either in suspension or in cantilever position, and the strain measurements as the vibrational loads were measured in peak-to-peak.

$$\bar{\varepsilon} = \frac{\sum_{i=1}^{n} \varepsilon_i}{n} \tag{3.4}$$

$$\overline{\varepsilon_b} = \frac{\sum_{i=1}^{n} \varepsilon_{b\,i}}{n} \tag{3.5}$$

where n represents the number of peak-to-peak strain observations, the i^{th} individual strain or loads recorded by the unit of time.

3.5 Summary

The VRTC has been used as an indoor laboratory facility for the tests. The bending amplitude procedure was used for the measurement of the dynamic loads of the vibrating conductor and its influences on the strain of composite insulators (suspension or line post) mounted on a support configuration placed at mid-span. Two types of ACSR conductors have been tested at four different static tensions (% UTS). A force transducer mounted to the anchor tower was used to measure the mechanical loads, while an LVDT placed at 89 mm from the last point of contact (LPC) of the suspension clamp measured the bending amplitude. Strain gauges applied on the FRP of the rod measured the strains. All sensor signals were connected to a comprehensive data-

logging system, mainly from the NI or Puma control system. The Puma software was used during the swept frequency-shaker-excitation method while the LabView software was used during the steady frequency-shaker-excitation method. Thus, the dynamic loads of the vibrating conductors and its influences on the strain of the suspension insulator or the bending strain of the line post insulator have been collected. In the next chapter, those results and their analysis will be presented and discussed.

CHAPTER 4
EXPERIMENTAL RESULTS & DISCUSSION

4.1 Introduction

This chapter outlines the experimental findings of the testing procedures used in this research. All dynamic loads or strain measurements collected were functions of the alternating peak-to-peak bending amplitude of the conductor at 89 mm of the last point of contact (LPC) between the conductor and the clamp [1]. For each support configuration (suspension or cantilever), the tests were performed at four static tensions (% UTS) which using sweep and steady frequency excitation methods. The steady frequency method was based on the swept frequency method which provided peak loads and bending amplitude values as functions of the driven frequency of the shaker. Thus, the graphs of loads of the conductors and the strains of the composite insulators were plotted for all support configurations and tensions (Figures 3-6, 3-21 and 3-22). The following results have been considered:

- Swept frequency results provided the peak of both vibrational loads and their bending amplitudes;
- Vibrational loads generated by the vibrating conductors on the clamp (blocked and articulated);
- Vibrational loads generated by the vibrating conductor on the suspension insulator, and the corresponding axial strain on the surface of the FRP rod of the suspension insulator; and
- Bending strains of the FRP rod of the line post insulator generated by the vibration of the conductor.

Owing to the large number of tests and data (accelerations, velocity, displacement, and frequency) of the vibrating conductor, only the 20% UTS of ACSR Pelican and 25% UTS of ACSR Tern conductors will be presented here, referring to the Eskom C value as explained in Section 3.4.3 [54].

4.2 Swept frequency results

The sweep method has given an overview of the relationship between vibrational loads of the overhead line conductors and their bending amplitude at 89 mm from the last point of contact (LPC) between the conductor and the clamp at the suspension support placed at mid-span. The blocked clamp configuration was considered the reference measurement, this method is detailed in IEEE committee report [33]. These tests were conducted with the Puma system, which used the frequency and time as input parameters (Section 3.3.3).

4.2.1 ACSR Pelican conductor

On the basis of the sweep frequency results at different static tensions on levels (15, 20, 25 and 30% UTS) of the Pelican conductor, the zero-to-peak values of vibrational loads and bending amplitudes are shown as functions of the driving frequency of the shaker. All clamp configuration results are represented in Figures 4-1 to 4-3. This shows a good correlation between the mechanical loads and the bending amplitudes generated by the Pelican conductor in the 5 to 70 Hz range frequency at all four static tensions (% UTS). The difference between these various configurations was the magnitude of the peak value of the dynamic loads and the bending amplitudes.

The graph 4-1 shows the overall trend of the loads and bending amplitudes. It is clear that higher vibrational loads and the bending amplitudes of the Pelican conductor were located between 7 and 10 Hz. From 10 Hz the peak value of both (loads and bending amplitudes) decreased fairly rapidly till 16 Hz and then increased slightly. At ± 21 Hz another peak value was reached, before decreasing at 32 Hz, thereafter dropping constantly to the lowest magnitude. The same behaviour of the Pelican swept results was almost identically evident at 15, 20 and 30% UTS using the blocked clamp. The difference detected was the magnitude of those both parameters (the bending amplitude and vibrational loads of the conductors). The difference detected was the magnitude of those both parameters. Higher vibrational loads were found at 30% UTS .When the frequency was lower than 10 Hz its corresponding bending amplitude reached its peak value around 17Hz.

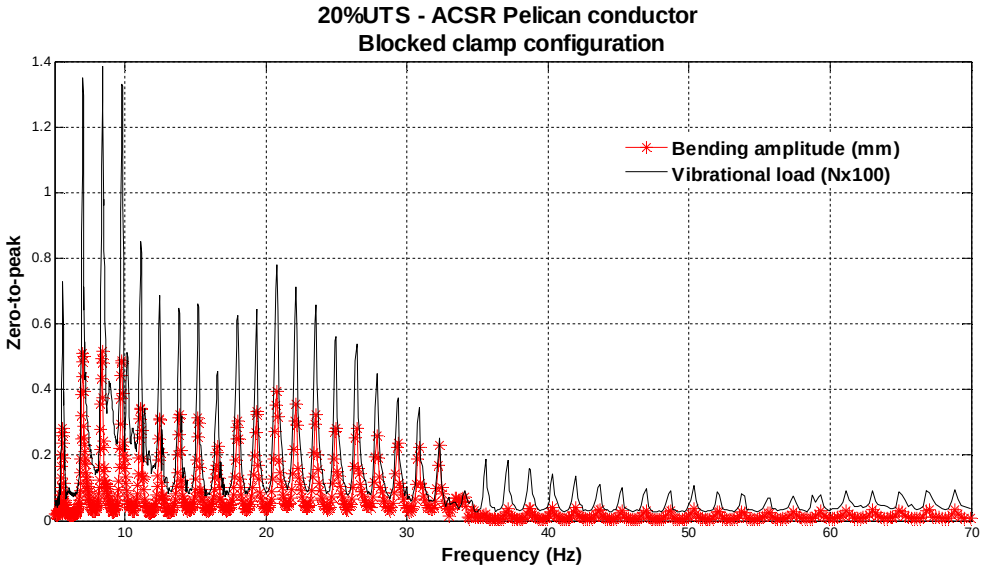

Figure 4-1: Mechanical loads and bending amplitudes vs. frequency at 20% UTS for the ACSR Pelican conductor with the blocked clamp

As shown in Figure 4-2, for all four static tensions of the ACSR Pelican conductor tested with an articulated clamp, the frequency dropped at 40 Hz and the bending amplitudes and the vibrational loads were not in perfect correlation, such as for the blocked clamp configuration. This means that the higher bending amplitudes may or may not correspond to higher vibrational loads.

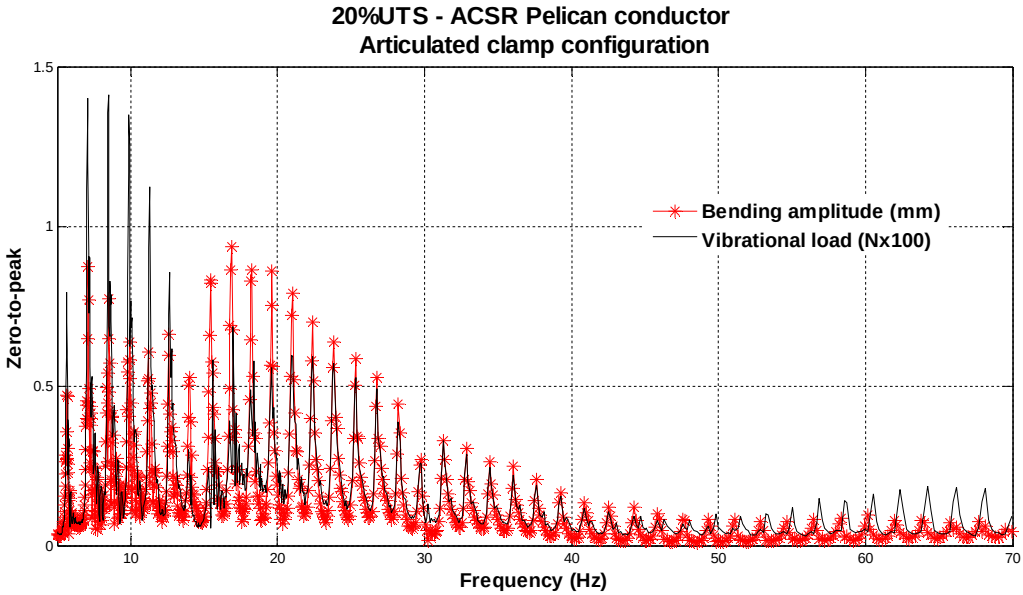

Figure 4-2: Mechanical loads and bending amplitudes vs. frequency at 20% UTS for the ACSR Pelican conductor with the articulated clamp

Figure 4-3 presents a quite different case from the previous clamp configurations, the suspension insulator being used. As there was not any movement restriction of the clamp, the bending amplitude was greater compared with its vibrational loads produced at low static tension of the ACSR Pelican conductor (15% UTS). The bending amplitude then gradually decreased over the swept frequency range. Mostly, the drop in frequency after which the bending amplitude and the loads were steadily reduced was noticed at around 41 Hz. This was so even when the loads and the bending amplitudes rose again around 48 Hz. The highest vibrational loads were reached around 6 Hz at 15% UTS. For the other three tensions (20, 25 and 30%), their loads were higher at the frequency of nearly 8 Hz; their bending amplitudes reaching the peak value at 17 Hz.

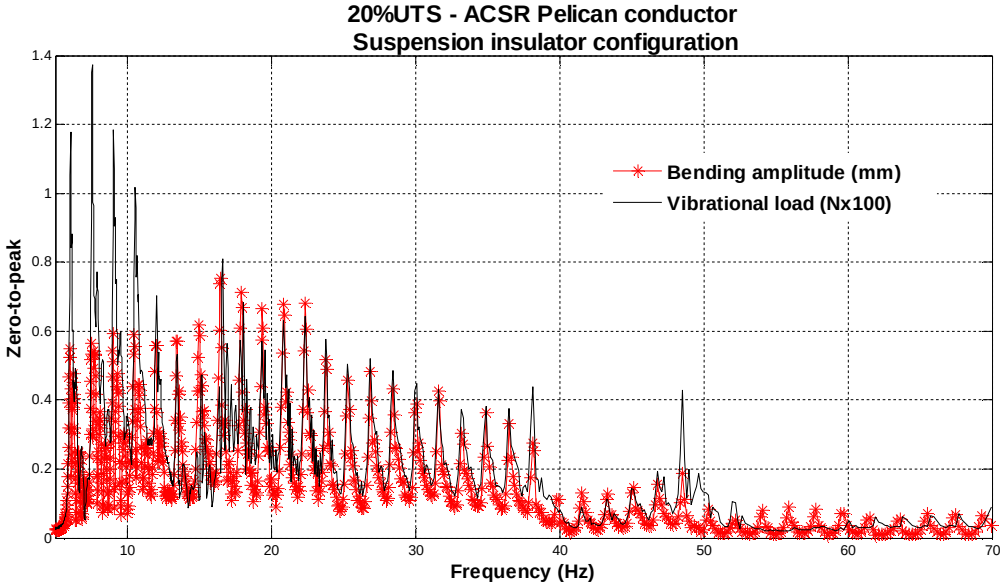

Figure 4-3: Mechanical loads and bending amplitudes vs. frequency at 20% UTS for the ACSR Pelican conductor with the suspension insulator

4.2.2 ASCR Tern conductor

The graphs of the Tern conductor presented identical mechanical behaviour to the ACSR Pelican with the swept frequency method. Because of the higher weight of the ACSR Tern conductor compared with the Pelican conductor, the Tern conductor showed the greater magnitude of mechanical loads (Table 3-2). For the blocked clamp, the swept results showed that the drop frequency for all tensions was nearly at 36 Hz. The peak values of the vibrational loads and the bending amplitudes were reached at the frequency close to 10 Hz for 15% UTS. The peak frequency loads decreased gradually from 10 Hz, while the tension was increased by a 5% UTS increment (Figure 4-4) by

considering all frequency scan of different tensions of the conductors used for the tests. (Table 3-7).

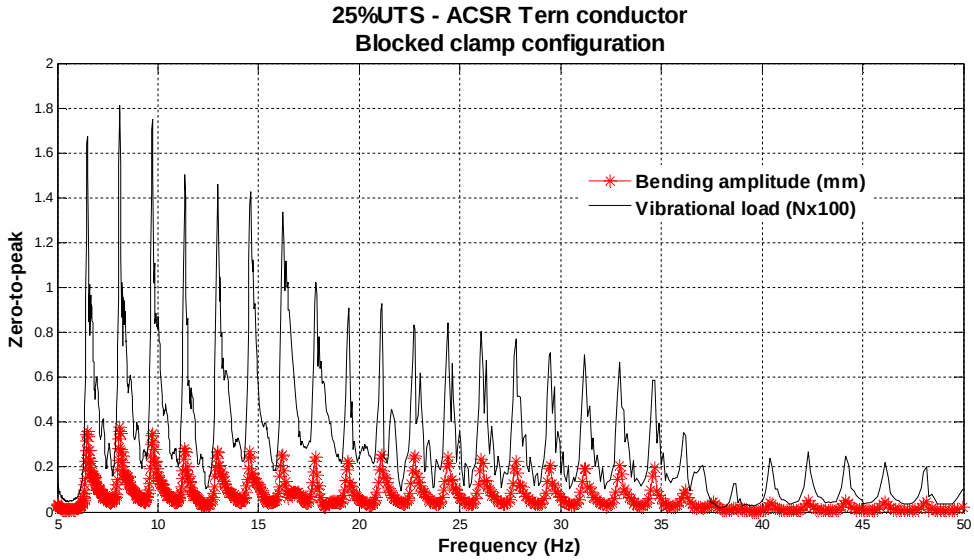

Figure 4-4: Mechanical loads and bending amplitudes vs. frequency at 25% UTS for the ACSR Tern conductor with the blocked clamp

For the articulated clamp configuration (Figure 4-5), the vibrational loads were higher at low frequency.

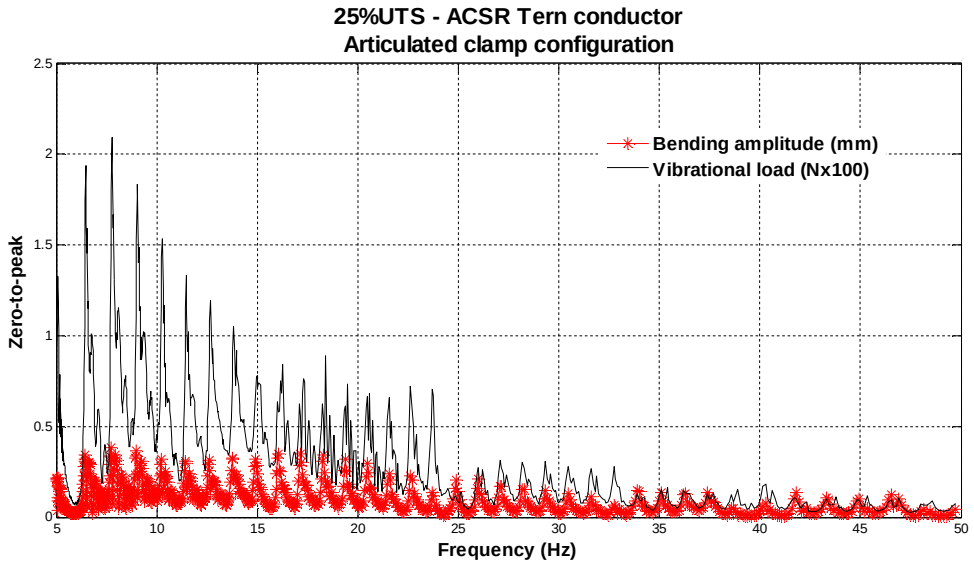

Figure 4-5: Mechanical loads and bending amplitudes vs. frequency at 25% UTS for the ACSR Tern conductor with the articulated clamp

The drop frequency changed according to the static tension of the conductor, that is, 35 Hz for 15% UTS, while for 20, 25 and 30% UTS was around 24Hz.

The highest peak value of the bending amplitude decreased continuously after reaching peak value at nearly 7 Hz for 15% UTS.

Figure 4-6 shows the influence of the suspension insulator on its mechanical behaviour using the ACSR Tern conductor being identical to the tension of the conductor tested previously for the ACSR Pelican conductor and ACSR Pelican. However, this particular behaviour has been noticed at 20, 25, and 30% UTS at which the peak value of the vibrational loads was almost constant in the frequency range of 20 to 40 Hz before dropping down at 40 Hz.

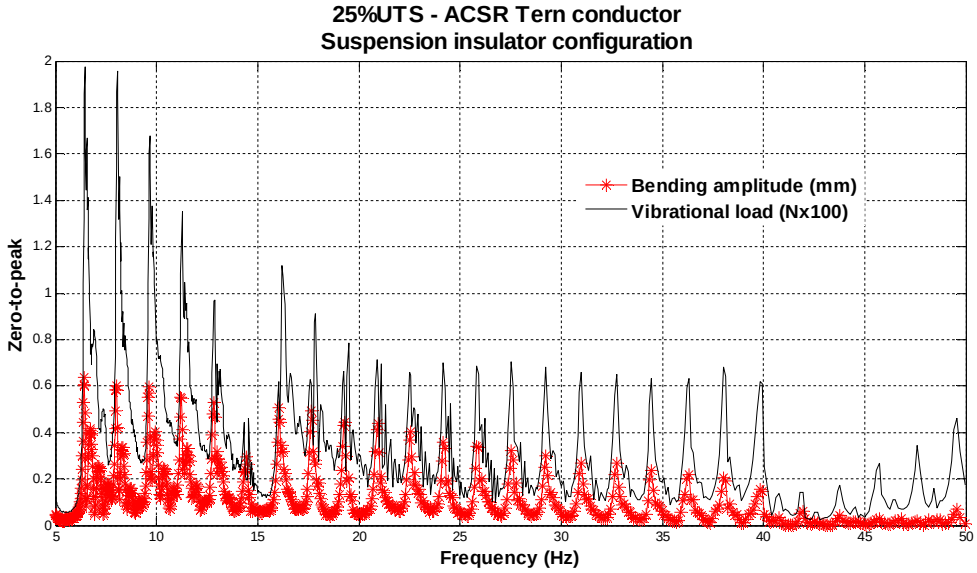

Figure 4-6: Mechanical loads and bending amplitudes vs. frequency at 25% UTS for the ACSR Tern conductor with the suspension clamp

4.3 Steady frequency results

The steady frequency measurements were under 20 Hz and mostly around 9 Hz and 15 Hz. The averages of the vibrational loads were found for each static tension used at two different frequencies. The peak value of the vibrational loads from the conductor vibration line was sinusoidal with constant amplitude [19]. It has been observed that the conductor vibrations were pure sinusoidal waves at resonance frequencies.

4.3.1 Dynamic loads of ACSR Pelican conductor

The vibrational loads versus the bending amplitude results of various clamp configurations plotted, presented similar characteristics at different tensions (Figures 3-6, 3-21 and 3-22). The vibrational loads generated by the vibrating conductor at the

clamp configuration showed that, generally, the blocked clamp configuration loads were greater than the articulated clamp and suspension insulator configuration (Figure 4-7 to 4-9). As described in section (3.4.2), the alternating peak-to-peak bending amplitude range used was 0.1 to 1.0 mm. A linear regression of loads could be observed in both conductors.

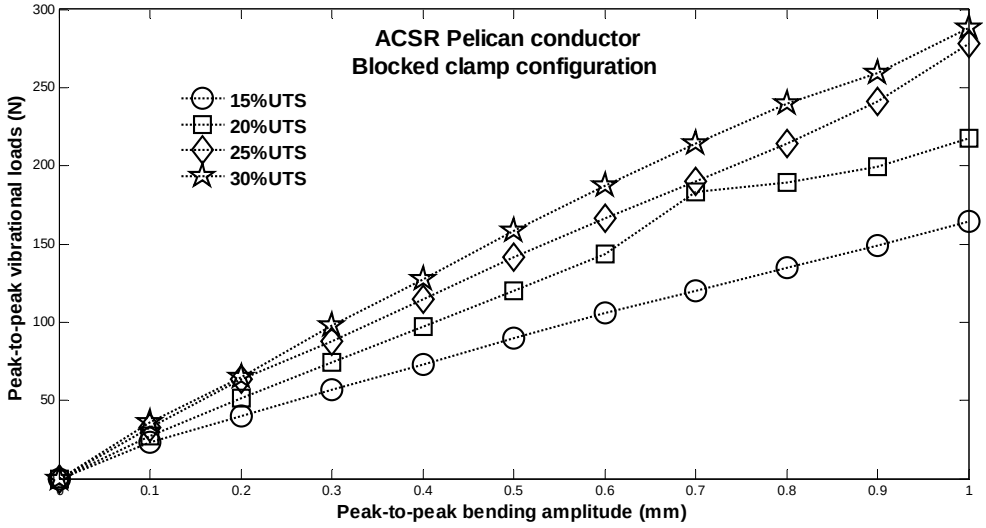

Figure 4-7: ACSR Pelican conductor held by the blocked clamp: Bending amplitudes vs. vibrational loads

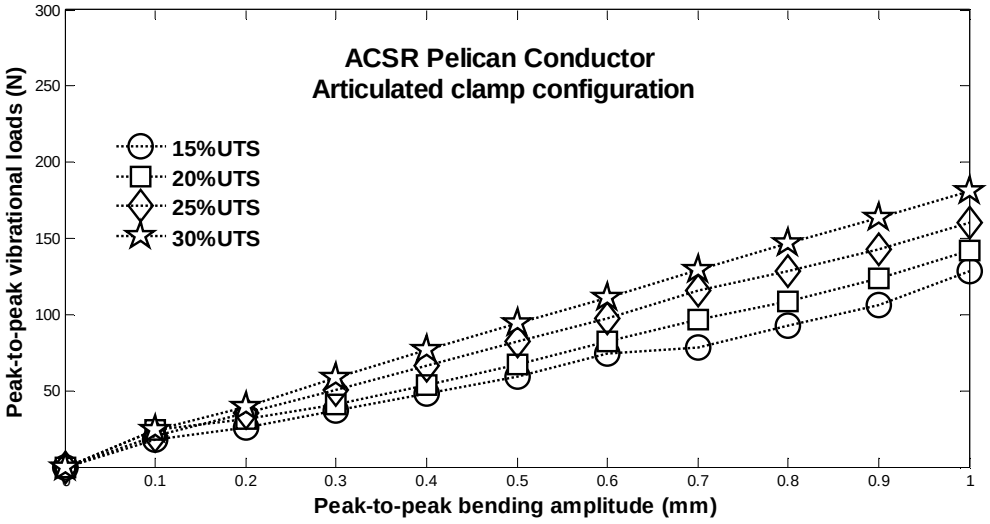

Figure 4-8: ACSR Pelican conductor held by the articulated clamp: Bending amplitudes vs. vibrational loads

These have been noticed for both ACSR conductors, i.e the Pelican and Tern conductors. For the same bending amplitude, the influence of the static tensions has shown that at higher tensions, the loads were higher than using the lower static tensions.

At 1.0 mm peak-to-peak, the blocked clamp configuration yielded nearly 288 N, while the conductor was tensioned at 16.610 kN (Table 3-7). At the same tension, the articulated clamp and insulator configuration yielded almost 182 N (Table 4-2 and 4-3).

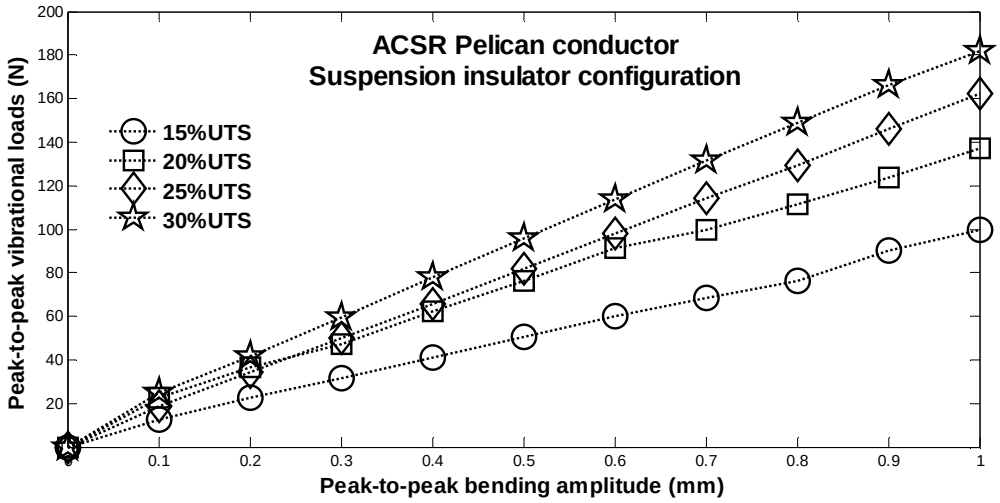

Figure 4-9: ACSR Pelican conductor held by the suspension insulator: bending amplitudes vs. vibrational loads

In conclusion, it has been observed, that that the vibrational loads of the vibrating Pelican conductor are roughly linear for all clamp configurations and for all static tensions (15, 20, 25 and 30% UTS). The highest vibrational loads were detected for blocked clamps at 30% UTS (Table 4-1).

4.3.2 Dynamic loads of ASCR Tern conductor

Owing to its mechanical properties, mostly because of its weight of 1.34 kg/m, the ACSR Tern conductor presented higher peak-to-peak loads compared with the ACSR Pelican conductor (0.97 kg/m) (Table 3-2).

The peak-to-peak vibrational loads of the Tern conductor have been compared for different clamp configurations at static tensions. It may be clearly seen as previously for the blocked clamp of the Pelican conductor, that the blocked clamp configuration presented greater alternating mechanical loads. This is shown in graphs 4-10, 4-11, and 4-12.

Using the suspension insulator has considerably reduced the vibrational loads as shown in Figure 4-12, compared with the blocked and articulated clamp configurations for the same conditions and parameters.

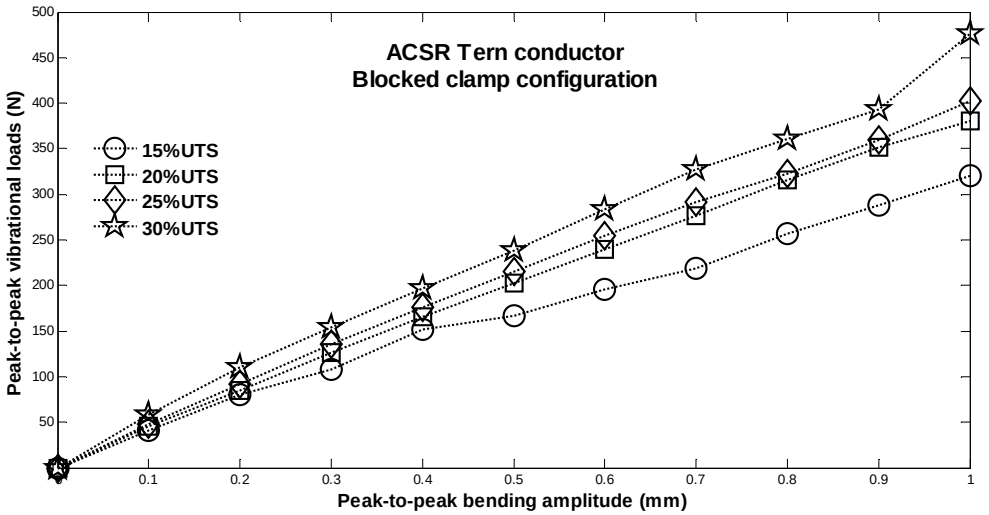

Figure 4-10: ACSR Tern conductor held by the blocked clamp: bending amplitudes vs. vibrational loads

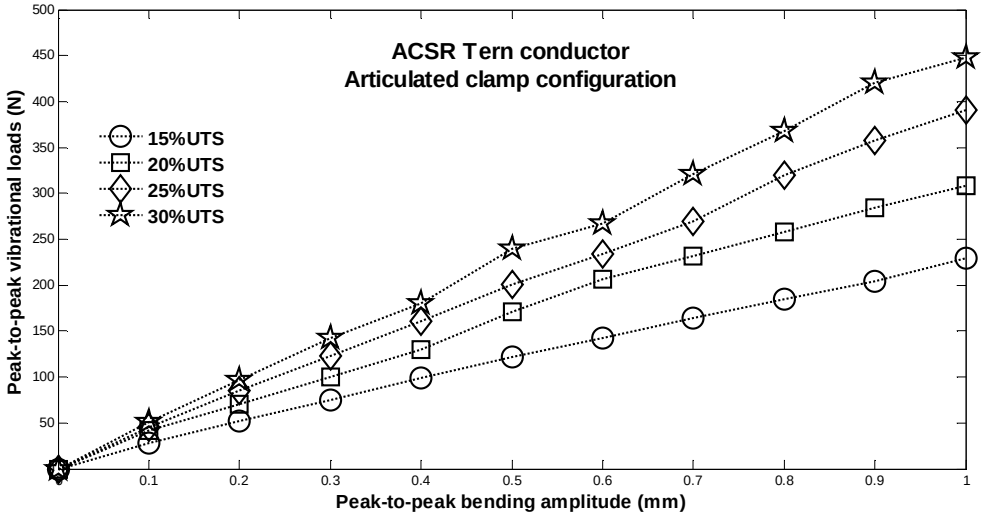

Figure 4-11: ACSR Tern conductor held by the articulated clamp: bending amplitudes vs. vibrational loads

Figure 4-12, At 1.0 mm peak-to-peak, the blocked clamp configuration yielded almost 476 N, while the conductor was tensioned at 30% UTS (Table 3-7). At the same tension, the articulated clamp and insulator configuration afforded almost 447 N and 435 N, respectively, as shown in Table 4-2.

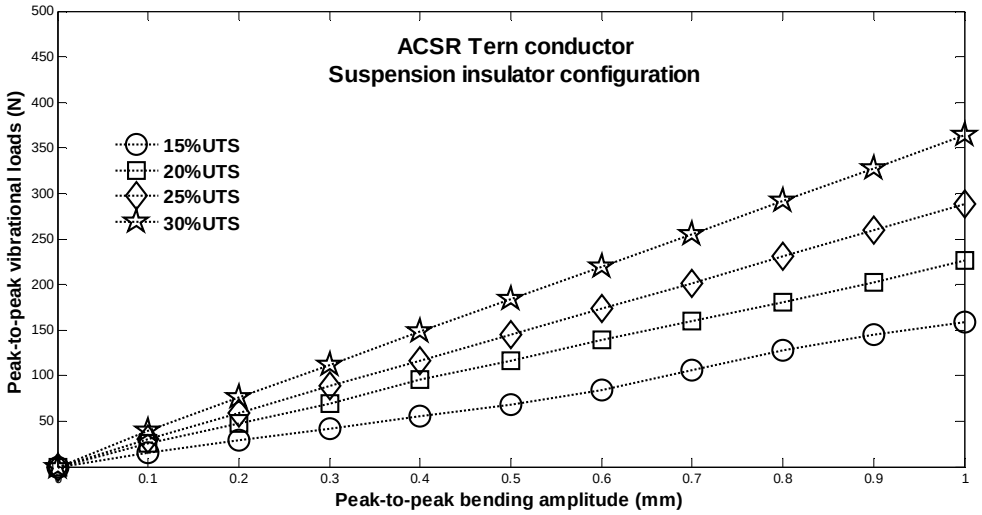

Figure 4-12: ACSR Tern conductor held by the suspension clamp: bending amplitudes vs. vibrational loads

Table 4-1: ACSR Pelican conductor: vibrational loads at 1.0 mm (peak-to-peak)

UTS (%)	Vibrational loads (N)		
	Blocked clamp	Articulated clamp	With insulator
15	164	105	99
20	217	142	137
25	278	160	162
30	288	180	182

Table 4-2: ACSR Tern conductor: vibrational loads at 1.0 mm (peak-to-peak)

UTS (%)	Vibrational loads (N)		
	Blocked clamp	Articulated clamp	With insulator
15	320	228	187
20	380	307	265
25	402	390	342
30	476	447	435

4.4 Strain of suspension insulator

Figure 4-13 shows the location of the strain gauges and their numbering during the data collection: 3 pairs of strain gauges were mounted on the FRP rod to measure the axial strain along the three areas.

4.4.1 Static measurement of the strain of the insulator

This depicts the static measurement of the strain gauges of the suspension insulator loaded gradually with 100 N till it reaches 800 N. It has been noted that the FRP rod of the insulator close to the end fittings was less sensitive to the axial tensile loads than the FRP rod in the middle of the suspension insulator (Figure 4-13). Gauges 1 and 3 seemed to have the same strain behaviour in contrast with gauge 2 which increased rapidly to the first 400 N that was applied. In the middle of the insulator (gauge 2) there is more mechanical stresses (tensile) than the FRP area closed to the two end-fittings of the composite insulator (gauges 1 & 3). The maximum tensile load applied was almost 750 N which represents 0.625% of SML.

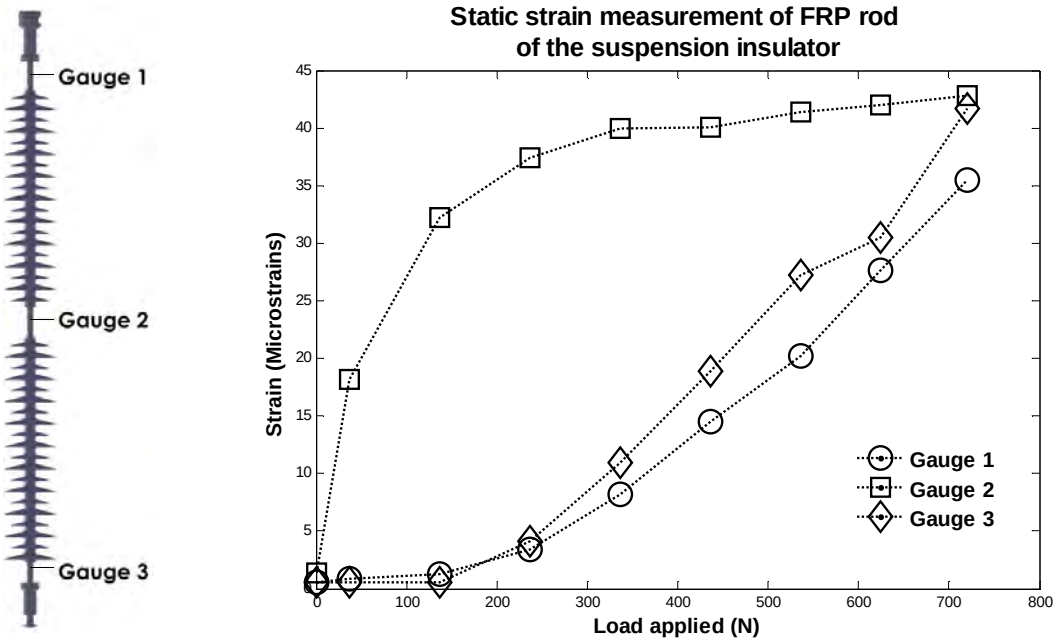

Figure 4-13: Location and numbering of strain gauges and the static measurement of the strain on the FRP rod of the suspension insulator

4.4.2 ACSR Pelican: Strain of the suspension insulator

The dynamic measurement of the strain gauges attached on the surface of the FRP rod of the suspension insulator has displayed behaviour differing from the static measurement. The tests were conducted at two different frequencies. The vibrational loads on the suspension were acting axially on the suspension insulator.

Figure 4-14 interprets the mechanical behaviour of the insulator by the strain generated at different frequencies. At 9.25 Hz, the strain increased slightly as a function of the peak-to-peak bending amplitudes of 0.1 mm increment on each level. For the

measurement conducted at 15.13 Hz, the same increment was observed until the 0.8 mm peak-to-peak bending amplitude; and at 0.9 mm the strain increased dramatically. It appeared apparently that the second frequency measurement of the vibrating conductor increased the effect of dynamic loads (No damping effect) on the composite insulator. Further study should be investigated on the reason of this increment as both the conductor and the composite insulator do not have same resonance frequency.

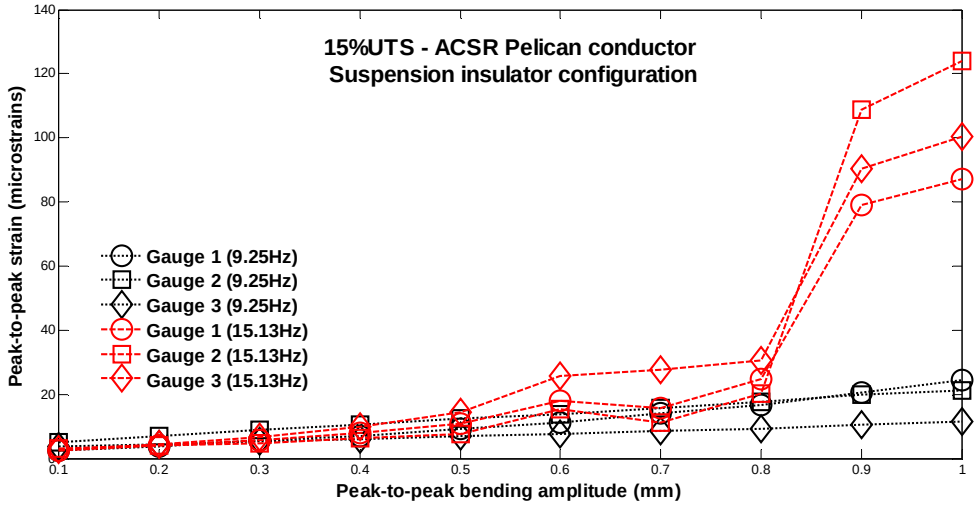

Figure 4-14: Dynamic strain of the FRP rod of insulator vs. the bending amplitudes of the ACSR Pelican conductor at 15% UTS

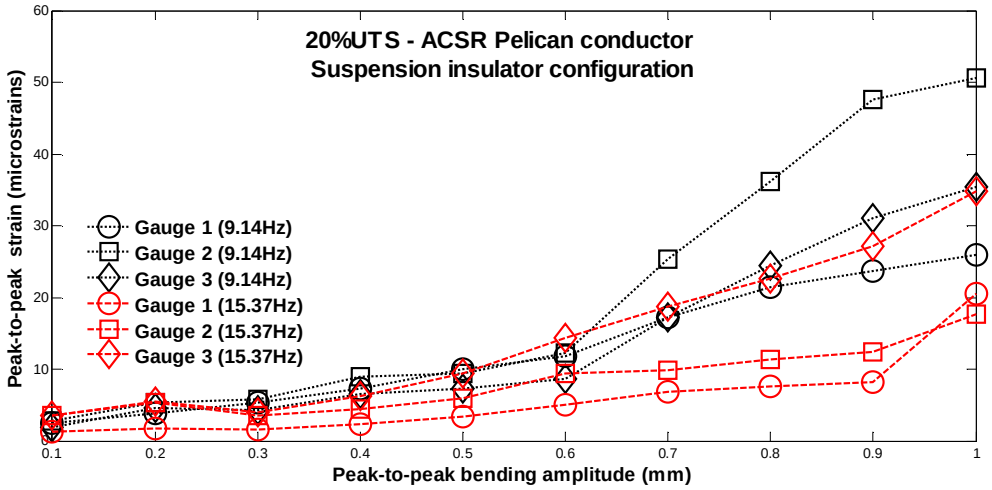

Figure 4-15: Dynamic strain of the FRP rod of insulator vs. the bending amplitudes of the ACSR Pelican conductor at 20% UTS

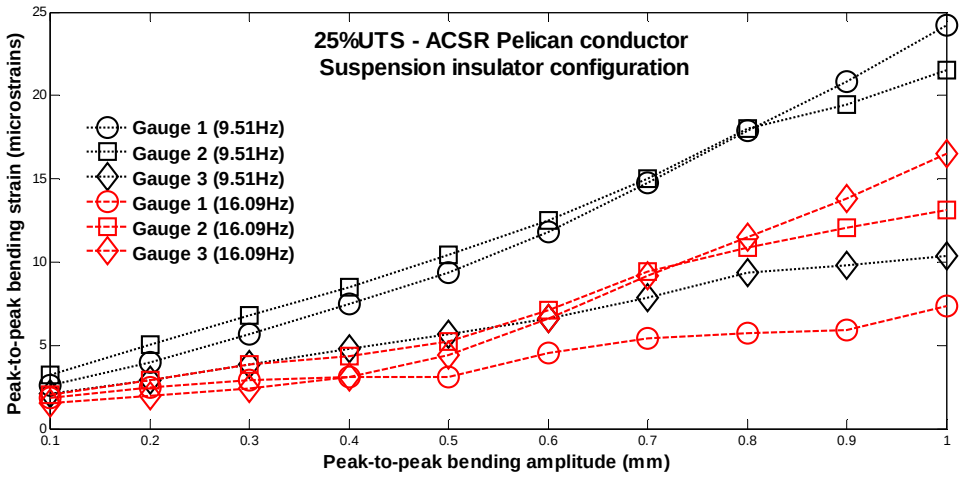

Figure 4-16: Dynamic strain of the FRP Rod of insulator vs. the bending amplitudes of the ACSR Pelican conductor at 25% UTS

Figures 4-15 (20% UTS) and 4-16 (25% UTS) show the strain curves of the FRP rod of the insulator increasing steadily while the ACSR Pelican was vibrating.

Referring to the graph 4-17, at 30% UTS, the peak-to-peak values of the FRP rod strain measured at 10.1 Hz has increased moderately, seeming to be linear, however, at 0.1 mm and 1.0 mm, the strains have considerably increased at 15.25 Hz.

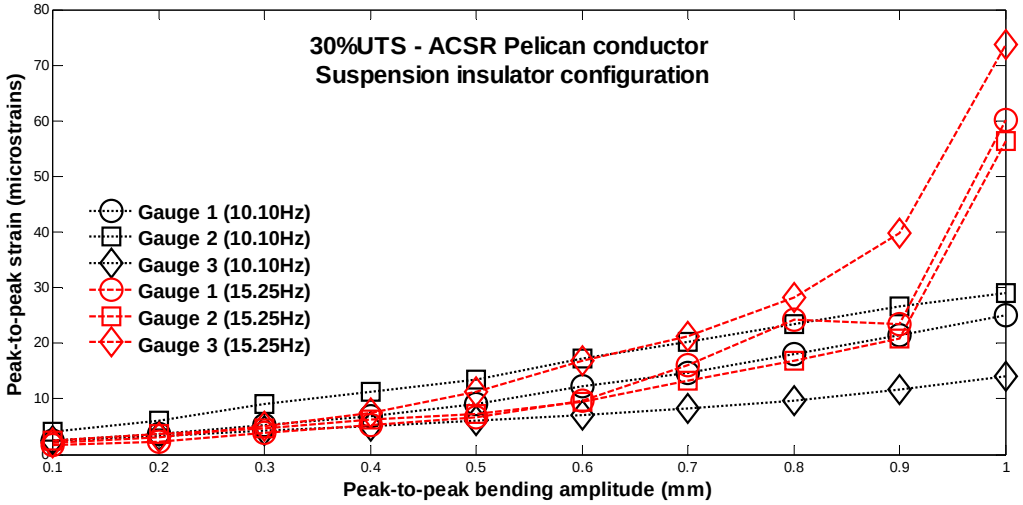

Figure 4-17: Dynamic strain of the FRP rod of insulator vs. the bending amplitudes of the ACSR Pelican conductor at 30% UTS

4.4.3 ACSR Tern: Strain of the insulator

Figures 4-18, 4-19 and 4-20 show the axial strain of the FRP rod of the suspension insulator generated by the vibration of the ACSR Tern conductor under the chosen frequencies.

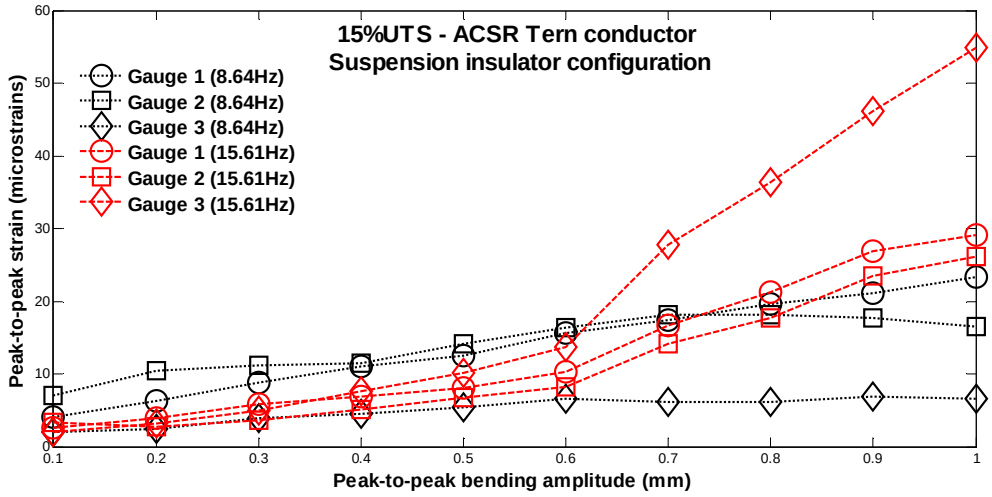

Figure 4-18: Dynamic strain of the FRP Rod of insulator vs. the bending amplitudes of the ACSR Tern conductor at 15% UTS

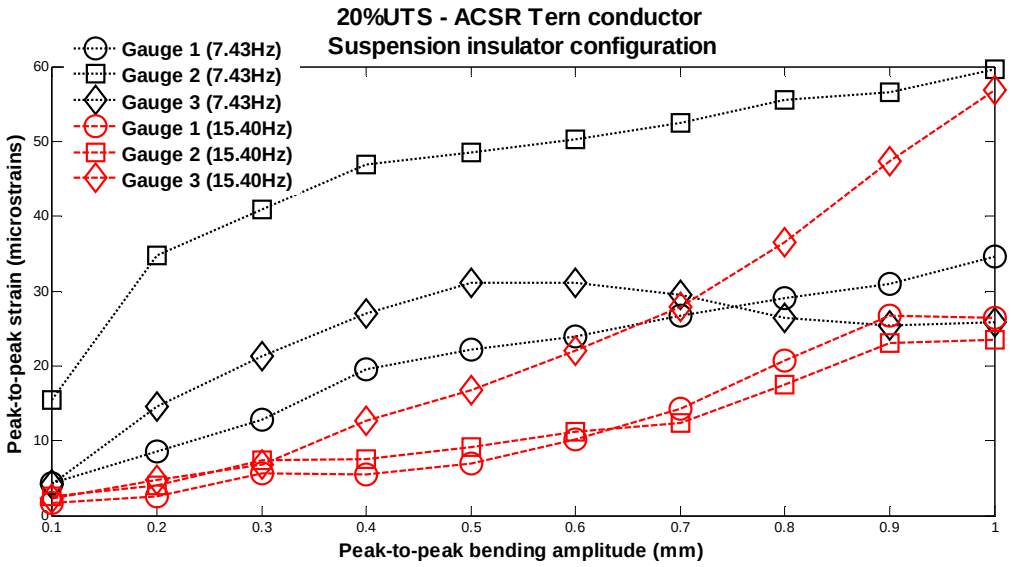

Figure 4-19: Dynamic strain of the FRP Rod of insulator vs. the bending amplitudes of the ACSR Tern conductor at 20% UTS

At 25% UTS of the ACSR Tern conductor, all strains measured at both frequencies started to increase gradually, continuing to 1.0 mm bending amplitude (Figure 4-20). At 30% UTS, only the strain measured by strain gauge 3 at 15.25 Hz had increased

strongly, while all other strains measured for both frequencies increased gradually but only slightly, without any disturbance.

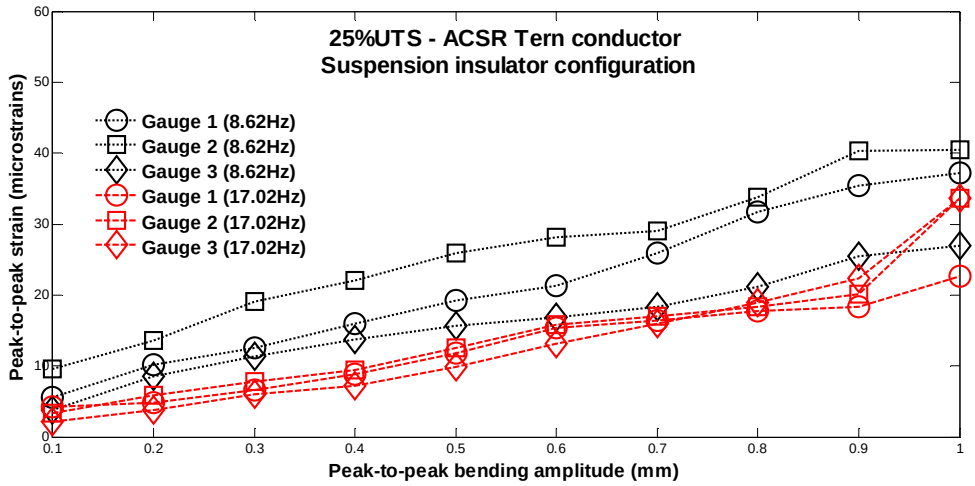

Figure 4-20: Dynamic strain of the FRP Rod of insulator vs. the bending amplitudes of the ACSR Tern conductor at 25% UTS

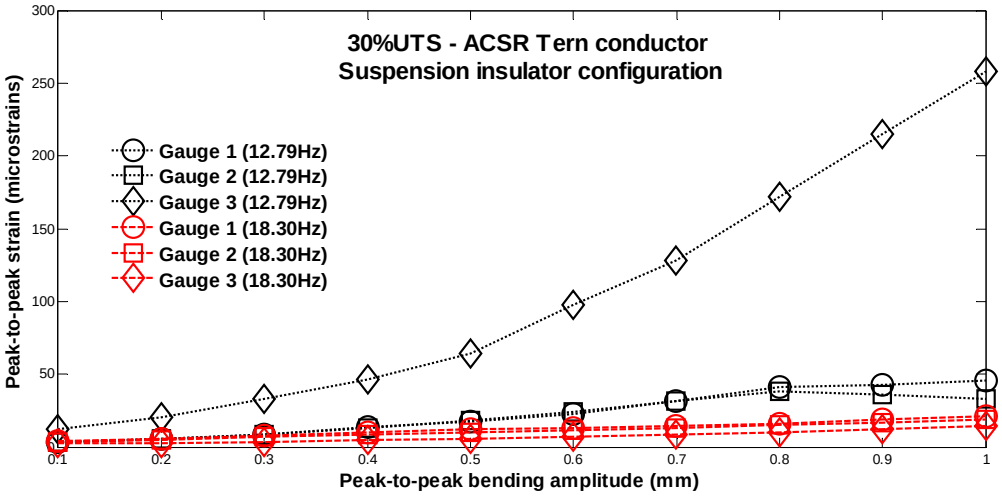

Figure 4-21: Dynamic strain of the FRP Rod of insulator vs. the bending amplitudes of the ACSR Tern conductor at 30% UTS

4.5 Bending strain of line post insulator

4.5.1 Static measurement of the strain of the insulator

The location of strain gauges around the FRP rod of line post insulator was checked by a static measurement. The strain gauges were separated close to 180 degrees apart (See Figures 3-7b, 3-8, and 3-16). This helped to quantify approximately the vibrational bending loads acting on the line post insulator while the conductor was vibrating. The

line post insulator was gradually loaded with 100 N. The bending load during the static test began at 0 kN reaching barely more than 57% MDCL (3.5 kN) of the line post insulator. The figure 4-22 shows the static measurement of the 4 strain gauges.

Figure 4-22 shows that the strain measurements of gauges 1 and 2 at the top and the bottom of the insulator are approaching symmetrical to the x-axis (cantilever load). Also, both gauges 3 and 4 on the neutral axis showed nearly the same value (theoretically zero) as stipulated in Bernoulli's hypothesis [59].

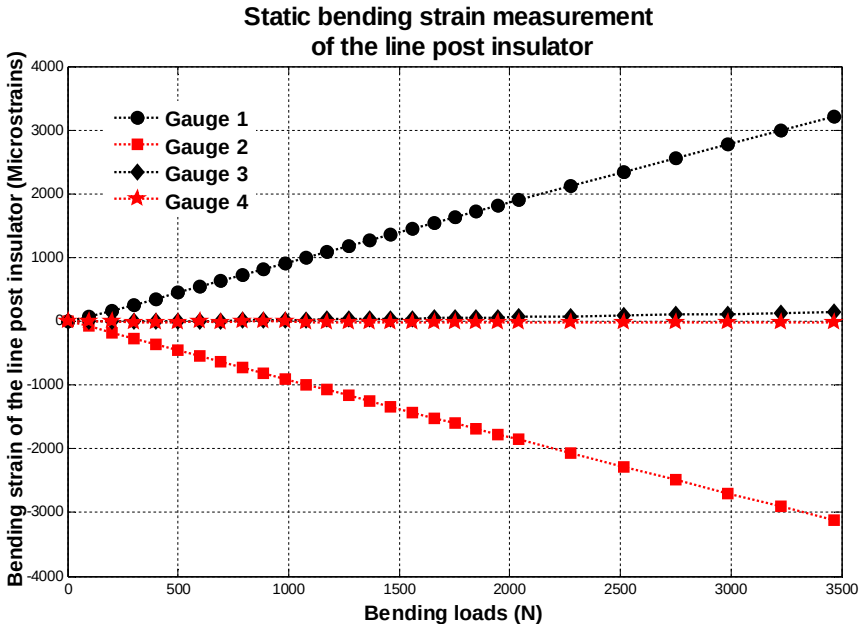

Figure 4-22 : Static measurement of four strain gauges attached around the FRP rod of the line post insulator

4.5.2 ACSR Pelican: Bending strain of the insulator

In order to investigate the influence of the suspension clamp movement on the mechanical behaviour (bending strain) of the line post insulator, it has been proposed to restrict (block) the movement to the suspension clamp during vibration of the conductor (Figure 3.22).

4.5.2.1 Blocked clamp

Figures 4-23 and 4-24 depict the situation in which the clamp was blocked while Figures 4-25 and 4-26 present the normal case (articulated clamp). The strain gauges 1 and 2 measured mainly the alternating peak-to-peak vertical mechanical loads (bending loads), while any slight increase or fluctuation of longitudinal loads affected the strain

gauges 3 and 4. This may be explained in that, as the conductor vibrated, the tensile force of the conductor was changing (longitudinal loads).

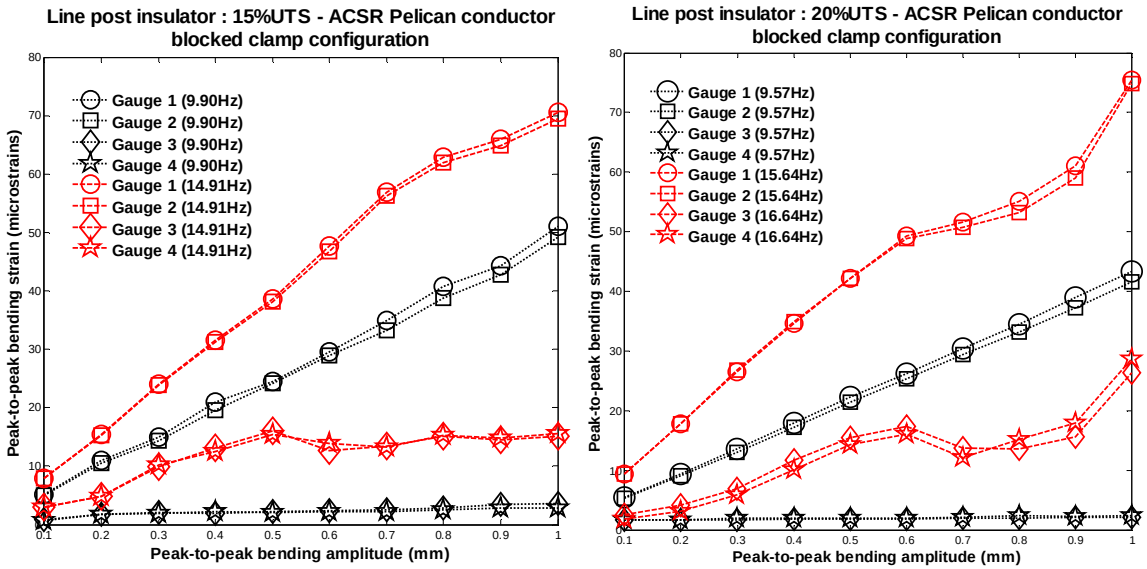

Figure 4-23: Alternating bending strains of the FRP rod of the line post insulator: blocked clamp with the Pelican conductor tensioned at 15% UTS (a) and 20 % UTS (b)

It has been observed that there is a positive correlation between each of the two opposite strains measured (gauges 1-2 and gauges 3-4). This means that gauges 1 and 2, which were subjected to vertical dynamic loads presented the same graph, although the strain measured by the gauge 2 was slightly smaller to the strain measured by gauge 1; that is, for 1.0 mm peak-to-peak bending amplitude at 9.6 Hz and at 20% UTS of Pelican conductor (Figure 4.23b), the bending strains measured at gauge 1 showed 43.3 με, while gauge 2 yielded 41.6 με; and at 15.64 Hz, gauge 1 presented 75.5 με, while gauge 2 yielded 74.8 με. The same behaviour has been observed for gauges 3 and 4. As with Figure 4-23, Figure 4-24 also presents the perfect correlation between each opposite gauge (180 degrees) at different frequencies of the conductor tested. At the lowest frequencies tested, all strain measurements presented the same mechanical behaviour: gauges 3 and 4 were close to zero; while gauges 1 and 2 could steadily but slightly increase till reaching 1.0 mm. At the highest frequencies tested, the strains were moderately increased.

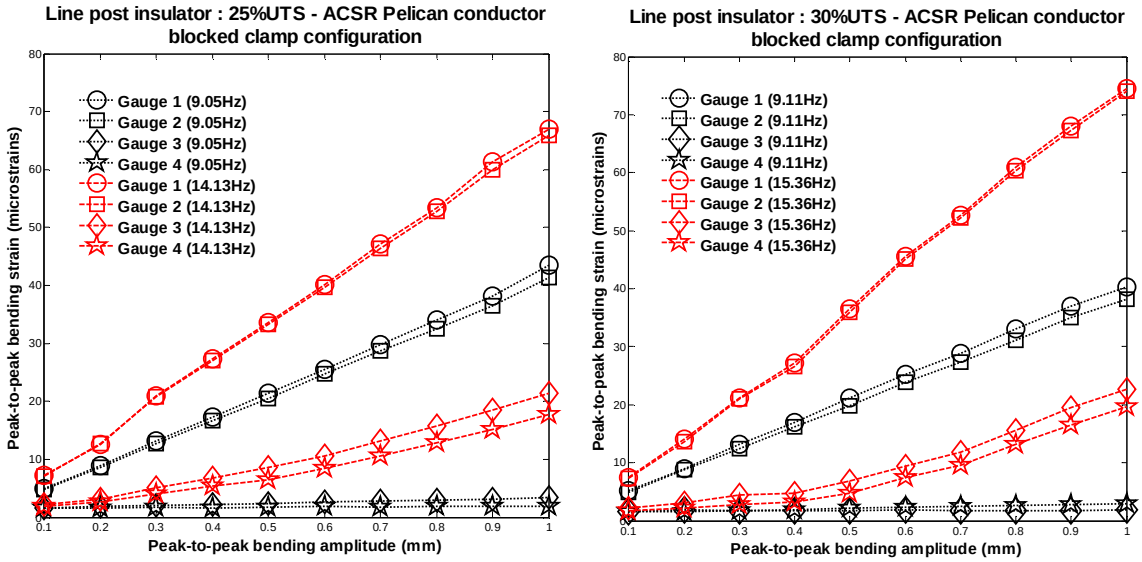

Figure 4-24: Alternating bending strains of the FRP rod of the line post insulator: blocked clamp with Pelican conductor tensioned at 25% UTS (a) and 30% UTS (b)

4.5.2.2 Articulated clamp

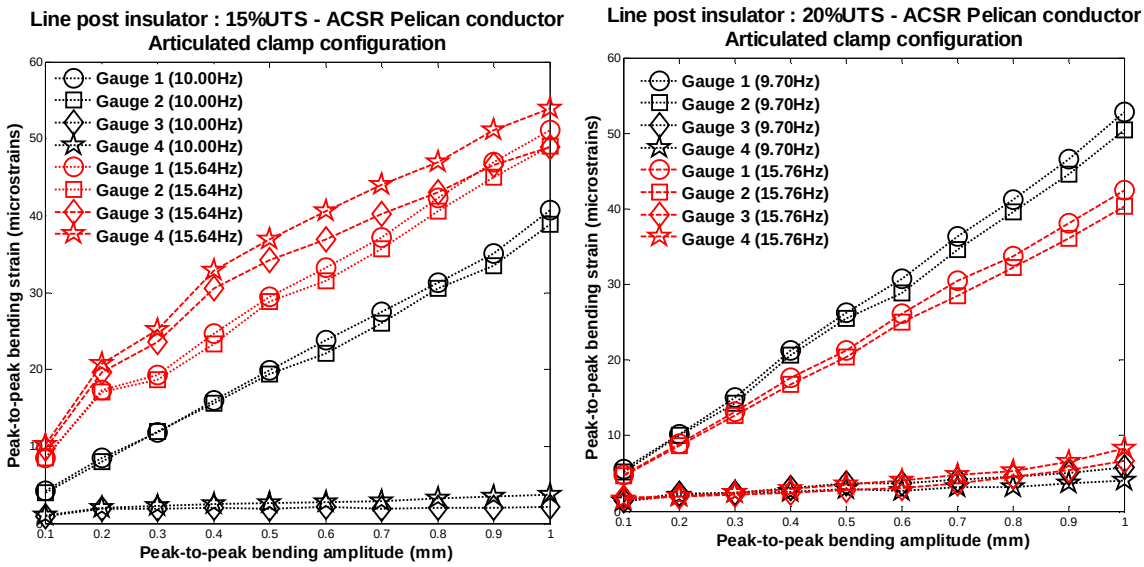

Figure 4-25: Alternating bending strains of the FRP rod of the line post insulator: articulated clamp with the Pelican conductor tensioned at 15% UTS (a) and 20% UTS (b)

The strain measurements of gauges 3 and 4 are steadily growing; this may be explained by the increasing of the dynamic longitudinal loads (Figure 4-26).

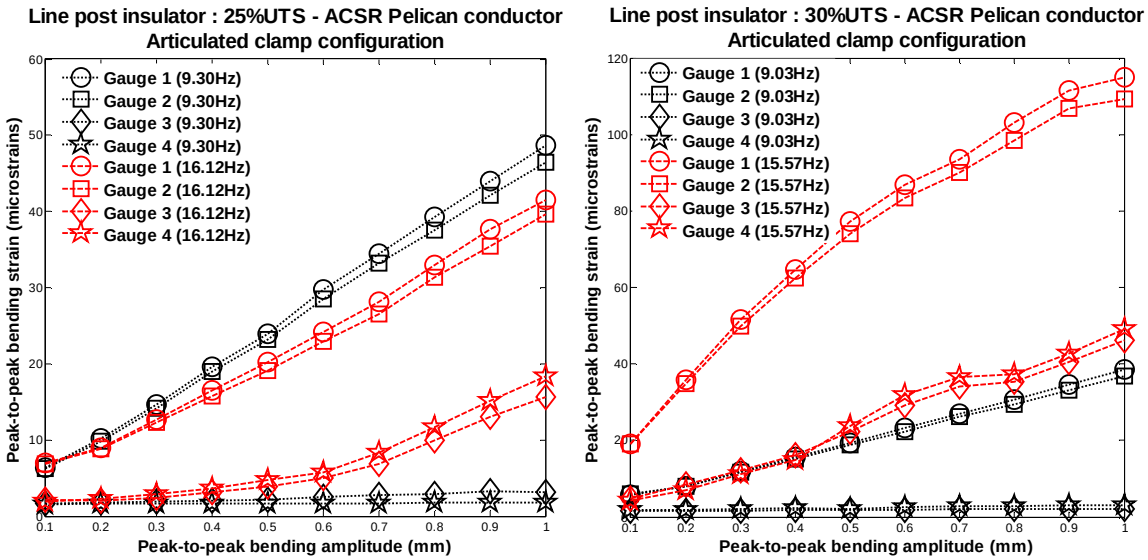

Figure 4-26: Alternating bending strains of the FRP rod of the line post insulator: articulated clamp with the Pelican conductor tensioned at 15% UTS (a) and 20% UTS (b)

4.5.3 ACSR Tern: Bending strain of the composite insulator

4.5.3.1 Blocked clamp

As previously with the ACSR Pelican conductor, the ACSR Tern conductor presented very similar graph behaviour (Figure 4-27 and 4-28).

The strain measurement of gauges 1 and 2 was seen to be linear at the lowest frequencies tested, while at the highest frequencies some non-linearity was recorded. Gauges 3 and 4 measured the strain having a lower value, closer to zero.

At certain frequencies tested, higher longitudinal loads generated by the vibrating conductor have been recorded (Figure 4-28a).

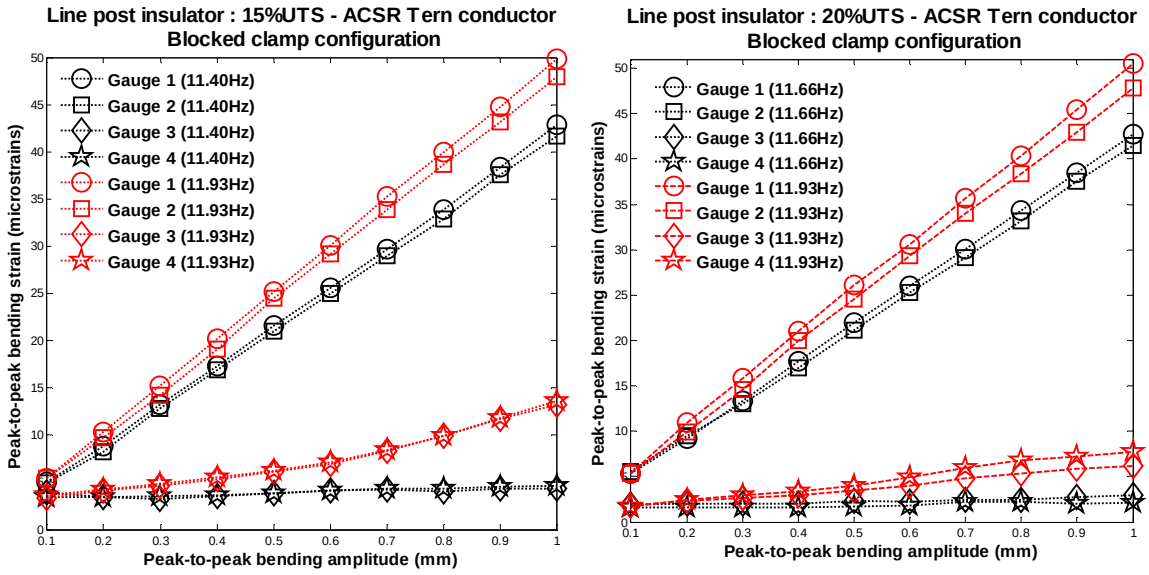

Figure 4-27: Alternating bending strains of the FRP rod of the line post insulator: articulated clamp with the Tern conductor tensioned at 25% UTS (a) and 30% UTS (b)

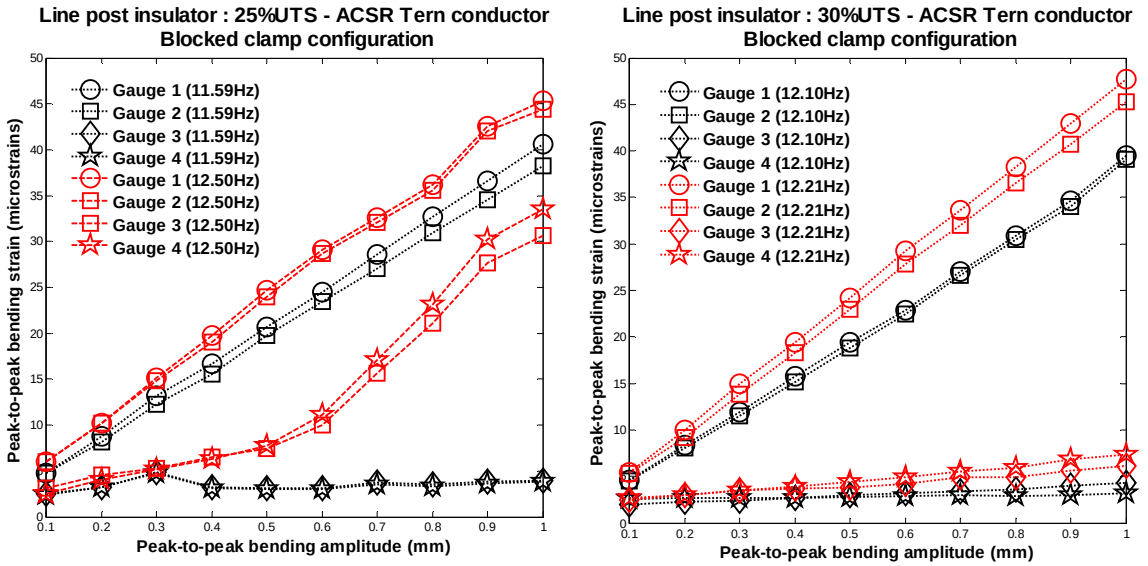

Figure 4-28: Alternating bending strains of the FRP rod of the line post insulator: blocked clamp with the Tern conductor tensioned at 25% UTS (a) and 30% UTS (b)

4.5.3.2 Articulated clamp

The dynamic bending strain of the line post insulator vibrating with the Tern conductor is illustrated by Figures 4-29 and 4-30, presenting the measurements conducted at four tension levels.

As with previous strain measurements, the mechanical behaviour of the FRP rod of the line post insulator presented the same characteristics. Although at 25% UTS for the articulated clamp, the longitudinal loads gradually increased.

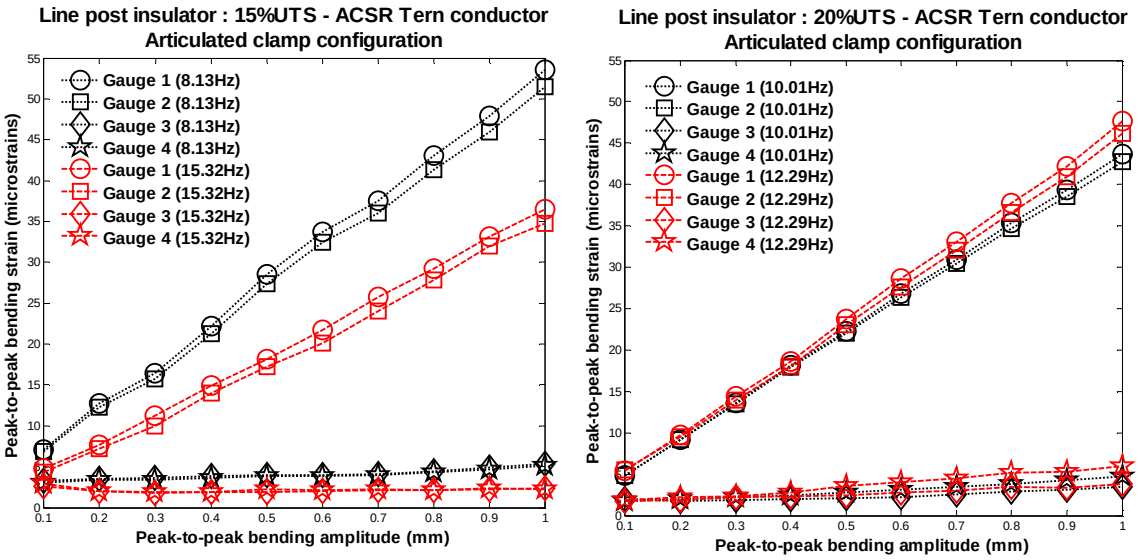

Figure 4-29: Alternating bending strains of the FRP rod of the line post insulator: articulated clamp with the Tern conductor tensioned at 15% UTS (a) and 20% UTS (b)

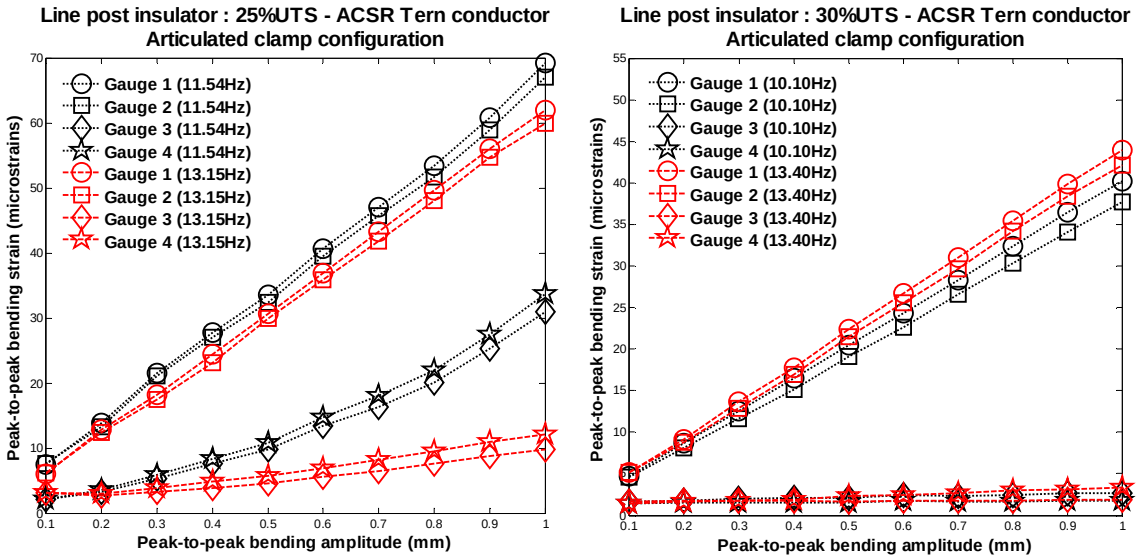

Figure 4-30: Alternating bending strains of the FRP rod of the line post insulator: articulated clamp with the Tern conductor tensioned at 25% UTS (a) and 30% UTS (b)

4.6 Discussion and analysis

4.6.1 Swept frequency results

The ACSR conductors (Pelican and Tern conductor) used for the study of mechanical loads while they are under Aeolian vibration showed that the mechanical properties of the conductor are the most important parameter (mass of the conductor) on the generation of vibrational loads (Table 3-2). It has been concluded that on the curves of the vibrational loads and the bending amplitude during the swept frequency method as a function of the driven frequency of the shaker:

- The bending amplitude and the vibrational load curves of the ACSR Pelican conductor are well correlated for the blocked clamp configuration at most of static tensions used (15 to 25% UTS). This means that each peak value of the vibrational loads corresponds with higher bending amplitude. This changed at a higher tension (30% UTS) at which higher peak dynamic loads did not correspond with higher bending amplitudes; and
- As with the ACSR Pelican conductor, the swept frequency results of both curve bending amplitudes and loads of the ACSR Tern conductor presented a perfect correlation for all tensions used; however, this situation was quite different for 15% and 20% UTS of the clamp configuration using an insulator. The configuration using a suspension insulator presented a nearly constant peak value of the loads at the frequency range from 15 to 40 Hz before declining and remaining at the lowest magnitude value.

It has further been observed that highest peak values of the mechanical loads were located at frequencies lower than 10 Hz for both conductors (Figures 4-1 to 4-6). This is due to the greater bending amplitudes obtained around that frequency as it has been shown by Figures 4-1 to 4-6.

4.6.2 Steady frequency results

Each steady state of alternating peak-to-peak bending amplitude measurement conducted on both conductors showed a wide variation in the accuracy of dynamic loads obtained at different conductor tensions.

4.6.2.1 Vibrational loads

The vibrational loads measured, whether with the suspension clamp or the suspension insulator, which are dynamic tensile loads and, consist of peak values, whether in axial compression or tension (figures 3-6, 3-21 and 3-22). The dynamic loads of the conductors, according to their bending amplitude, displayed a linear regression trend. The results showed clearly that the heaviest conductor produced higher vibration loads (From figure 4-7 to 4-12).

The results of the loads generated (Table 4-1 and 4-2) during the test suggested focusing attention on higher tensions of the conductor, the dynamic loads created by the Aeolian vibration of the conductor being higher than the other tensions. This is valid for both conductors (Tern and Pelican) (Figure 4-7 and 4-10).

According to the mechanical properties of both conductors (Tables 4-1 and 4-2), the ACSR Tern conductor presented higher vibrational loads at 1.0 mm peak-to-peak bending amplitude of the conductor, at 89 mm from the last point of conductor (LPC) (Figure 4-10). A simple explanation may be that the weight of the ACSR Tern conductor is higher than the ACSR Pelican conductor. The blocked clamp configuration presented the highest loads at frequencies tested, and for the bending amplitude ranged from 0.1 mm to 1.0 mm.

The slip-stick phenomenon of the individual wires may be observed at the lowest bending amplitude for both ACSR conductors, resulting in a non-linearity [6]. The static tension of the conductor, frequencies and the support configuration at mid-span support greatly influenced the vibrational loads of the overhead line conductor.

4.6.2.2 Influence of the clamp configuration

The dynamic measurement of mechanical loads of the vibrating conductors has shown that the worst case was represented by the blocked clamp configuration which provided higher mechanical loads on the clamp (Figures 4-7 to 4-10). This may be seen in Tables 4-1 and 42. This scenario may be explained by the effect of the restriction of movement (no degree of freedom) of the clamp. All the forces of the mechanical waves of the vibration conductor were entirely concentrated on the force transducer.

The articulated clamp showed mechanical loads much smaller in magnitude to the vibrational loads. This was understandable in that there was a degree of freedom of the clamp to rock around the axis of the pin on the clamp suspension (Figures 4-8 and 4-11).

The mechanical loads recorded while using the suspension insulator were considerably lower. They rose, however, when using the suspension composite insulator; a scenario explained by its damping effect on the transmission line conductor (Figures 4-9 and 4-12). This reduces the vibration level of the conductor, there being no restriction of the clamp held by the insulator; it is free to move (vertically, longitudinally, and in a transverse direction) [60] .

4.6.2.3 Dynamic behaviour of the composite insulator

For more conclusive results on the axial strains of suspension insulator and the bending strains of line post insulators, two frequencies close to resonance were used in evaluating the effect or the impact of the mechanical loads generated by the vibrating ACSR conductor (Pelican and Tern) on the surface of the fibre-reinforced plastic (FRP) rod of these composite insulators.

a) Dynamic behaviour of the suspension insulator

It has been noticed that the suspension insulator was subjected to compression or axial tensile loads while the conductor was vibrating. Measuring by means of the strain gauge subjected to vertical loads (gauges 1 and 2) showed that strains of the suspension insulator are proportional to the bending amplitudes and the frequencies of the vibrating conductor. The entire system is fairly complex as the conductor was held by the insulator (Figures 4-14 to 4-19). The situation of the suspension insulator may be compared with a rod subjected to longitudinal vibrations [61]. The variations of axial strains of the FRP rod surface recorded at three locations as shown by Figure 4-13 revealed that the axial strain increased its magnitude, while the bending amplitudes of the conductor at 89 mm of the LPC (last point of contact) increased, being widely dependent on the frequency of measurements. This can be seen in Figures 4-14 to 4-21). The conclusion raised from the measurements was that the strain gauges 2 and 3 showed higher strain peak-to-peak value; this could be interpreted by the mechanical loads tagging the lower part of the insulator.

b) Dynamic behaviour of the line post insulator

The FRP rod of the line post insulator has similar properties as the composite suspension insulator, however, with a large FRP rod diameter (63.5 mm) and with different end fittings (flanges) (Tables 3-4 and 3-5). Initially, the line post insulator bears the -static- bending load produced by the weight of the overhead line conductor and further the dynamic loads caused by the vibration of the conductor..

The mechanical behaviour of the line post insulator was as described by four strain gauges attached around the FRP rod, as shown by Figures 3-7, 3-8, and 3-16. Previously, in Figures 2-9, three types of mechanical load were presented according to the loading direction. The opposite gauges are well-correlated and dependent, with the frequencies as shown in the graph (Figures 4-25 to 4-30).

As defined in Figure 2-9, the dynamic loads of the vibrating conductor acted strenuously in a vertical direction but moderately in a longitudinal direction except at 15% UTS with the articulated clamp configuration (Figure 4-25a). At low frequencies of both conductors (below 10 Hz), the vibrational loads seemed to act more vertically. This may be seen by the bending strain measurement taken by gauges 1 and 2. However, at higher frequencies (up to 15 Hz), in addition to vertical vibrational loads acting on the end of the line post insulator, the longitudinal vibration loads collected by gauges 3 and 4 were increased concomitantly with the peak-to-peak bending amplitude of the conductor at the suspension point (Figures 4-23b, 4-24, 4-26, 4-28b, 4-27 and 4-30).

In order to comprehend the influence of the movement restriction of the clamp, the tests were conducted first with the blocked clamp and secondly with the articulated clamp.

- For the ACSR Pelican conductor, the blocked clamp presented higher peak-to-peak bending strain measurements, while the articulated clamp showed a lower value of the peak-to-peak bending strain compared with the blocked clamp exception at 30% articulated clamp configuration (Figure 4-26b); and
- For the ACSR Tern conductor, there were not high differences between the peak-to-peak bending amplitude of the blocked and articulated clamps. However, the peak-to-peak bending strains generated by the vibration of the

ACSR Tern conductor on the line post insulator were generally lower than generated by the ACSR Pelican conductor.

This situation can be explained because of the weight of the overhead line conductor and the conductor stiffness. The bending of the line post insulator once loaded with the weight of the conductor is moderately greater while using the ACSR Tern conductor than when using the ACSR Pelican conductor. While vibrating, the dynamic effects of the ACSR Tern conductor seemed to be more subdued than those of the ACSR Pelican conductor.

4.6.3 Fatigue considerations

Considerations were conducted into whether the Aeolian vibrational loads could cause fatigue on the composite insulators. The swept results indicated that the higher peak loads could be obtained at the lowest frequencies. The data obtained by cycling loading as shown by Figure 2-18 showed that the loads were much smaller (Tables 4-1 and 4-2).

The reason of lower loading on insulators is explained by the lower dynamic loads produced by both vibrating conductors. The loads generated had no major effects on the composites insulators tested which is due to the mechanical properties of these insulators (SML, MDLC). These dynamic loads were still low even with measurements taken at 1.0 mm peak-to-peak (worst case) as bending amplitude of the conductor which can be considered as critical scenario.

The interaction of these mechanical loads can be observed in different plotted graphs (Figure 4-14 to 4-21). All vibrational loads measured which were generated by the vibrating conductors were acting vertically on the suspension insulator and were identified as tension and compression loads with nearly equal magnitudes. The vibrational loading's combination of the line post insulators which are composed of vertical loads (Cantilever loads: up and down), longitudinal loads (side loads) are interpreted by the bending strain graphs (Figure 4-23 to 4-30). Transversal loads could not be evaluated in this study because it was assuming that these loads were nearly inexistent and difficult to create such scenario in the laboratory with the electrodynamic shaker.

It was concluded after many experimental investigations on the vibration of fatigue of the insulators that the mechanical loads of the vibrating conductor were much lower and

thus, the fatigue of composite insulators due to dynamic loads caused by overhead line vibration under Aeolian vibrations condition was not an issue. The S/N curves of composite insulators of composite suspension insulators flatten out at dynamic loads at the range of 20-30% of the SML. The same is true for composite posts [4].

The peak-to-peak loads collected by the force transducer were maximum 435 N. This represents only 0.4% of SML of the suspension insulator. It can be thus reasonably concluded that cyclic loading will not have a major effect on the fatigue performance of the insulator, the highest loads at which a run-out (non-failure) occurs was not taken as the fatigue threshold [44, 46, 62].

As previously mentioned, De Toureil found that the mechanical strength of the insulators subjected to cyclic loads could be from 22-75% lower than their static strength [3, 4]. For the line post insulator, the strain measurements of static load tests carried out on the insulator were used as reference data for the dynamic load tests.

Table 4-3: Strains of the line post insulator owing to ACSR Pelican vibrational loads at 1.0 mm (peak-to-peak) with a blocked clamp

UTS (%)	Peak-to-peak bending strains (με)			
	Gauge 1	Gauge 2	Gauge 3	Gauge 4
15	70.5	69.4	15.0	15.5
20	75.4	74.8	26.3	28.7
25	67.0	65.8	21.3	17.8
30	74.5	74.0	22.7	19.9

Table 4-4: Strains of the line post insulator owing to ACSR Tern vibrational loads at 1.0 mm (peak-to-peak) with a blocked clamp

UTS (%)	Peak-to-peak bending strains (με)			
	Gauge 1	Gauge 2	Gauge 3	Gauge 4
15	49.9	48.0	10.5	13.6
20	50.5	47.8	6.18	7.78
25	45.3	44.4	30.6	33.5
30	47.7	45.3	5.1	7.3

Table 4-5: Strains of the line post insulator owing to static loads

Force (N)	Peak bending strains (με)			
	Gauge 1	Gauge 2	Gauge 3	Gauge 4
0	15.2	-13.4	0.5	0.0
98.6	21.5	-20.0	0.3	-0.1
198.5	30.5	-30.1	-0.8	-0.9
298.4	38.8	-40.2	-2.2	-2.1
398.3	48.1	-49.6	-2.0	-2.2
498.2	57.1	-58.7	-1.9	-2.1
598.1	66.9	-67.7	-1.0	-1.6
694.1	76.0	-76.5	-0.6	-1.7
790.5	85.1	-85.1	-0.0	-1.5

The peak-to-peak bending strain measurements of the line post insulator subjected to vibrational loads generated by 1.0 mm bending amplitudes of both conductors (Pelican and Tern) were compared with the static peak bending strain measurements which the bending loads propelled almost to 57% MDLC. The dynamic loads acting on the insulator were approximately 298.4 N. This represents only 4.97% of MDLC. The effects of this cyclic loading amplitude of the ACSR conductor on the line post insulator are much lower compared to its fatigue characteristics.

4.7 Summary

In this chapter, the data measurements collected of two ACSR conductors (Pelican and Tern) at different clamp configurations, were presented and compared in plotted graphs. The measurements were conducted at different frequencies and at four tensions, with an increment of 5% UTS provided by the swept frequency excitation method. The peak-to-peak measurements of the vibrational loads of the vibrating conductors, the axial strain of the FRP rod of the suspension insulator, and the bending strain of the line post insulator, were taken as functions of the peak-to-peak bending amplitude at the last point of contact (LPC) between the clamp and the conductor. The mechanical behaviour of both the ACSR conductor and the composite insulator under Aeolian vibration conditions were interpreted by graphs. The conclusion reached was that the heaviest conductor produced higher dynamic loads on the major set-up configuration (clamp and suspension insulator), except on the line post configuration, which seems to show the reverse scenario.

CHAPTER 5
CONCLUSION

5.1 Research summary

Since their advent in the 1950s in the power line industry, the mechanical properties of the FRP used for the core of the composite insulator are still under investigation, even though much progress has been made in the manufacture of these materials. Actually, the mechanical standard tests proposed for composite insulators are limited mainly to static load conditions. This could be insufficient in making decisions on the mechanical loading considerations of these insulators. This is because, while in service, insulators are exposed to dynamic loads generated by the conductor's oscillation, namely, Aeolian vibrations.

It was thus the intention of this research to determine experimentally the mechanical loads generated by overhead conductors stretched at different tensions. Once those loads were known and applied to the composite insulators, the mechanical behaviour of these insulators (suspension and line post) was investigated. The wind effect simulated on the overhead line conductors was under Aeolian vibration conditions. Two major types of tests were conducted: the swept frequency method, and the steady frequency method. Three support configurations were used.

The swept frequency method conducted by the Puma control system provided the dynamic response of the bending amplitude and the vibrational loads of the overhead conductors under a range of frequency provided by the Strouhal formula.

Interesting results are found on the relationship between the dynamic loads and the bending amplitude, which reached highest peak value at the lowest frequencies (under 10 Hz). The heaviest conductor has a smaller range of frequency (5-50 Hz) where peak value of loads and bending amplitudes are higher before the constant damping state, while the lighter conductor presented a long and valuable frequency range (5-70 Hz).

The steady frequency method was conducted at multiple values of the alternating peak-to-peak bending amplitudes from 0.1 to 1.0 mm as the standard values. Thus, the

dynamic loads of the overhead conductors at different tensions (15, 20, 25 and 30% UTS) were measured by a force transducer, while the LVDT was measuring the peak-to-peak bending amplitudes.

In order to study more in-depth the dynamic load effects, the articulated clamp used was blocked, as described in [33]. The blocked clamp configuration presented high loads compared with the articulated clamp. These experiments showed that for all clamp configurations, the axial compressive and tensile loads are of nearly the same intensity.

The vibrational loads of the vibrating conductor collected by the force transducer while using the suspension insulator were much lower compared to the blocked and articulated clamp configuration. It has been noticed that the suspension insulator was also subjected to compression or axial tensile loads, which may be compared with a rod subjected to longitudinal vibrations [61]. Like the presence of both composite insulators in the line (suspension and line post) reduced considerably the oscillation force of the conductor at the suspension point, this has led to conclude that the composite insulator have some damping properties which reduce the impact of mechanical load generated by the vibrating conductor. The dynamic behaviour of the suspension insulator collected by strain gauge measurements on the FRP rod of the insulator showed that the inferior part of the suspension insulator closed to its end fittings was more exposed to the vibrational loads of the conductor.

The dynamic loads on the line post insulator were even lower than using a suspension insulator. This conclusion arose while comparing the static measurement with the dynamic. The mechanical behaviour of the line post insulator with the strain gauges attached to the FRP rod indicated that at low frequency only vertical mechanical loads were considered. While the frequency was increased, this brought more stress to the insulators by increasing the longitudinal vibrational loads, which was nearly insignificant at low frequency.

The axial strain of the suspension insulator or the bending strain of the FRP rod or the line post insulator subjected to vertical loads measured by the strain gauges showed that strains of those insulators were proportional to the bending amplitudes of the vibrating conductor.

The combination and orientation of insulator's mechanical loading depend on the type of insulators used (suspension or line post) and the effects generated by the two types of conductors used (ACSR) were slightly the same as mentioned. It is well known that composite material (Fiberglass reinforced plastic) resist badly to the torsion but once mounted on the overhead line, composite insulators experience less torsion in service because of their assembly configurations:

- For the suspension insulator: there was a rotation freedom of the long rod insulators according to its axis allowed by the insulator end fittings.
- For the line post insulator, the suspension clamp mounted to the insulator is free to rock according to its pin axis. This makes the insulator to avoid torsion. The configuration of the line post with the suspension clamp blocked was careful studied in this research. It was found that the twisted movement (torsion forces) created by the vibrating conductor around the line post insulator was mainly avoided by the cantilever position of the insulator. This action was reacting like a spring beam that was going up and down.

The vibrational loads created by the vibrating conductor showed that the lowest part of the suspension insulator (from the middle to the end-fitting close to the suspension clamp of the conductor) was more exposed to high mechanical stresses as indicated by the strain gauge measurement. For the line post insulator, the stressed area of the insulator is the area close to the end-fitting that is mounted to the support tower. This scenario is comparable to a cantilever beam subjected to a vertical point load at its free end. The static tests done confirmed the Bernoulli's theorem: The strains on the top and the bottom of the insulator were nearly symmetrical to the x-axis (Figure 4-22). Also both gauges on the neutral axis had the same value (theoretically zero) [59].

The movement of the suspension clamp mounted to the line post insulator showed that there is no major difference either the suspension clamp is articulated or blocked. The torsion forces on the line post insulator which could be caused by greater longitudinal loads were minimised by the rocking movement of the suspension clamp and the bending movement of the whole line post insulator. All restrictions on the suspension clamp seemed to be converted more in bending of the insulator which acted like a spring beam.

5.2 Research outcomes

This project has showed experimentally the conductor behaviour under Aeolian vibration in which a prediction of their dynamic loads can be made. Many experimental tests of the steady frequency method were conducted in order to arrive at conclusions apropos of the vibrational loads generated by both overhead line conductors at four different tensions on composite insulators tested. The swept frequency results indicated:

- A trend overview of dynamic loads and bending amplitudes given by the swept frequency method for all clamp configurations;
- The dynamic loads with a suspension clamp (blocked and articulated) and a suspension insulator according to its set-up configuration;
- Mechanical behaviour of the suspension insulator subjected to the alternating axial loads interpreted by strain measurements of its FRP rod. The tension and compression forces are nearly equal in magnitude value at opposite directions; and
- Mechanical behaviour of the line post insulator subjected to the vertical and lateral alternating bending loads was also interpreted by the strain measurements of its FRP rod. The suspension clamp was either blocked or articulated in order to ascertain the influence of clamp movement.

Thus, scrutinising the very low values of the dynamic loads measured at very high bending amplitudes (1.0 mm peak-to-peak) of the conductor at the suspension point at mid-span, fatigue investigations are not required. Previous investigations have showed that the S/N-curve of composite suspension insulators flattens out at dynamic loads in the range of 20-30% of the SML. This also holds true for composite posts [5].

The research has shown by means of carefully planned experiments that the real dynamic loads occurring when the conductor is under Aeolian vibration condition are too low to cause fatigue failures on the composite insulators. Thus, fatigue of composite insulators due to dynamic loads caused by Aeolian vibrations is not an issue. This information would be of great interest to the power industry (manufactures and users) and to academia at large.

This research work has presented the case of the vibrating conductor without dampers held by the composite insulators (bundle conductors were not considered). This is represented as close as possible to the real case on the field but the following limitations can be observed:

- The height of the suspension point and the length of the conductor's span using for both types of insulators in the laboratory. Generally the lengths of the span vary from 200 m to 600 m and this depends on the landscape of the area. Thus, no major conductor sag was observed during the tests due to the dimensions of the indoor laboratory.
- Difficult to generate the transversal loads using the electrodynamic shaker which could act on the line post insulator while the conductor was vibrating. These loads are composed of tension loads and compression loads. Tension loads which are pulling the conductors perpendicularly away from the tower, essentially putting the line post insulator in tension. The compression loads pull perpendicularly the conductor into the tower, compressing the line post insulator towards the tower. According to the standard test done on the line post insulators, it is assumed that these transversal loads are easily supported by the insulators as the main loading issues arise from cantilever loads (MDCL, RCL or SCL).
- Environmental issues have to be taken in account for all types of insulators according to the area where they are placed.

5.3 Recommendations

From this experimental investigation into the dynamic loads caused by conductors on composite insulators, in order to improve future research, certain recommendations for future investigations may be made:

- Applicability to other types and sizes of conductors and to another conductor test span arrangements with a suspension clamp could be standardised [33]. It would also be helpful to test a long span of the conductors;
- Evaluation of Aeolian vibrational loads on the end fittings of the composite insulators (suspension and line post);
- As remarked, regarding high loads at low frequencies, more profound investigation should also be made into other conductor oscillations, particularly

galloping conductors, and the shock loads (ice shedding, short circuit loads, etc.) of overhead lines;

- More investigation into the damping effect of the composite insulator should be undertaken;
- Investigations should be made using other analytical or finite element analysis (FEA) approach under Aeolian vibrations conditions, of :
    - the dynamic loads of the overhead conductors; and
    - the effect of these dynamic loads on composite insulators (suspension or line post);
- It would also be interesting to investigate the mechanical behaviour and fatigue of string composite insulators under Aeolian vibration;
- Concerning the line post insulator, the longitudinal loads should be deeply also investigated during power line motions and conductor's breakage.

References

[1] EPRI, *EPRI Transmission Line Reference Book: Wind-Induced Conductor Motion* second edition ed. Palo Alto, C. A. 1012317, USA: EPRI, 2009.

[2] F. Kiessling, P. Nefzger, U. Kaintzyk, and J. F. Nolasco, *Overhead Power Lines: Planning, Design, Construction*: Springer, 2003.

[3] C. de Tourreil, R. Roberge, and P. Bourdon, "Long-term mechanical properties of high voltage composite insulators," *Power Engineering Review, IEEE*, vol. PER-5, pp. 52-52, 1985.

[4] C. H. de Tourreil, "Response of composite insulators to dynamic mechanical loads," *Power Delivery, IEEE Transactions on*, vol. 5, pp. 379-383, 1990.

[5] K. O. Papailiou and F. Schmuck, *Silicone Composite Insulators: Materials, Design, Applications*: Springer, 2012.

[6] A. Cardou, *Stick-slip Mechanical Models For Overhead Electrical Conductors In Bending (with Matlab applications)*. Université Laval, Québec: GREMCA, 2013.

[7] R. E. T. K. Sharma. Polymeric Insulators [Online]. Available: http://www.appstate.edu/~clementsjs/surfaceflashover/insulatortesting.pdf

[8] IEEE, "IEEE Guide for Application of Composite Line Post Insulators," in *IEEE Std 1572-2004*, ed, 2004, pp. 0_1-16.

[9] ANSI, "ANSI C29.11, American National Standard for composite suspension insulators for overhead transmission lines, ed. New York: ANSI, 1989.

[10] A. C. Baker, "Insulators 101 Section C - Standards," in *Transmission and Distribution Conference and Exposition, 2010 IEEE PES*, 2010, pp. 1-5.

[11] E. Palazuelos and A. Fernandez, "Aeolian vibration recording and control," in *Overhead Line Design and Construction: Theory and Practice, 1989., International Conference on*, 1988, pp. 56-59.

[12] J. D. Mozer, J. C. Pohlman, and J. F. Fleming, "Longitudinal load analysis of transmission line systems," *Power Apparatus and Systems, IEEE Transactions on*, vol. 96, pp. 1657-1665, 1977.

[13] T. Krauthammer, "A numerical study of wind-induced tower vibrations," *Computers & Structures*, vol. 26, pp. 233-241, // 1987.

[14] R. C. Battista, R. S. Rodrigues, and M. S. Pfeil, "Dynamic behavior and stability of transmission line towers under wind forces," *Journal of Wind Engineering and Industrial Aerodynamics,* vol. 91, pp. 1051-1067, 8// 2003.

[15] G. Diana, S. Bruni, F. Cheli, F. Fossati, and A. Manenti, "Dynamic analysis of the transmission line crossing “Lago de Maracaibo”," *Journal of Wind Engineering and Industrial Aerodynamics,* vol. 74–76, pp. 977-986, 4/1/ 1998.

[16] A. R. E. Oliveira and D. G. Freire, "Dynamical modelling and analysis of aeolian vibrations of single conductors," *Power Delivery, IEEE Transactions on,* vol. 9, pp. 1685-1693, 1994.

[17] D. Brika and A. Laneville, "An Experimental Study of the Aeolian vibrations of a Flexible Circular Cylinder at Different Incidences," *Journal of Fluids and Structures,* vol. 9, pp. 371-391, 5// 1995.

[18] M. Kraus and P. Hagedorn, "Aeolian vibrations: wind energy input evaluated from measurements on an energized transmission line," *Power Delivery, IEEE Transactions on,* vol. 6, pp. 1264-1270, 1991.

[19] P. W. Davall, M. M. Gupta, and P. R. Ukrainetz, "Mathematical analysis of transmission line vibration data," *Electric Power Systems Research,* vol. 1, pp. 269-282, 12// 1978.

[20] P. Hagedorn, "Wind-excited vibrations of transmission lines: A comparison of different mathematical models," *Mathematical Modelling,* vol. 8, pp. 352-358, // 1987.

[21] A. Leblond and C. Hardy, "Assessment of safe design tension with regard to Aeolian vibrations of single overhead conductors," in *Transmission and Distribution Construction, Operation and Live-Line Maintenance Proceedings. 2000 IEEE ESMO - 2000 IEEE 9th International Conference on*, 2000, pp. 202-208.

[22] F. Lévesque, S. Goudreau, L. Cloutier, and A. Cardou, "Finite element model of the contact between a vibrating conductor and a suspension clamp," *Tribology International,* vol. 44, pp. 1014-1023, 8// 2011.

[23] F. Schmuck, S. Aitken, and K. O. Papailiou, "A proposal for intensified inspection and acceptance tests of composite insulators as an addition to the guidelines of IEC 61109 Ed. 2: 2008 and IEC 61952 Ed. 2: 2008," *Dielectrics and Electrical Insulation, IEEE Transactions on,* vol. 17, pp. 394-401, 2010.

[24] A. M. Loredo-Souza and A. G. Davenport, "The effects of high winds on transmission lines," *Journal of Wind Engineering and Industrial Aerodynamics,* vol. 74–76, pp. 987-994, 4/1/ 1998.

[25] I. Giosan, Vortex Shedding Induced Loads on Free Standing Structures [Online]. Available: http://www.wceng-fea.com/vortex_shedding.pdf

[26] M. A. Baenziger, W. D. James, B. Wouters, and L. Li, "Dynamic loads on transmission line structures due to galloping conductors," *Power Delivery, IEEE Transactions on,* vol. 9, pp. 40-49, 1994.

[27] P. Du Plessis, *Mechanical Oscillations on Overhead Transmission Lines.* Randse Afrikaanse Universiteit. Department Meganiese en Siviele Ingenieurswese: Rand Afrikaans University, 1994.

[28] W. Jeff, "Overhead Transmission Line Vibration and Galloping," in *High Voltage Engineering and Application, 2008. ICHVE 2008. International Conference on,* 2008, pp. 120-123.

[29] H. Jicai, Z. Song, M. Jianguo, and W. Shijing, "Model for comprehensive simulation of overhead high voltage power transmission line galloping and protection," in *Electrical Insulation and Dielectric Phenomena, 2006 IEEE Conference on,* 2006, pp. 190-193.

[30] N. Barbieri, O. H. d. S. Júnior, and R. Barbieri, "Dynamical analysis of transmission line cables. Part 1—linear theory," *Mechanical Systems and Signal Processing,* vol. 18, pp. 659-669, 5// 2004.

[31] L. Y.-b. W. Hong, D. Yu-ming, X. Hong, "The study of conductor fatigue test amplitude of overhead lines " *Proceedings of the CSEE,* vol. 28, 2008.

[32] G. B. Tebo, "Measurement and control of conductor vibration," *Electrical Engineering,* vol. 60, pp. 1188-1193, 1941.

[33] I. C. Report, "Standardization of Conductor Vibration Measurements," *Power Apparatus and Systems, IEEE Transactions on,* vol. PAS-85, pp. 10-22, 1966.

[34] J. C. Poffenberger and R. L. Swart, "Differential Displacement and Dynamic Conductor Strain," *Power Apparatus and Systems, IEEE Transactions on,* vol. 84, pp. 281-289, 1965.

[35] K. O. Papailiou, "On the bending stiffness of transmission line conductors," *Power Delivery, IEEE Transactions on,* vol. 12, pp. 1576-1588, 1997.

[36] S. Bisnath, T. Pillay, and E. (Firm), *The Planning, Design and Construction of Overhead Power Lines* vol. 1. Johannesburg: Crown Publications, 2005.

[37] S. Bisnath, T. Pillay, and E. (Firm), *The Fondamental and Pratice of Overhead Power Lines* vol. 2. Johannesburg: Crown Publications, 2004.

[38] EPRI, "Polymer Insulator Survey 2002: Utility Field Experience and In-Service Failures," EPRI, Palo Alto2003.

[39] A. Bansal, "Finite element simulation of mechanical characterization of composite insulators," Thesis, Dept. of Materials Science and Engineering, Oregon Graduate Institute of Science & Technology, Oregon 1996.

[40] D. Dumora, M. Gaudry, D. Feldman, "Mechanical behaviour of flexurally stressed composite insulators," *IEEE Transactions on Power Delivery,* vol. 5, No2, 1990.

[41] R. Mier-Maza, J. Lanteigne, and C. de Tourrell, "Failure Analysis of Synthetic Insulators with Fiberglass Rod Submitted to Mechanical Loads," *Power Engineering Review, IEEE,* vol. PER-3, pp. 44-44, 1983.

[42] F. Schmuck and C. de Tourreil, "Brittle Fractures of Composite Insulators an Investigation of their Occurrence and Failure Mechanisms and a Risk Assessment," *CIGRE WG 22-03*.

[43] B. Mobasher, D. Kingsbury, J. Montesinos, and R. S. Gorur, "Mechanical aspects of crimped glass reinforced plastic (GRP) rods," *Power Delivery, IEEE Transactions on,* vol. 18, pp. 852-858, 2003.

[44] J.Wańkowicz, J.Bielecki, and E.Strużewska, "Damage Limit of Composite Long Rod Insulators Subjected to Cyclic Loads," presented at the 41st International Council on Large Electric Systems CIGRÉ, Paris 2010.

[45] A. Prenleloup, T. Gmu, J. Botsis, and K. O. Papailiou, "Stress and failure analysis of crimped metal-composite joints used in electrical insulators subjected to bending," *4th International conference on NDT*, 2007.

[46] J. G. Wankowicz and J. Bielecki, "Life estimation for long rod composite insulators subjected to accelerating ageing by combined static and cyclic loading," *Dielectrics and Electrical Insulation, IEEE Transactions on,* vol. 18, pp. 106-113, 2011.

[47] M. Serridge and T. R. Licht, *Piezoelectric Accelerometers and Vibration Preamplifiers : Theory and Application Handbook*. DK-2600 Glostrup, Denmark, 1987.

[48] NI. Strain gauge configuration types [Online]. Available: http://www.ni.com/white-paper/4172/en/, 12/10/2014

[49] NI. Measuring with strain gauges [Online]. Available: http://www.ni.com/white-paper/3642/en/, 12/10/2014

[50] "IEEE Guide for Laboratory Measurement of the Power Dissipation Characteristics of Aeolian Vibaration," *IEEE Std 664-1993*, p. i, 1993.

[51] C. R. F. Azevedo, A. M. D. Henriques, A. R. Pulino Filho, J. L. A. Ferreira, and J. A. Araújo, "Fretting fatigue in overhead conductors: Rig design and failure analysis of a Grosbeak aluminium cable steel reinforced conductor," *Engineering Failure Analysis*, vol. 16, pp. 136-151, 1// 2009.

[52] S. Goudreau, F. Levesque, A. Cardou, and L. Cloutier, "Strain measurements on ACSR conductors during fatigue tests II - Stress fatigue indicators," *Power Delivery, IEEE Transactions on*, vol. 25, pp. 2997-3006, 2010.

[53] S. Guerard, B. Godard, and J. L. Lilien, "Aeolian vibrations on power-line conductors, evaluation of actual self damping," *Power Delivery, IEEE Transactions on*, vol. 26, pp. 2118-2122, 2011.

[54] Y. Kubelwa, "The relationship between the bending amplitude and bending stress/strain at the mouth of a so-called square-faced clamp for different conductor sizes and different tensile loads : Experimental Approach," MSc, Mechanical Engineering UKZN, Durban, 2013.

[55] F. Levesque, S. Goudreau, A. Cardou, and L. Cloutier, "Strain Measurements on ACSR Conductors During Fatigue Tests I : Experimental Method and Data," *Power Delivery, IEEE Transactions on*, vol. 25, pp. 2825-2834, 2010.

[56] O. Nigol, R. C. Heics, and H. J. Houston, "Aeolian vibration of single conductors and its control," *Power Apparatus and Systems, IEEE Transactions on*, vol. PAS-104, pp. 3245-3254, 1985.

[57] IEEE, "IEEE Guide for Aeolian vibration field measurement of overhead conductors," *IEEE Std 1368-2006*, pp. 1-35, 2006.

[58] J. S. Barrett and Y. Motlis, "Allowable tension levels for overhead-line conductors," *Generation, Transmission and Distribution, IEE Proceedings-*, vol. 148, pp. 54-59, 2001.

[59] M. Sochor, *Strength of Materials I*: České vysoké učení technické, 2011.

[60] T. Gopalan, "Fatigue failure of insulator string of overhead transmission line," *J. Eng. Mech.*, vol. 117(1), pp. 88–99, 1991.

[61] C. M. Harris and C. E. Crede, *Shock and Vibration Handbook*: McGraw-Hill, 1976.

[62] J. Wankowicz and J. Bielecki, "Models of the long-term mechanical strength of long rod composite insulators," *Dielectrics and Electrical Insulation, IEEE Transactions on,* vol. 17, pp. 360-367, 2010.

Appendices

Appendix A: Characteristics of different types of power line motion

From the EPRI Transmission Line Reference Book, “Wind-induced conductor Motion”, based on EPRI Research Project 792.

	Aeolian Vibration	Conductor Galloping	Wake-induced Oscillation
Types of Overhead Lines Affected	All	All	Limited to lines with bundled conductors
Approx. Frequency Range (Hz)	3 to 150	0.08 to 3	0.15 to 10
Approx. Range of Vibration Amplitudes (Peak-to-Peak) (Expressed in conductor diameters)	0.01 to 1	5 to 300	Rigid-Body Mode: 0.5 to 80 Subspan Mode: 0.5 to 20
Weather Conditions Favoring Conductor Motion			
Wind Character	Steady	Steady	Steady
Wind Velocity	1 to 7 m/s (2 to 15 mph)	7 to 18 m/s (15 to 40 mph)	4 to 18 m/s (10 to 40 mph)
Conductor Surface	Bare or uniformly iced (i.e. hoarfrost)	Asymmetrical ice deposit on conductor	Bare, dry
Design Conditions Affecting Conductor Motion	Line tension, conductor self-damping, use of dampers, armor rods	Ratio of vertical natural frequency to torsional natural frequency; sag ratio and support conditions	Subconductor separation, tilt of bundle, subconductor arrangement, subspan staggering
Damage			
Approx, time required for severe damage to develop	3 mos to 20 + years	1 to 48 hours	1 mo to 8 + years
Direct causes of damage	Metal fatigue due to cyclic bending	High dynamic loads	Conductor clashing, accelerated wear in hardware
Line components most affected by damage	Conductor and shield wire strands	Conductor, all hardware, insulators, structures	Suspension hardware, spacers, dampers, conductor strands

Appendix B: Mechanical and Electrical characteristics of the composite insulators

Mechanical and Electrical characteristic	Line post insulator	Suspension Insulator
One minute power frequency withstand voltage (50Hz, wet) (kV)	385	395
One minute power frequency withstand voltage (50Hz, dry) (kV)	445	465
Lightning impulse withstand voltage (1.2/50, positive) (kV)	775	775
Minimum dry arcing distance (mm)	1218	1321
Minimum creepage distance (mm)	4500	4525
Specified cantilever load (SCL) (kN)	13.3	-
Specified mechanical load (SML)	-	120
Maximum design cantilever load (MDCL) (kN)	6	-
Routine Test Load (kN)	-	60
Maximum design torsional load (MDTL) (Nm)	3200	-
Termination	Flange	Ball & Socket
Number of sheds (small / large)	19/20	23/24
Mass (approx.) (kg)	26.54	5.36

Appendix C: Overall Dimensions of the insulator supports (Suspension and line post)

All supports were designed using Solidworks.

Anchor tower (Suspension insulator)

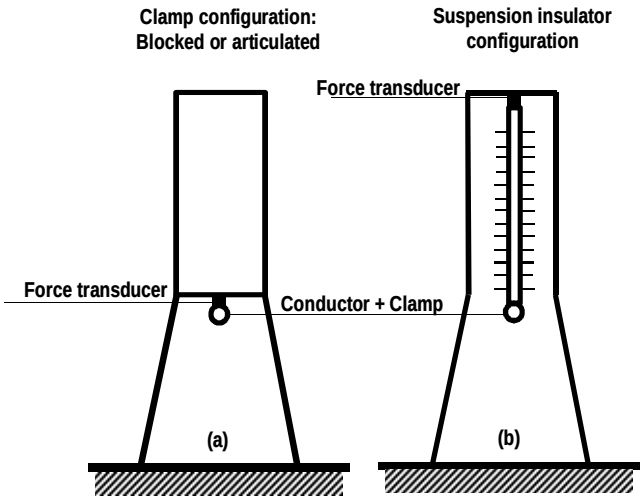

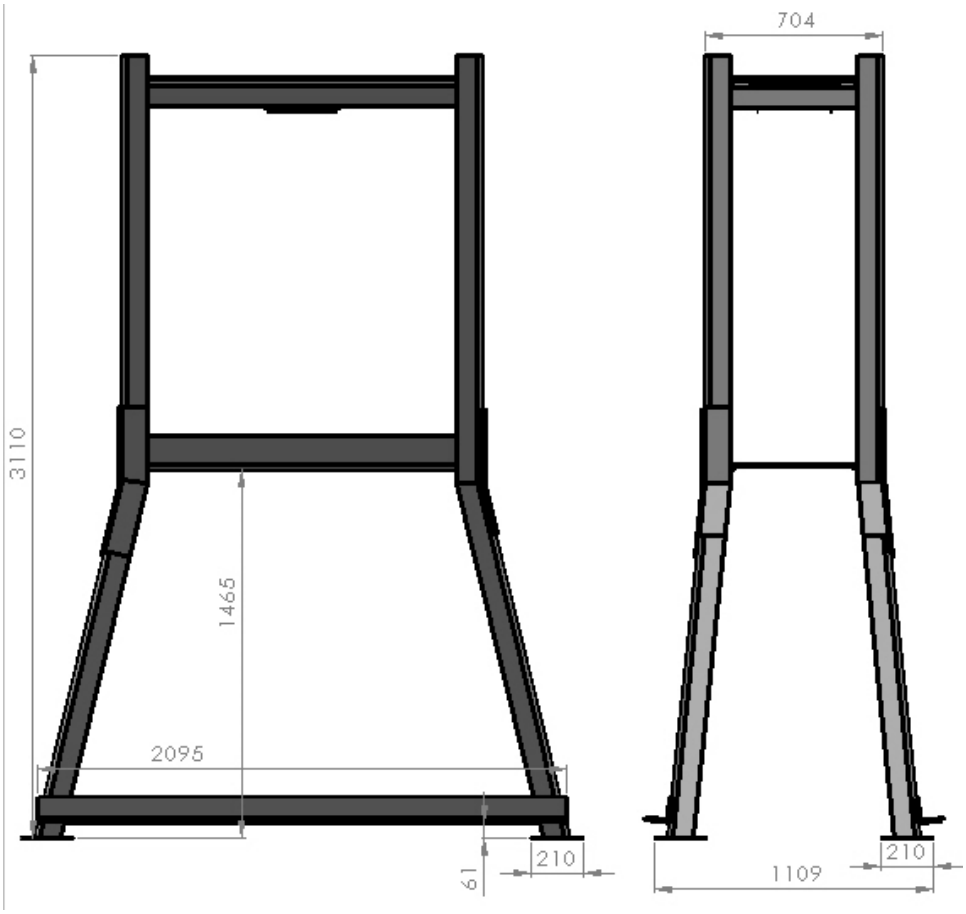

Line post support

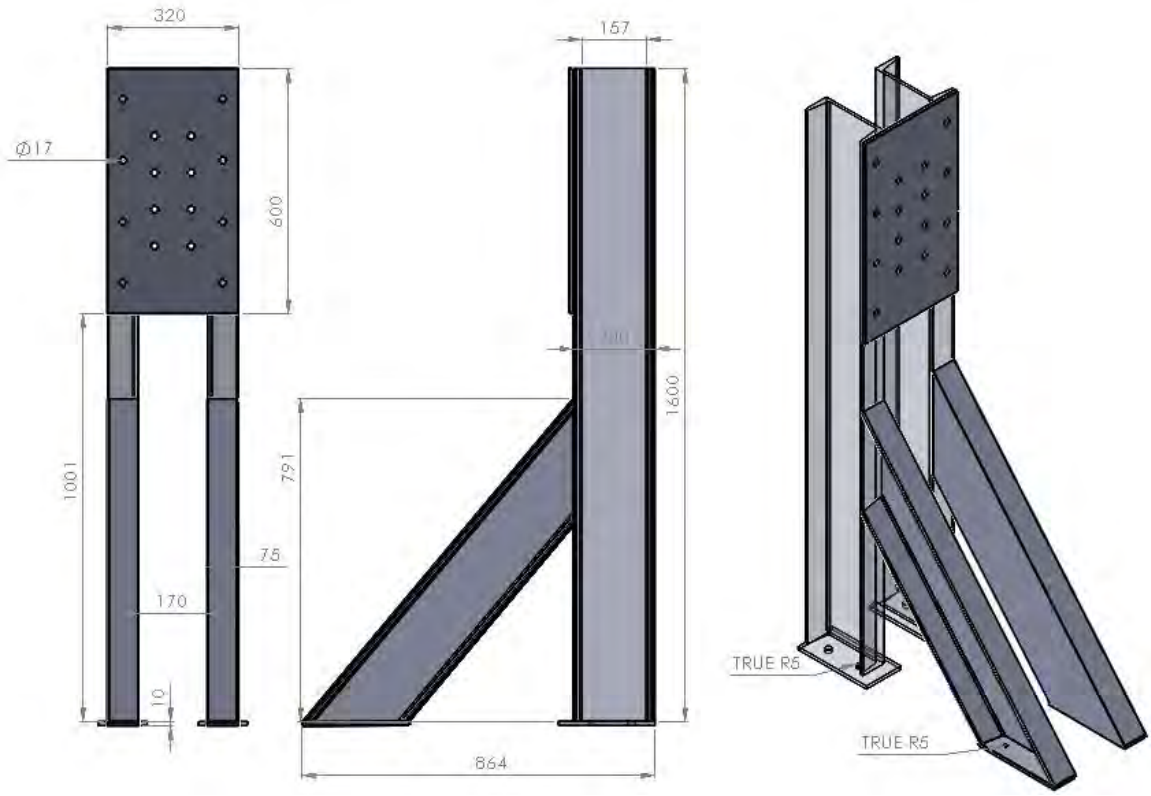

Appendix D: Static tension of the conductors

The limits of the static tension (%UTS) proposed here are the intersection point between the conductor's sag and the ESKOM's EDS corresponded to transmission line in SA for the conductors mentioned.

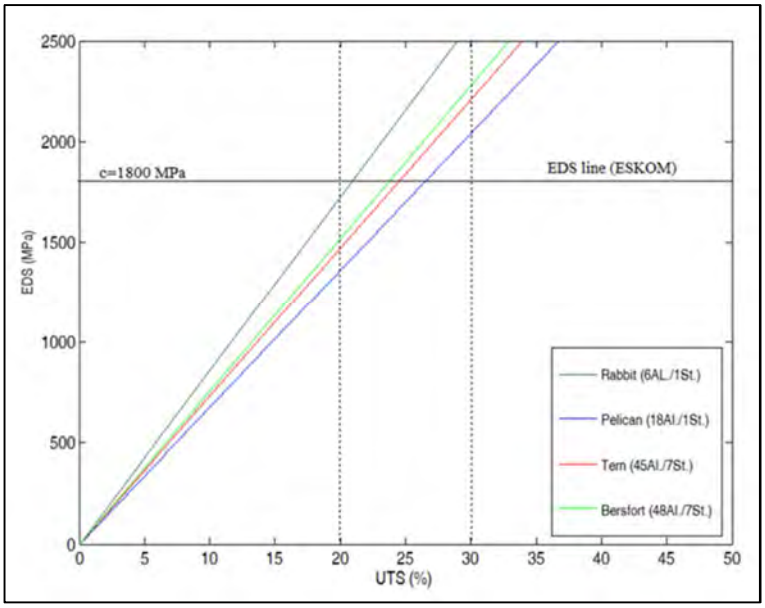

Figure C.1: Recommended static tension for major ACSR conductors (Rabbit, Pelican, Tern and bersfort) used by ESKOM

Appendix E: Swept frequency results of conductors

E.1: Pelican conductor

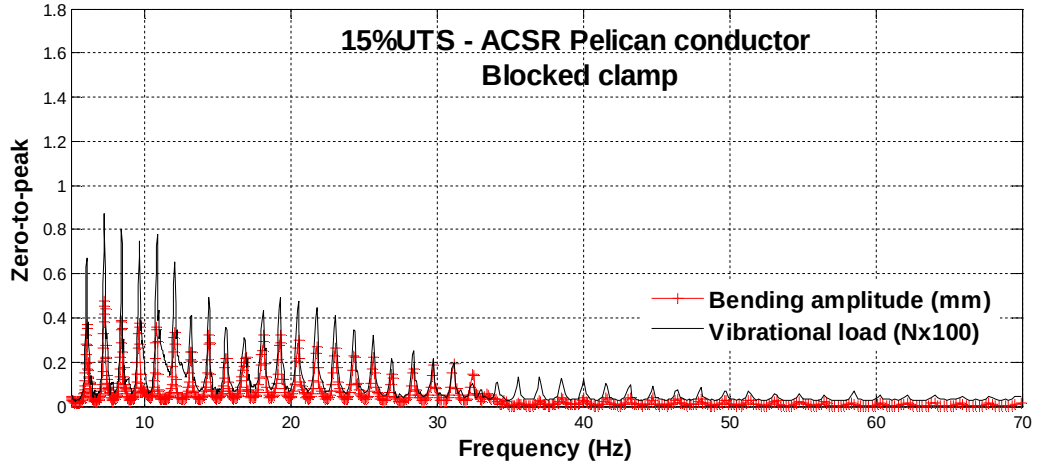

Figure E.1: Mechanical loads and bending amplitudes vs. frequency at 15% UTS for the ACSR Pelican conductor with the blocked clamp

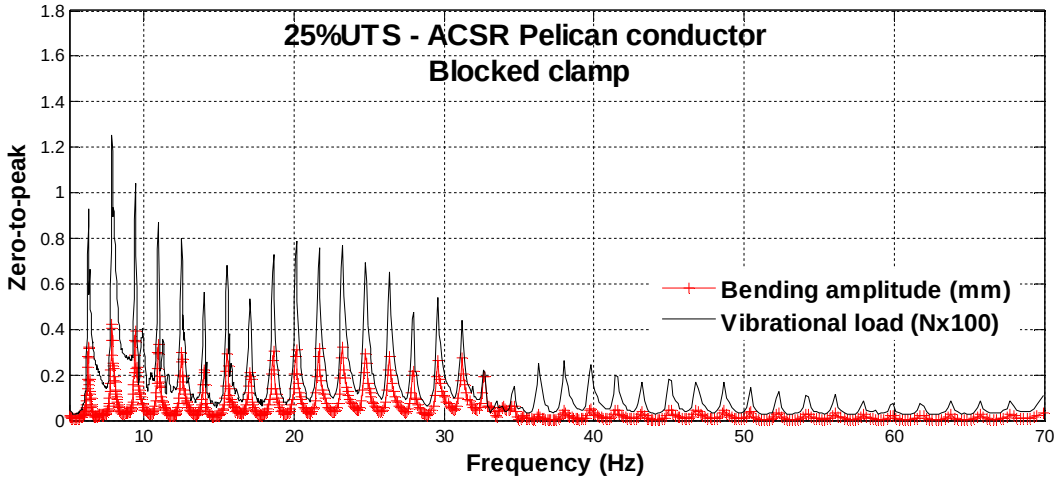

Figure E.2: Mechanical loads and bending amplitudes vs. frequency at 25% UTS for the ACSR Pelican conductor with the blocked clamp

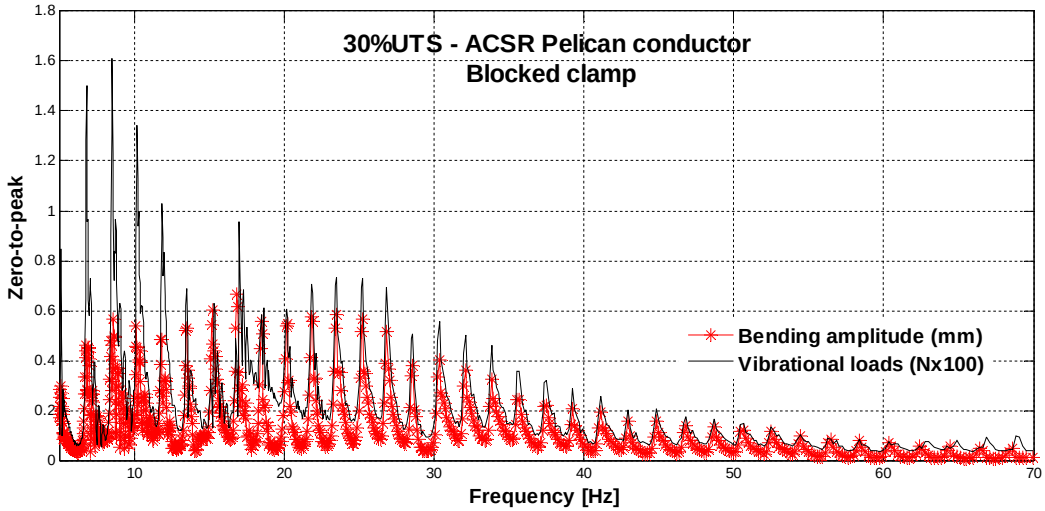

Figure E.3: Mechanical loads and bending amplitudes vs. frequency at 30% UTS for the ACSR Pelican conductor with the blocked clamp

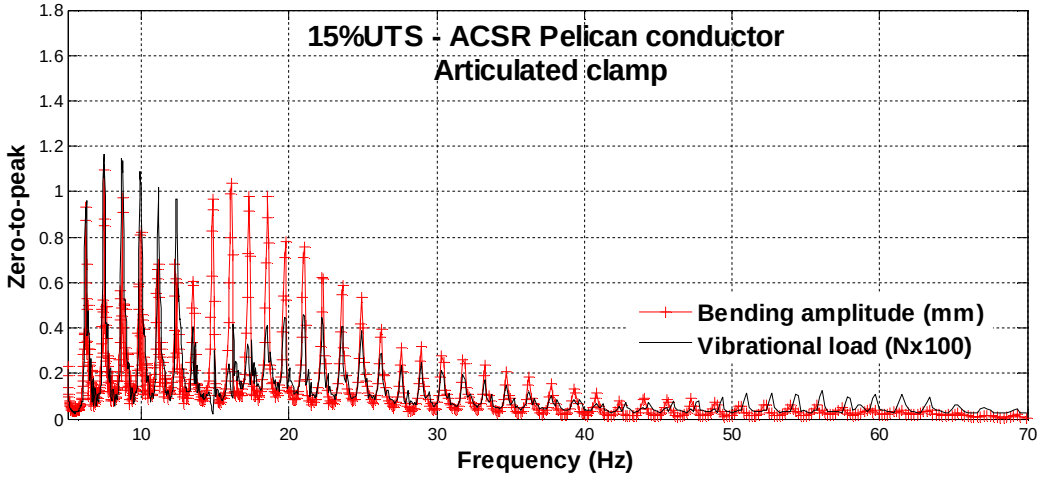

Figure E.4: Mechanical loads and bending amplitudes vs. frequency at 15% UTS for the ACSR Pelican conductor with the articulated clamp

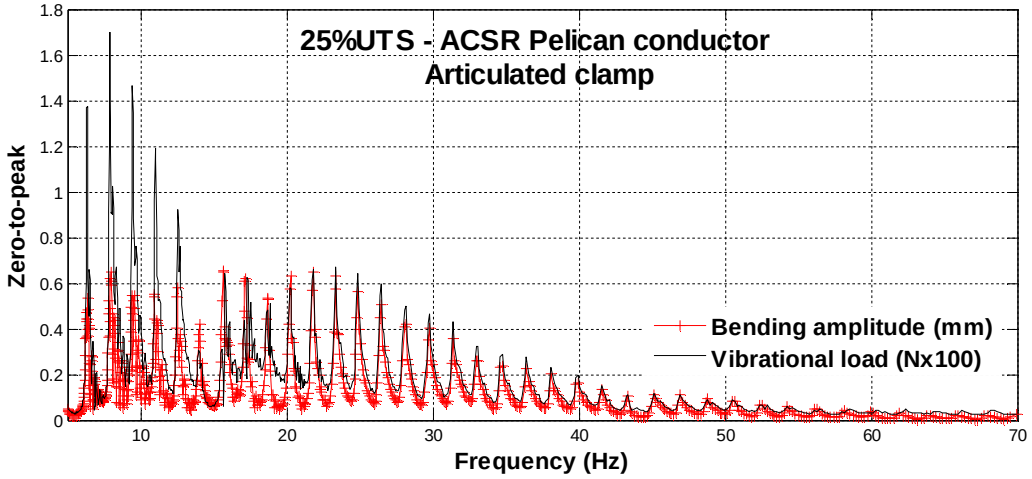

Figure E.5: Mechanical loads and bending amplitudes vs. frequency at 25% UTS for the ACSR Pelican conductor with the articulated clamp

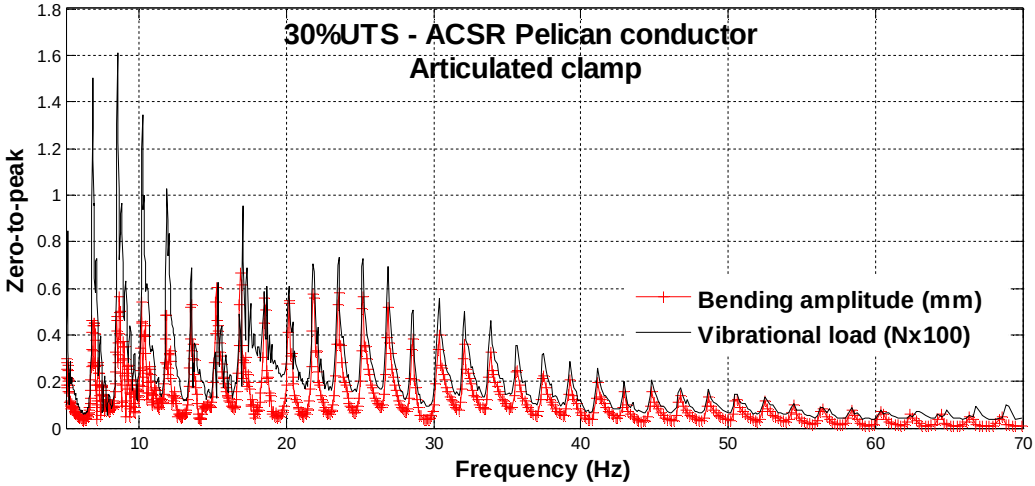

Figure E.6: Mechanical loads and bending amplitudes vs. frequency at 30% UTS for the ACSR Pelican conductor with the articulated clamp

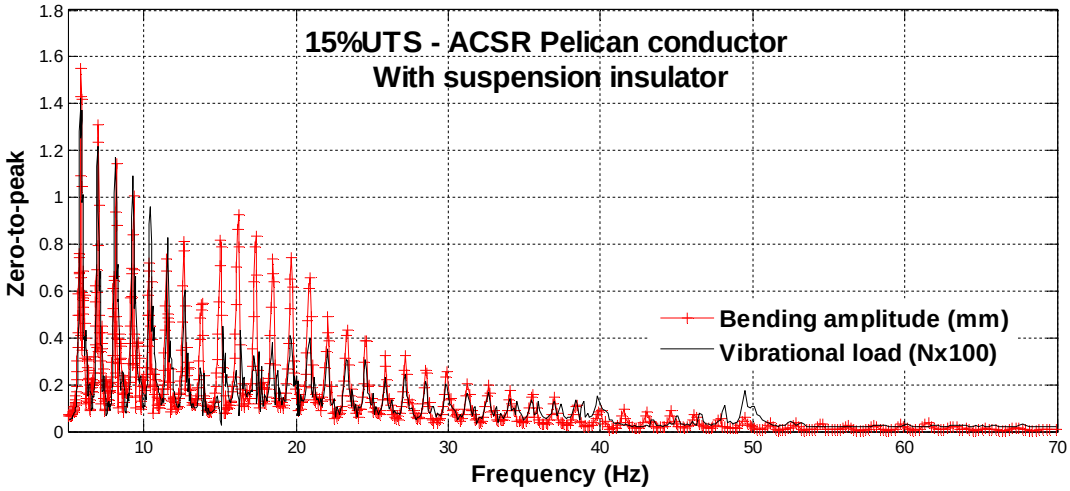

Figure E.7: Mechanical loads and bending amplitudes vs. frequency at 15% UTS for the ACSR Pelican conductor with the suspension insulator

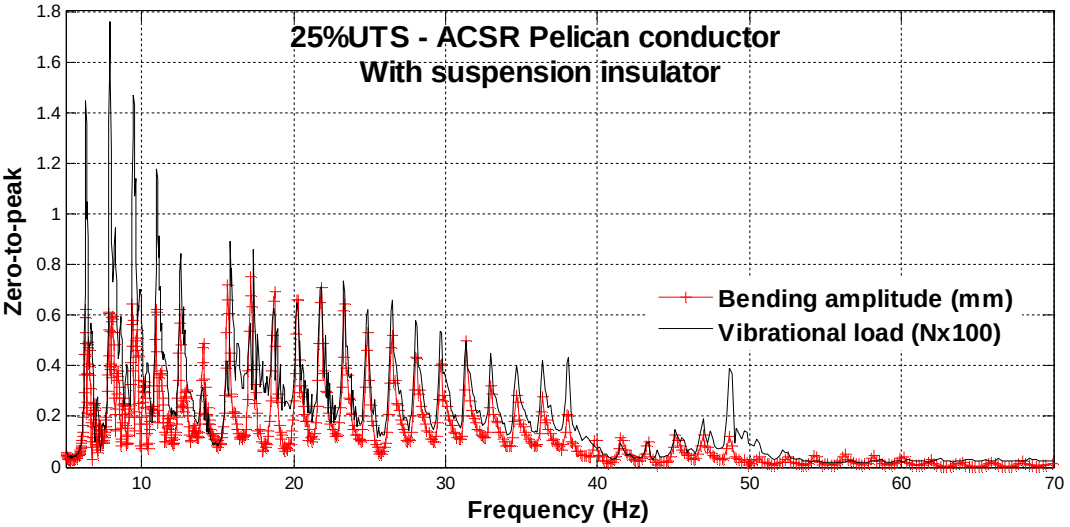

Figure E.8: Mechanical loads and bending amplitudes vs. frequency at 25% UTS for the ACSR Pelican conductor with the suspension insulator

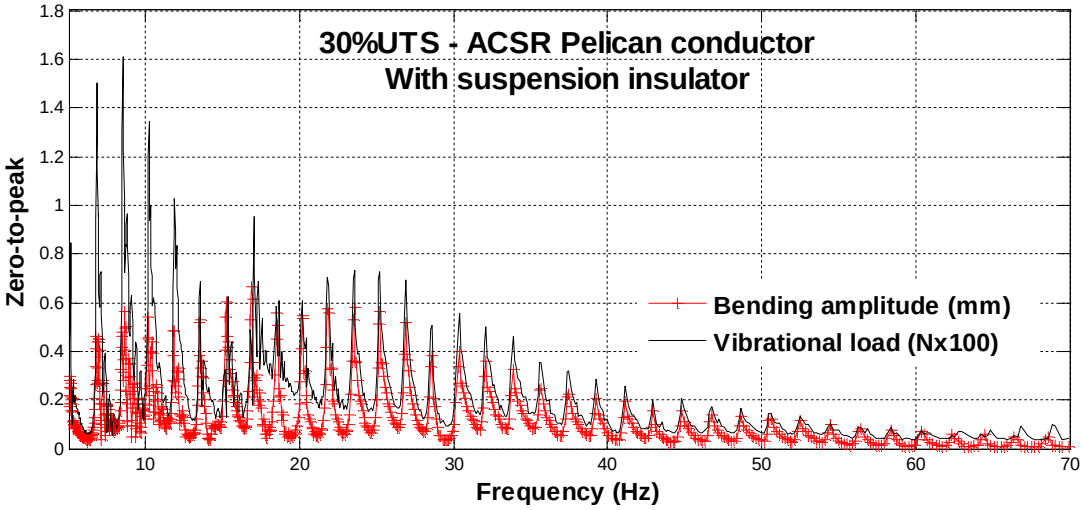

Figure E.9: Mechanical loads and bending amplitudes vs. frequency at 30% UTS for the ACSR Pelican conductor with the suspension insulator

E.2: Tern conductor

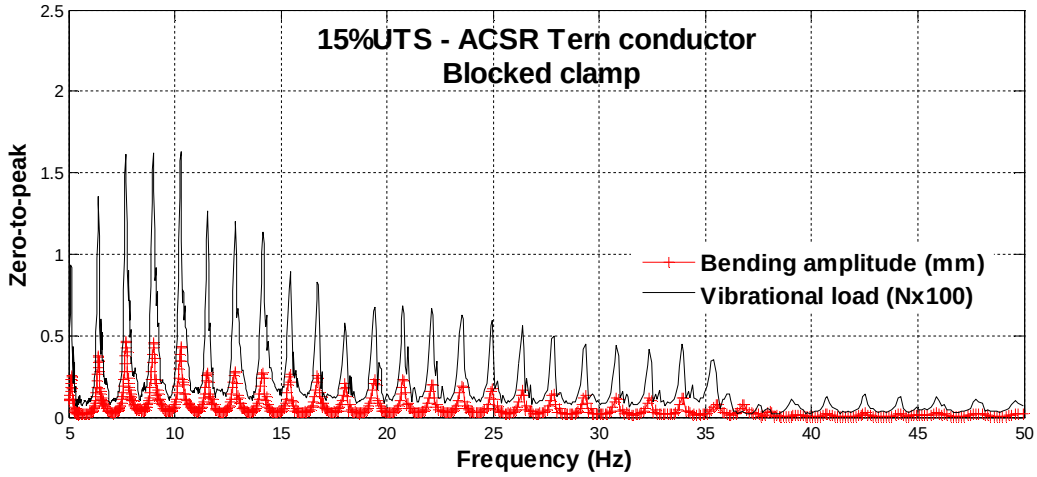

Figure E.10: Mechanical loads and bending amplitudes vs. frequency at 15% UTS for the ACSR Tern conductor with the blocked clamp

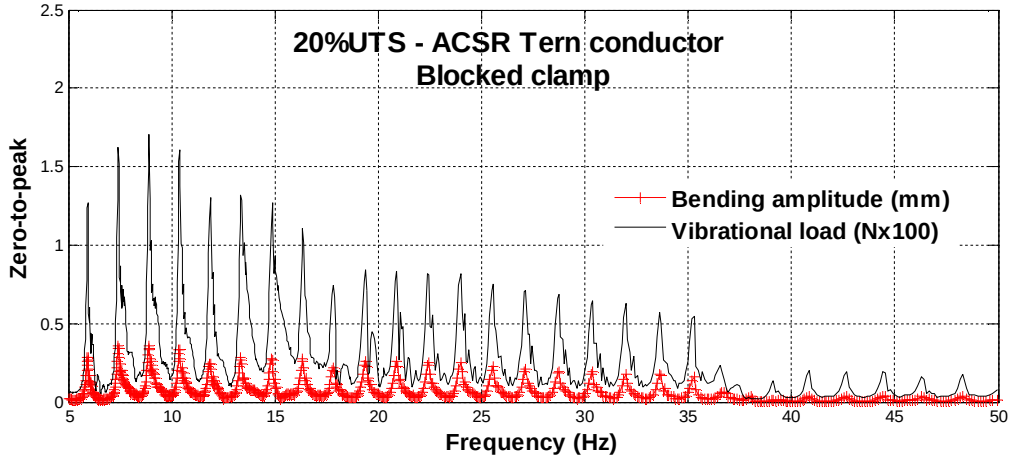

Figure E.11: Mechanical loads and bending amplitudes vs. frequency at 20% UTS for the ACSR Tern conductor with the blocked clamp

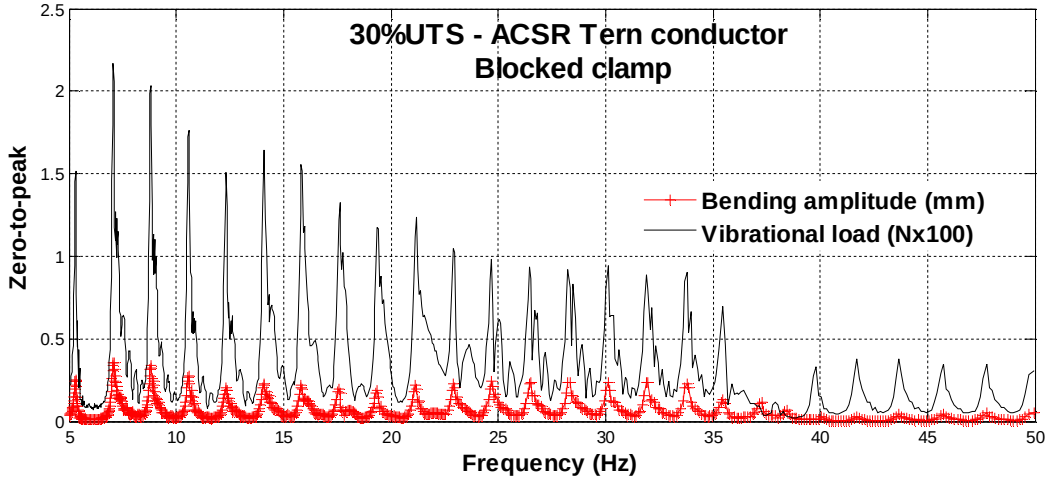

Figure E.12: Mechanical loads and bending amplitudes vs. frequency at 30% UTS for the ACSR Tern conductor with the blocked clamp

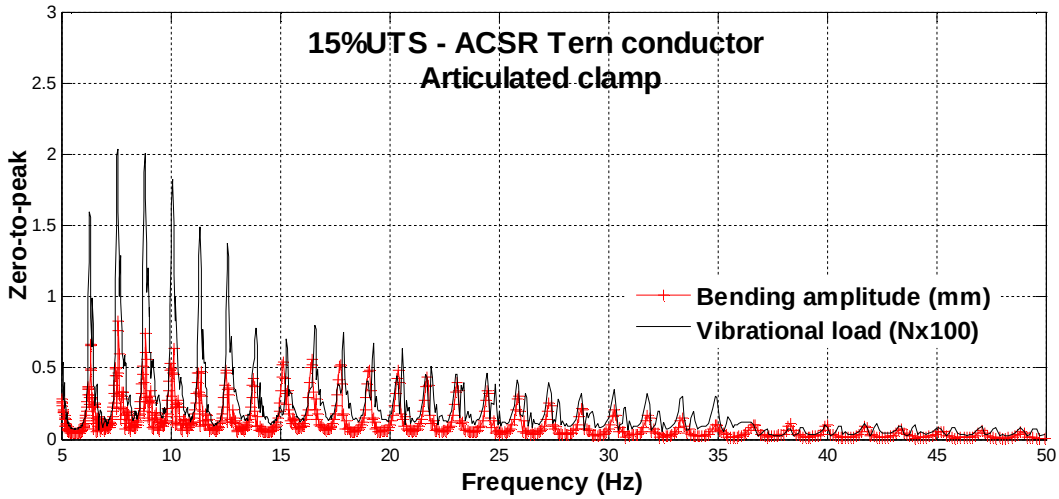

Figure E.13: Mechanical loads and bending amplitudes vs. frequency at 15% UTS for the ACSR Tern conductor with the articulated clamp

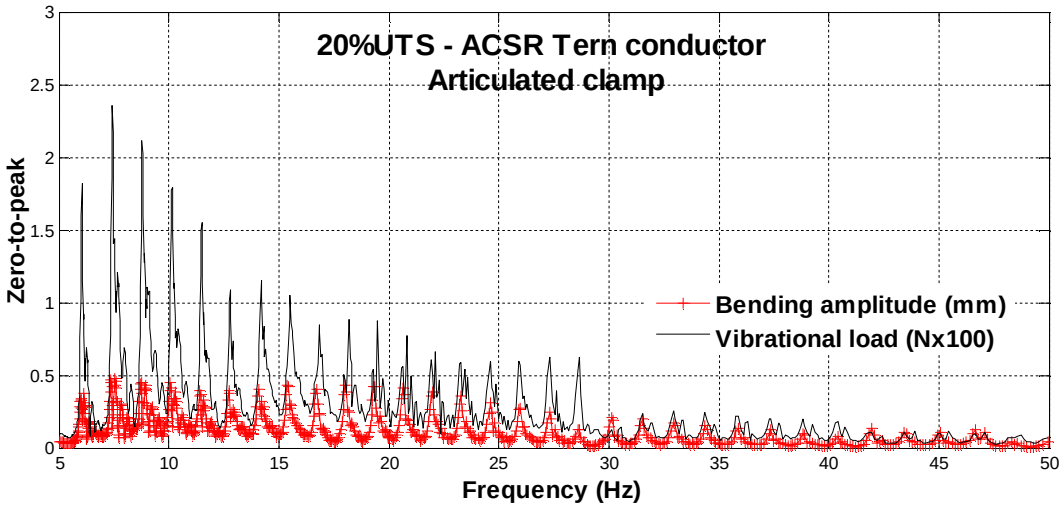

Figure E.14: Mechanical loads and bending amplitudes vs. frequency at 20% UTS for the ACSR Tern conductor with the articulated clamp

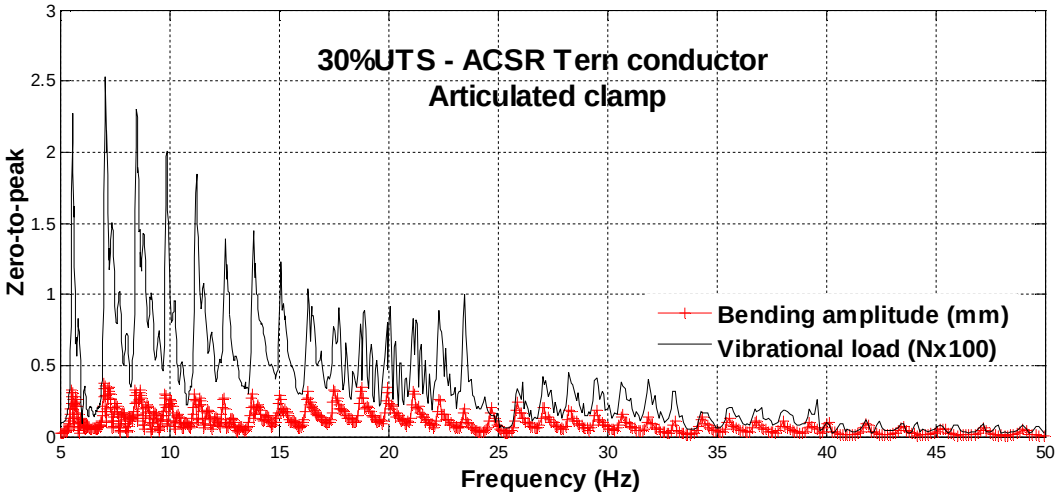

Figure E.15: Mechanical loads and bending amplitudes vs. frequency at 30% UTS for the ACSR Tern conductor with the articulated clamp

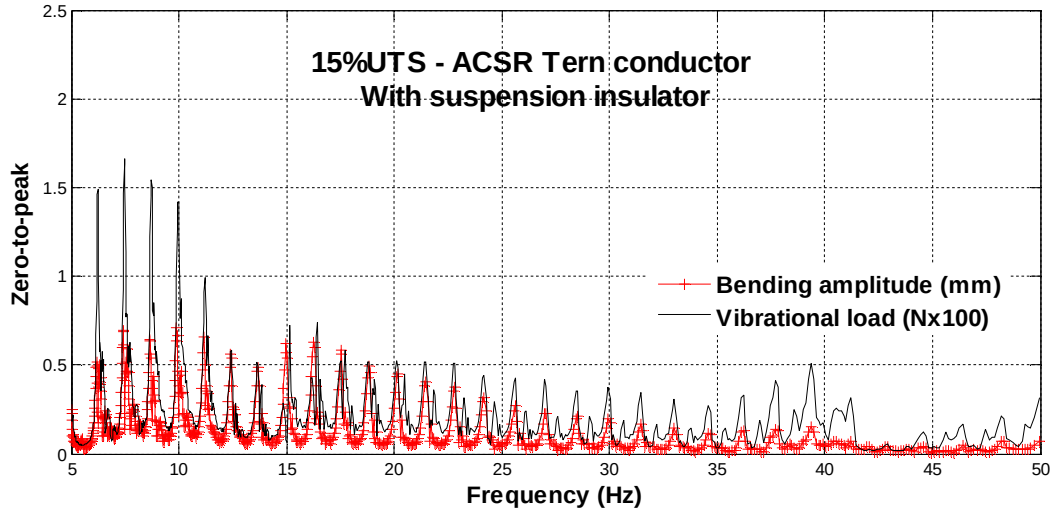

Figure E.16: Mechanical loads and bending amplitudes vs. frequency at 15% UTS for the ACSR Tern conductor with the suspension insulator

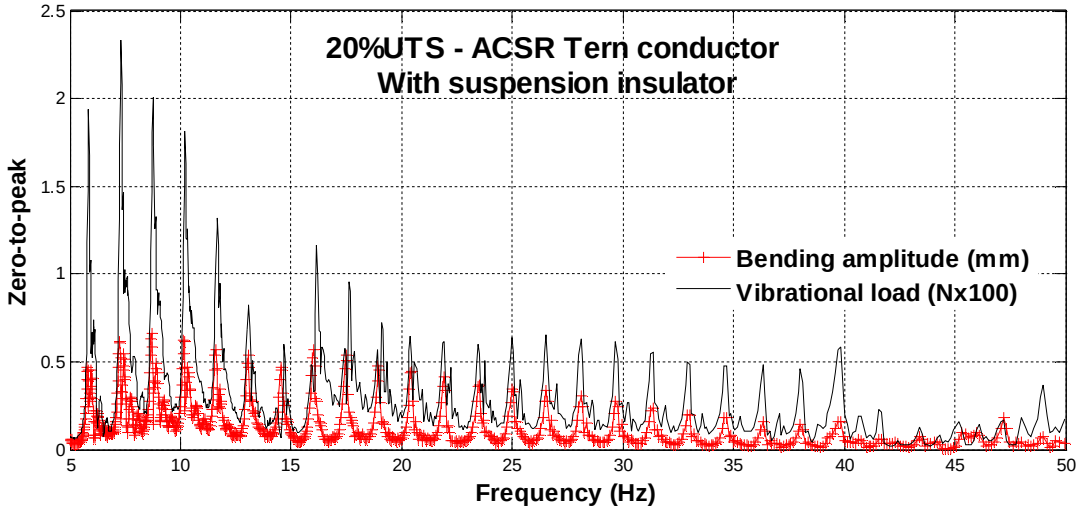

Figure E.17: Mechanical loads and bending amplitudes vs. frequency at 20% UTS for the ACSR Tern conductor with the suspension insulator

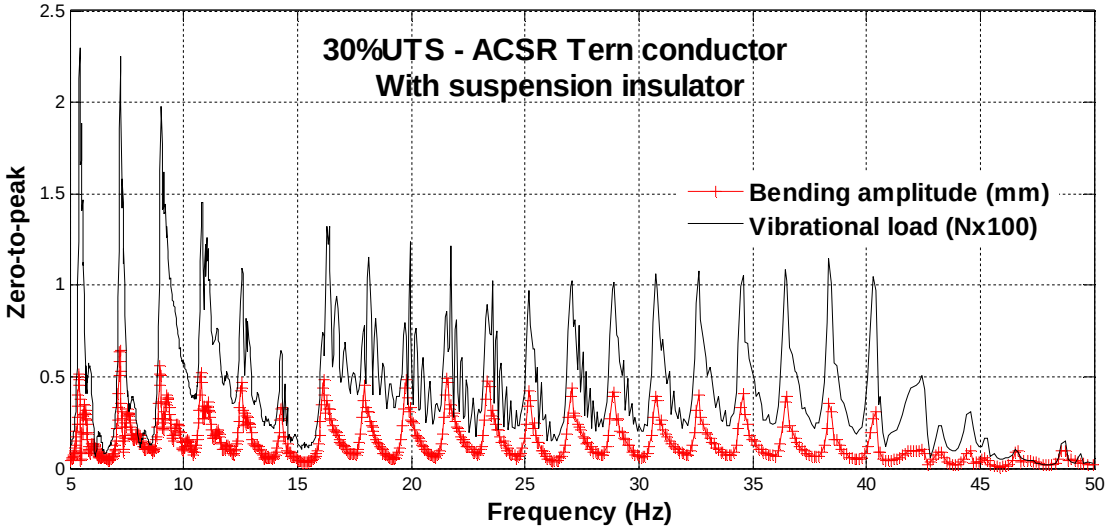

Figure E.18: Mechanical loads and bending amplitudes vs. frequency at 30% UTS for the ACSR Tern conductor with the suspension insulator

Appendix F: Results of dynamical loads of conductors at different clamp configurations

Table F.1: Pelican conductor - Frequencies of dynamical loads measurements

UTS (%)	Frequency of dynamical loads measurements (hz)					
	Articulated suspension clamp		Blocked suspension clamp		Composite insulator	
	I	II	I	II	I	II
15	9.97	15.27	8.47	15.40	9.25	15.14
20	9.90	15.78	9.70	15.42	9.14	15.37
25	9.40	15.71	9.43	15.90	9.51	16.09
30	8.69	15.50	8.47	15.40	10.10	15.25

Table F.2: Pelican conductor - Dynamical loads measurements

Peak-to-peak bending amplitude (mm)	Vibrational loads (N)											
	Blocked clamp configuration				Articulated clamp configuration				Suspension insulator configuration			
	15	20	25	30	15	20	25	30	15	20	25	30
0.1	23	27	32	36	13	25	20	24	13	22	19	25
0.2	40	52	63	65	23	32	35	39	23	37	34	42
0.3	57	74	88	98	33	41	50	58	32	47	50	60
0.4	73	97	115	127	42	54	66	77	41	63	65	78
0.5	90	120	141	158	51	67	82	94	51	76	82	96
0.6	106	144	167	187	62	82	98	111	60	91	98	114
0.7	120	183	190	214	73	96	116	129	69	100	114	132
0.8	135	189	214	240	79	109	128	147	77	112	130	149
0.9	149	199	241	259	90	124	143	164	90	123	146	166
1.0	165	217	278	288	99	142	161	181	100	137	163	182

Table F.3. Tern conductor - Frequencies of dynamical loads measurements

UTS (%)	Frequency of dynamical loads measurements (hz)					
	Free suspension clamp		Blocked suspension clamp		Composite insulator	
	I	II	I	II	I	II
15	10.170	18.000	10.400	17.160	8.640	15.364
20	16.630	18.900	8.990	15.120	7.430	15.400
25	17.192	20.520	11.350	16.420	8.624	17.024
30	16.928	17.797	10.810	12.530	12.790	18.300

Table F.4. Tern conductor - Dynamical loads measurements

Peak-to-peak bending amplitude (mm)	Vibrational loads (N)											
	Blocked clamp configuration				Articulated clamp configuration				Suspension insulator configuration			
	15	20	25	30	15	20	25	30	15	20	25	30
0.1	41	45	47	58	16	26	30	40	16	26	30	40
0.2	80	84	91	111	29	48	59	76	29	48	59	76
0.3	108	126	135	155	42	70	89	112	42	70	89	112
0.4	152	166	177	197	56	96	116	148	56	96	116	148
0.5	167	202	216	238	69	116	145	184	69	116	145	184
0.6	196	240	254	283	84	139	174	219	84	139	174	219
0.7	218	277	291	327	106	160	201	256	106	160	201	256
0.8	257	316	323	361	127	181	231	292	127	181	231	292
0.9	289	351	360	394	145	202	259	327	145	202	259	327
1.0	320	380	403	476	159	226	288	364	159	226	288	364

Appendix G: Results of strains of the suspension insulator

G.1: Static bending strain measurement

Table G.1: Static bending strain measurement

Force applied (N)	Strain (με) of the suspension insulator		
	Gauge 1	Gauge 2	Gauge 3
0.0000	0.5713	1.3584	0.5387
37.0818	0.8662	18.2228	0.5632
136.8986	1.2807	32.1781	0.5635
236.7644	3.4310	37.3677	4.1553
336.6302	8.2402	39.9584	10.9804
435.7112	14.5353	40.0674	18.8954
535.5770	20.2245	41.3663	27.2254
623.8670	27.6103	41.9880	30.4773
719.9559	35.4623	42.7839	41.7279

G.2: Pelican conductor

Table G.2: Strain (με) of the suspension insulator with ACSR Pelican conductor (15%UTS)

Peak-to-peak bending amplitude (mm)	Frequency (Hz)					
	9.25			15.13		
	Gauge 1	Gauge 2	Gauge 3	Gauge 1	Gauge 2	Gauge 3
0.1	2.3033	4.9693	3.8462	2.4515	3.1683	2.8824
0.2	3.6311	6.8596	4.4120	3.9685	4.0129	4.2707
0.3	5.5061	8.8459	5.4500	5.6907	4.6571	6.7044
0.4	7.1024	10.3683	5.9359	7.9759	6.2138	9.8412
0.5	9.1962	12.2920	6.8742	10.9221	7.6347	14.3094
0.6	11.1595	13.7424	7.5291	17.9159	15.4218	25.5492
0.7	13.9777	15.6577	8.6137	15.6898	11.1361	27.7162
0.8	16.6017	17.5590	9.2007	24.8044	20.0729	30.5738
0.9	20.5074	19.7912	10.4625	79.1791	108.9190	90.5036
1.0	24.3407	21.3222	11.3871	87.2268	124.0956	100.4634

Table G.3: Strain (με) of the suspension insulator with ACSR Pelican conductor (20%UTS)

Peak-to-peak bending amplitude (mm)	Frequency (Hz)					
	9.14			15.37		
	Gauge 1	Gauge 2	Gauge 3	Gauge 1	Gauge 2	Gauge 3
0.1	2.5496	2.7489	1.8480	1.3212	3.5801	3.5246
0.2	3.7770	5.3998	4.5312	1.7356	5.2887	5.5185
0.3	5.3702	5.7884	4.2470	1.6198	3.5578	4.0439
0.4	7.3114	8.9654	6.6071	2.3729	4.3980	6.1815
0.5	9.9350	9.3398	7.2901	3.3435	5.9572	9.4612
0.6	11.8425	12.2518	8.6395	5.0647	9.4217	14.3472
0.7	17.1485	25.2888	17.1926	6.8403	9.8632	18.7793
0.8	21.3888	36.1746	24.4394	7.5849	11.4166	22.6513
0.9	23.7245	47.6205	31.1029	8.2288	12.3357	27.1573
1.0	25.9621	50.5866	35.4225	20.5522	17.7158	34.8865

Table G.4: Strain (με) of the suspension insulator with ACSR Pelican conductor (25%UTS)

Peak-to-peak bending amplitude (mm)	Frequency (Hz)					
	9.51			16.09		
	Gauge 1	Gauge 2	Gauge 3	Gauge 1	Gauge 2	Gauge 3
0.1	2.6027	3.2039	2.1081	1.8686	2.0549	1.5433
0.2	3.9807	5.0370	2.9304	2.5057	2.9248	1.9755
0.3	5.6421	6.7996	3.8451	2.9167	3.8260	2.3914
0.4	7.5076	8.5152	4.7633	3.0720	4.3592	3.0962
0.5	9.3910	10.4447	5.6628	3.0781	5.2008	4.4203
0.6	11.8380	12.5043	6.6227	4.5219	7.1121	6.6347
0.7	14.7467	15.0167	7.8552	5.4107	9.4411	9.1955
0.8	17.9127	18.0434	9.3825	5.7490	10.8542	11.5159
0.9	20.8625	19.4619	9.8199	5.9419	12.0646	13.7960
1.0	24.2373	21.5507	10.3927	7.3495	13.1285	16.5068

Table G.5: Strain (με) of the suspension insulator with ACSR Pelican conductor (30%UTS)

Peak-to-peak bending amplitude (mm)	Frequency (Hz)					
	10.10			15.25		
	Gauge 1	Gauge 2	Gauge 3	Gauge 1	Gauge 2	Gauge 3
0.1	2.4034	4.0808	2.4516	1.6494	2.5676	2.1047
0.2	3.6580	6.1292	3.3765	2.3794	3.5949	3.1148
0.3	5.2563	8.9803	4.2108	3.8434	4.7326	5.0243
0.4	6.8031	11.2547	4.9888	5.2366	6.2096	7.4339
0.5	9.0627	13.3765	6.1503	6.7825	7.3228	11.2690
0.6	12.2153	17.2943	7.1423	9.6907	9.5734	16.9527
0.7	14.6133	20.1861	8.3046	16.0179	13.2205	21.2868
0.8	17.9854	23.3443	9.7172	24.1783	16.7616	28.1852
0.9	21.4931	26.5872	11.7400	23.5027	20.8612	39.7385
1.0	24.9531	29.0913	14.0032	60.0546	56.3694	73.7584

G.3: Tern conductor

Table G.6: Strain (με) of the suspension insulator with ACSR Tern conductor (15%UTS)

Peak-to-peak bending amplitude (mm)	Frequency (Hz)					
	8.64			15.61		
	Gauge 1	Gauge 2	Gauge 3	Gauge 1	Gauge 2	Gauge 3
0.1	4.1203	7.0316	2.0227	2.5742	3.2832	2.0338
0.2	6.3275	10.4206	2.4500	3.9589	2.7021	3.1589
0.3	8.8652	11.1143	3.8549	5.8859	3.6263	5.0206
0.4	11.0752	11.4567	4.4529	6.8288	5.1051	7.6212
0.5	12.5175	14.1183	5.3360	8.1210	6.7283	10.1649
0.6	15.6528	16.4409	6.5675	10.2301	8.2419	13.6688
0.7	17.4647	18.1875	6.1754	16.6810	14.1142	27.7174
0.8	19.6880	18.1826	6.1217	21.3107	17.6453	36.3119
0.9	21.1378	17.7355	6.8899	26.8317	23.4916	46.2013
1.0	23.2756	16.5862	6.6074	29.1384	26.1099	54.8395

Table G.7: Strain (με) of the suspension insulator with ACSR Tern conductor (20%UTS)

Peak-to-peak bending amplitude (mm)	Frequency (Hz)					
	7.43			15.40		
	Gauge 1	Gauge 2	Gauge 3	Gauge 1	Gauge 2	Gauge 3
0.1	4.3397	15.3932	4.1930	1.7561	2.5960	2.3393
0.2	8.4980	34.8262	14.5382	2.6049	4.0684	4.7822
0.3	12.7938	40.9391	21.2459	5.6074	7.3895	6.7577
0.4	19.5326	46.9172	26.9400	5.5189	7.6086	12.6872
0.5	22.1232	48.4973	31.1534	6.8940	9.0933	16.6831
0.6	23.8927	50.2271	31.0622	10.1261	11.1227	22.0576
0.7	26.6457	52.4438	29.4460	14.2164	12.4219	27.9059
0.8	28.9841	55.5746	26.4375	20.6500	17.4356	36.5500
0.9	30.9860	56.5564	25.4129	26.7270	23.1021	47.3030
1.0	34.5706	59.6390	25.8867	26.4573	23.5478	56.8729

Table G.8: Strain (με) of the suspension insulator with ACSR Tern conductor (25%UTS)

Peak-to-peak bending amplitude (mm)	Frequency (Hz)					
	9.51			16.09		
	Gauge 1	Gauge 2	Gauge 3	Gauge 1	Gauge 2	Gauge 3
0.1	5.6300	9.6357	3.7742	4.2028	3.3570	2.2135
0.2	10.1398	13.6457	8.5794	4.7816	5.8561	3.8285
0.3	12.6199	19.0974	11.4106	6.6599	7.7864	5.9936
0.4	16.0082	22.1004	13.7756	8.8721	9.4302	7.2005
0.5	19.2885	25.8849	15.5831	11.8353	12.6175	9.9501
0.6	21.2618	28.0768	16.7724	15.3292	15.7501	13.1647
0.7	25.8825	29.1120	18.3201	16.4018	16.9546	15.8526
0.8	31.6632	33.7616	21.1179	17.6518	18.3613	18.8784
0.9	35.4293	40.2666	25.4209	18.4004	20.1156	22.3865
1.0	37.2245	40.4567	26.9526	22.6632	33.6715	33.7105

Table G.9: Strain (με) of the suspension insulator with ACSR Tern conductor (30%UTS)

Peak-to-peak bending amplitude (mm)	Frequency (Hz)					
	10.10			15.25		
	Gauge 1	Gauge 2	Gauge 3	Gauge 1	Gauge 2	Gauge 3
0.1	3.0984	3.1749	12.0278	4.1117	3.2496	2.3487
0.2	5.8217	5.8290	20.3146	5.3975	4.8516	2.6762
0.3	8.5287	8.7850	33.1062	7.7968	6.8765	3.5459
0.4	13.5316	13.0260	46.0419	10.1574	8.4693	4.5124
0.5	17.7291	18.4433	64.0624	12.2828	10.3557	5.7768
0.6	22.9878	24.4442	97.5855	13.2523	11.2217	6.9107
0.7	31.2242	31.6646	127.9485	14.1988	12.9274	8.4508
0.8	41.3792	38.2465	171.5508	16.1902	14.8766	10.2293
0.9	42.3670	36.2968	215.0421	18.6756	16.8095	12.1890
1.0	45.7629	33.0717	258.2287	21.1740	18.5682	14.7252

Appendix H: Results of bending strains of the line post insulator

H.1: Static bending strain measurement

Table H.1: Static bending strain measurement

Force applied (N)	Static bending strain measurement (με)			
	Gauge 1	Gauge 2	Gauge 3	Gauge 4
0.00	0.00	0.00	0.00	0.00
98.64	73.22	-77.77	0.19	-0.79
198.55	167.11	-175.35	-2.88	-4.69
298.47	257.69	-273.15	-8.05	-10.63
398.38	352.94	-367.73	-5.77	-12.25
498.25	446.79	-460.55	-3.51	-11.73
598.16	543.56	-551.18	3.01	-8.97
694.16	635.65	-639.49	7.12	-9.34
790.49	727.84	-727.59	12.39	-8.94
886.48	819.90	-815.86	17.21	-8.83
982.62	911.94	-904.32	21.75	-8.96
1078.71	1004.04	-992.82	25.73	-9.44
1173.28	1091.23	-1078.83	28.80	-10.57
1270.54	1183.69	-1167.28	33.70	-10.73
1366.14	1275.07	-1255.29	37.89	-11.37
1462.08	1362.40	-1340.22	41.31	-11.34
1559.30	1451.87	-1428.57	44.23	-12.86
1656.71	1543.07	-1515.51	50.21	-12.48
1753.19	1632.81	-1600.44	55.27	-12.48
1848.55	1722.06	-1687.11	58.78	-13.84
1943.80	1809.19	-1772.32	62.06	-15.40
2040.19	1898.75	-1859.09	65.97	-16.23
2277.34	2121.96	-2071.69	77.36	-17.45
2513.47	2346.58	-2280.22	90.21	-17.21
2748.22	2564.06	-2486.89	102.00	-18.03
2987.34	2784.56	-2698.68	112.83	-19.90
3228.13	3000.98	-2909.29	124.29	-21.90
3468.33	3217.40	-3116.82	136.16	-22.11

H.2: Blocked clamp configuration with Pelican conductor

Table H.2: Bending strain (με) of the line post insulator with ACSR Pelican conductor (15%UTS)

Peak-to-peak bending amplitude (mm)	Frequency (Hz)							
	9.10				14.91			
	Gauge 1	Gauge 2	Gauge 3	Gauge 4	Gauge 1	Gauge 2	Gauge 3	Gauge 4
0.1	5.2109	4.9798	0.7799	0.7405	7.8980	7.8448	2.9639	2.9883
0.2	11.0169	10.5814	1.8338	1.7816	15.4035	15.2884	4.8792	4.8027
0.3	15.0377	14.3176	2.0659	1.9207	24.0863	23.9357	9.9405	10.1389
0.4	20.9678	19.6058	1.9799	2.2430	31.6160	31.1995	13.0958	12.4586
0.5	24.4830	24.1552	2.1616	2.0633	38.6103	38.1062	16.0821	15.4589
0.6	29.5664	28.9480	2.3986	2.2364	47.6359	46.8071	12.6219	13.9371
0.7	34.9177	33.1756	2.4995	2.1602	56.9379	56.2863	13.4334	13.3549
0.8	40.7494	38.6988	2.7901	2.4952	62.8632	62.0153	15.1953	15.2351
0.9	44.3220	42.7603	3.3940	2.8968	65.8844	64.9058	14.5224	14.8457
1.0	51.0863	49.1756	3.6720	2.8300	70.5289	69.4765	15.0946	15.5639

Table H.3: Bending strain (με) of the line post insulator with ACSR Pelican conductor (20%UTS)

Peak-to-peak bending amplitude (mm)	Frequency (Hz)							
	9.57				15.64			
	Gauge 1	Gauge 2	Gauge 3	Gauge 4	Gauge 1	Gauge 2	Gauge 3	Gauge 4
0.1	5.4401	5.2794	1.6730	1.6773	9.3696	9.4313	2.5425	1.8870
0.2	9.4016	9.0737	1.6427	1.7271	17.7782	17.7757	4.1313	3.1743
0.3	13.5195	13.0563	1.7407	1.9549	26.5149	26.8080	6.9377	5.9460
0.4	17.9067	17.1660	1.7921	1.9266	34.6874	34.8585	11.6488	10.1500
0.5	22.3535	21.3874	1.8701	1.9697	42.1536	42.1383	15.5000	14.2834
0.6	26.2443	25.3505	1.8315	2.0265	49.2786	48.9264	17.3989	16.0217
0.7	30.4823	29.3701	1.9931	2.1336	51.5694	50.6724	13.7493	12.1135
0.8	34.5522	33.1402	1.9924	2.3327	55.1277	53.2127	13.5587	15.2255
0.9	39.0147	37.2649	2.1049	2.1814	61.0814	59.0223	15.5447	17.9250
1.0	43.2782	41.6042	2.1073	2.4081	75.4741	74.7840	26.3775	28.7433

Table H.4: Bending strain (με) of the line post insulator with ACSR Pelican conductor (25%UTS)

Peak-to-peak bending amplitude (mm)	Frequency (Hz)							
	9.05				14.13			
	Gauge 1	Gauge 2	Gauge 3	Gauge 4	Gauge 1	Gauge 2	Gauge 3	Gauge 4
0.1	5.0096	4.8682	1.6108	1.6311	7.2387	7.0659	2.2809	1.8604
0.2	8.8398	8.6357	1.8497	1.6561	12.6293	12.6807	3.1792	2.6408
0.3	13.1200	12.7126	2.0309	1.7446	20.9444	20.8594	5.0475	4.0741
0.4	17.2334	16.7563	2.2267	1.6247	27.3152	26.9745	6.7067	5.3656
0.5	21.3584	20.5278	2.4341	1.7131	33.5719	33.3018	8.6340	6.4778
0.6	25.5975	24.7634	2.6366	1.8411	40.1951	39.7651	10.6170	8.5253
0.7	29.8284	28.7577	2.8194	1.7796	47.1719	46.3844	13.1111	10.6332
0.8	33.9902	32.5529	2.9005	1.9015	53.4376	52.7521	15.7400	12.8609
0.9	38.0991	36.5575	3.1858	1.8725	61.2634	60.0257	18.5168	15.2037
1.0	43.4813	41.3820	3.4791	1.8864	66.9885	65.8303	21.3428	17.8115

Table H.5: Bending strain (με) of the line post insulator with ACSR Pelican conductor (30%UTS)

Peak-to-peak bending amplitude (mm)	Frequency (Hz)							
	9.11				15.36			
	Gauge 1	Gauge 2	Gauge 3	Gauge 4	Gauge 1	Gauge 2	Gauge 3	Gauge 4
0.1	5.1494	4.9461	1.6228	1.5711	7.4638	7.3187	2.1957	1.7191
0.2	9.0256	8.8154	1.8523	1.6178	14.0115	13.6988	3.1167	2.1364
0.3	13.1931	12.3608	1.7153	1.6860	21.2279	21.0376	4.4356	2.7250
0.4	17.0200	16.1435	1.7521	1.9031	27.1338	26.5272	4.8011	3.2092
0.5	21.2362	19.8549	1.7775	2.1135	36.5186	35.9847	6.8459	4.7229
0.6	25.2341	23.8211	1.8213	2.2920	45.5689	45.0694	9.3467	7.4458
0.7	28.8176	27.2741	1.7635	2.4349	52.5862	52.2518	11.7841	9.6257
0.8	33.0018	31.1401	1.7677	2.5797	60.9329	60.3459	15.5937	13.1593
0.9	36.9753	35.0541	1.7656	2.7642	68.0141	67.2092	19.4650	16.5353
1.0	40.2958	38.1914	1.8857	2.8771	74.4933	74.0708	22.6923	19.6895

H.3: Articulated clamp configuration with Pelican conductor

Table H.6: Bending strain (με) of the line post insulator with ACSR Pelican conductor (15%UTS)

Peak-to-peak bending amplitude (mm)	Frequency (Hz)							
	10.00				15.64			
	Gauge 1	Gauge 2	Gauge 3	Gauge 4	Gauge 1	Gauge 2	Gauge 3	Gauge 4
0.1	4.2021	3.9528	0.9349	1.0142	8.5643	8.4784	9.7344	10.2780
0.2	8.4873	7.9839	1.8884	2.0485	17.2981	17.1248	19.6615	20.7595
0.3	11.8494	11.9053	1.9463	2.2982	19.3146	18.6745	23.5136	25.2079
0.4	15.9652	15.6427	2.0369	2.4630	24.6290	23.3107	30.5875	32.8302
0.5	19.9197	19.3940	1.9411	2.6623	29.4315	28.7967	34.2325	36.8705
0.6	23.8697	22.0624	2.1016	2.6968	33.2922	31.4841	36.9206	40.6101
0.7	27.4425	26.0040	1.9484	2.8837	37.1741	35.6698	40.1908	44.0652
0.8	31.3377	30.5695	1.9938	3.2012	42.2639	40.5903	43.0867	46.9780
0.9	35.0911	33.5499	2.0485	3.5209	46.9558	44.9623	46.5947	51.1251
1.0	40.7585	38.8474	2.1103	3.7025	51.1775	49.0261	48.9174	53.9536

Table H.7: Bending strain (με) of the line post insulator with ACSR Pelican conductor (20%UTS)

Peak-to-peak bending amplitude (mm)	Frequency (Hz)							
	9.70				15.76			
	Gauge 1	Gauge 2	Gauge 3	Gauge 4	Gauge 1	Gauge 2	Gauge 3	Gauge 4
0.1	5.5106	5.1774	1.3759	1.2487	4.8109	4.6795	1.7515	1.5947
0.2	10.2040	10.0050	2.3289	2.0096	8.9751	8.6522	1.9634	1.9168
0.3	15.0289	14.2466	2.4046	2.4235	13.1217	12.6251	2.1634	2.4306
0.4	21.3019	20.6310	3.1093	2.5908	17.5904	16.7345	2.4531	2.9573
0.5	26.2721	25.4994	3.6292	2.8746	21.3046	20.4394	2.8631	3.6023
0.6	30.7685	28.9316	3.6460	2.7211	26.1703	25.0676	3.0734	4.0034
0.7	36.4199	34.6701	4.2149	3.2080	30.4850	28.4850	3.6235	4.8162
0.8	41.2515	39.6043	4.5232	3.1855	33.7311	32.2968	4.6037	5.3411
0.9	46.6405	44.5578	5.1037	3.6231	38.1653	36.1655	5.4319	6.5973
1.0	52.7797	50.3960	5.8100	4.0530	42.5068	40.3733	6.6813	8.2940

Table H.8: Bending strain (με) of the line post insulator with ACSR Pelican conductor (25%UTS)

Peak-to-peak bending amplitude (mm)	Frequency							
	9.30				16.12			
	Gauge 1	Gauge 2	Gauge 3	Gauge 4	Gauge 1	Gauge 2	Gauge 3	Gauge 4
0.1	6.3717	6.2670	1.7149	1.5090	7.0323	6.8192	2.1407	1.9360
0.2	10.1717	9.8320	1.7815	1.6746	8.9432	8.8287	2.0348	2.2635
0.3	14.6296	14.2148	1.9252	1.7249	12.7099	12.3318	2.4332	2.9522
0.4	19.5874	18.9895	2.0974	1.6772	16.4688	15.7239	3.1502	3.6771
0.5	23.9312	23.2104	2.2040	1.6135	20.2162	19.1393	3.9404	4.7591
0.6	29.7573	28.5563	2.5746	1.7032	24.2436	22.9636	5.0628	5.7447
0.7	34.4880	33.1925	2.7673	1.7211	28.1201	26.5455	6.9221	8.3268
0.8	39.2698	37.5884	2.9534	1.7443	32.9656	31.3430	9.9235	11.6753
0.9	44.0234	42.1213	3.2209	1.7734	37.6436	35.4324	13.0485	15.1503
1.0	48.6701	46.4822	3.1043	1.7921	41.5600	39.6631	15.6151	18.4260

Table H.9: Bending strain (με) of the line post insulator with ACSR Pelican conductor (30%UTS)

Peak-to-peak bending amplitude (mm)	Frequency							
	9.03				15.57			
	Gauge 1	Gauge 2	Gauge 3	Gauge 4	Gauge 1	Gauge 2	Gauge 3	Gauge 4
0.1	5.7480	5.9310	1.7191	1.7458	19.1246	18.9914	4.7793	4.2098
0.2	8.1030	7.9506	1.6930	1.9414	35.7590	34.7694	8.5694	7.0157
0.3	11.8576	11.8079	1.6579	2.0868	51.6016	50.0028	12.3062	11.1194
0.4	15.7166	15.2213	1.8107	2.2851	64.7835	62.3804	16.0887	14.9562
0.5	19.3783	18.7690	1.8547	2.1960	77.2974	74.1474	22.3887	23.7664
0.6	23.3404	22.2164	1.9707	2.4897	86.8643	83.4189	29.2880	31.8378
0.7	26.8662	26.1991	2.0679	2.7387	93.6023	90.0463	34.0837	36.6011
0.8	30.7899	29.3247	2.0351	2.8608	103.2090	98.5319	35.3128	37.3280
0.9	34.5599	33.0751	1.9746	3.0969	111.4110	106.7909	40.4506	42.7271
1.0	38.4538	36.7835	2.0670	3.1837	114.8303	109.2439	46.2216	49.1320

H.4: Blocked clamp configuration with Tern conductor

Table H.10: Bending strain (με) of the line post insulator with ACSR Tern conductor (15%UTS)

Peak-to-peak bending amplitude (mm)	Frequency (Hz)							
	11.40				11.93			
	Gauge 1	Gauge 2	Gauge 3	Gauge 4	Gauge 1	Gauge 2	Gauge 3	Gauge 4
0.1	5,0203	4,9787	3,9491	3,4054	5,4310	5,4855	3,3774	3,6331
0.2	8,7910	8,1996	3,3984	3,4701	10,3291	9,6839	4,0972	4,2713
0.3	13,1911	12,8000	3,21	3,5699	15,2670	14,2545	4,6850	4,8808
0.4	17,2732	16,8812	3,4991	3,6702	20,1625	19,1421	5,3876	5,5232
0.5	21,5729	21,0069	3,8093	3,8842	25,1833	24,5240	6,0986	6,2028
0.6	25,5930	25,0217	4,0980	4,1586	30,1204	29,2072	6,9709	7,1700
0.7	29,7182	29,0100	4,2150	4,3059	35,2351	33,8524	8,3243	8,4676
0.8	33,8778	32,8622	4,0084	4,3826	39,9401	38,6723	9,9392	9,9422
0.9	38,3686	37,5872	4,3340	4,5411	44,8060	43,1998	11,7058	11,8454
1.0	42,8246	41,6658	4,3000	4,6872	49,8460	47,9635	13,2516	13,5774

Table H.11: Bending strain (με) of the line post insulator with ACSR Tern conductor (20%UTS)

Peak-to-peak bending amplitude (mm)	Frequency (Hz)							
	11.66				11.93			
	Gauge 1	Gauge 2	Gauge 3	Gauge 4	Gauge 1	Gauge 2	Gauge 3	Gauge 4
0.1	5.3050	5.5174	1.9478	1.6113	5.3759	5.3064	1.8322	1.7508
0.2	9.2449	9.4811	2.0000	1.6241	10.9858	9.9486	2.3584	2.4467
0.3	13.2723	13.0319	2.0399	1.5784	15.8353	14.5940	2.6396	2.9841
0.4	17.6655	17.0198	2.0700	1.6095	20.9803	19.9660	2.9544	3.4074
0.5	21.9500	21.0974	2.3026	1.7447	26.0571	24.6387	3.4600	4.0296
0.6	26.0166	25.3134	2.2293	1.7840	30.6354	29.3423	3.9865	4.9129
0.7	30.1364	29.0768	2.3894	2.2667	35.7216	34.0006	4.7997	6.0015
0.8	34.3210	33.2240	2.4178	2.1960	40.3776	38.3539	5.3321	6.7704
0.9	38.5147	37.4570	2.7263	2.0478	45.4448	43.0096	5.8936	7.2492
1.0	42.7434	41.4962	2.9467	2.1688	50.5388	47.8256	6.1822	7.7773

Table H.12: Bending strain (με) of the line post insulator with ACSR Tern conductor (25%UTS)

Peak-to-peak bending amplitude (mm)	Frequency (Hz)							
	11.59				12.50			
	Gauge 1	Gauge 2	Gauge 3	Gauge 4	Gauge 1	Gauge 2	Gauge 3	Gauge 4
0.1	4.8155	4.7720	2.5030	2.5001	5.9957	6.0355	3.1810	2.4996
0.2	8.7886	8.1832	3.2244	3.1845	10.2067	10.1945	4.6124	4.0108
0.3	13.1829	12.2747	4.8366	4.7989	15.1093	14.8133	5.3118	5.1416
0.4	16.6893	15.5570	3.2676	3.2570	19.7277	19.0249	6.4835	6.3253
0.5	20.6666	19.7803	3.1604	3.1784	24.7027	23.9847	7.4555	7.7628
0.6	24.5339	23.4143	3.1306	3.1381	29.1548	28.7293	10.0071	11.1406
0.7	28.5858	27.0181	3.7398	3.7394	32.6034	32.0796	15.6739	17.0868
0.8	32.6879	30.9906	3.5591	3.5815	36.1409	35.5474	21.0767	23.1288
0.9	36.5908	34.5336	3.8012	3.7571	42.5865	42.0850	27.6709	30.2373
1.0	40.5744	38.2436	3.9346	3.8578	45.3211	44.3755	30.6366	33.4740

Table H.13: Bending strain (με) of the line post insulator with ACSR Tern conductor (30%UTS)

Peak-to-peak bending amplitude (mm)	Frequency (Hz)							
	12.10				12.21			
	Gauge 1	Gauge 2	Gauge 3	Gauge 4	Gauge 1	Gauge 2	Gauge 3	Gauge 4
0.1	4,6628	4,4981	1,9637	2,5912	5,4665	5,3304	2,5100	2,6858
0.2	8,3417	8,0485	2,2528	2,6737	9,9998	9,1767	2,9819	2,9918
0.3	11,8903	11,4810	2,4099	2,6610	14,9090	13,8413	3,4560	3,5219
0.4	15,7749	15,1530	2,7268	2,7049	19,3787	18,3468	3,6973	3,9126
0.5	19,4708	18,7954	2,9767	2,7840	24,2161	22,9327	3,8167	4,4521
0.6	22,8549	22,5077	3,222	2,9372	29,2327	27,8059	4,2474	4,9477
0.7	27,0583	26,6590	3,4318	2,9728	33,6167	31,9801	4,9608	5,4973
0.8	30,8692	30,4750	3,6341	2,8473	38,3286	36,5379	4,8700	5,9789
0.9	34,6510	34,0587	4,0330	2,9777	42,9215	40,6947	5,6351	6,8083
1.0	39,5138	39,0803	4,2962	3,2436	47,6972	45,3147	6,1594	7,3856

H.5: Articulated clamp configuration with Tern conductor

Table H.14: Bending strain (με) of the line post insulator with ACSR Tern conductor (15%UTS)

Peak-to-peak bending amplitude (mm)	Frequency (Hz)							
	8.13				15.32			
	Gauge 1	Gauge 2	Gauge 3	Gauge 4	Gauge 1	Gauge 2	Gauge 3	Gauge 4
0.1	7.1421	6.8564	3.2305	3.1013	4.7379	4.2786	2.6135	2.9254
0.2	12.7540	12.2438	3.4916	3.3519	7.6744	7.2469	1.9755	2.0512
0.3	16.3991	15.7432	3.5856	3.4422	11.2664	10.0158	1.7896	1.8736
0.4	22.1901	21.3025	3.8233	3.6703	14.9372	13.9815	1.8949	1.8682
0.5	28.5701	27.4273	3.9777	3.8185	18.1082	17.2154	1.9380	2.2069
0.6	33.7756	32.4246	4.0116	3.8511	21.7463	20.1596	2.0096	2.0764
0.7	37.5628	36.0602	4.0927	3.9290	25.7714	24.0333	2.1093	2.2135
0.8	43.0272	41.3061	4.4916	4.3119	29.2615	27.8738	2.1110	2.1095
0.9	47.8864	45.9710	4.9231	4.7261	33.1066	32.0512	2.2896	2.3558
1.0	53.6145	51.4699	5.3477	5.1338	36.5510	34.7537	2.3110	2.2886

Table H.15: Bending strain (με) of the line post insulator with ACSR Tern conductor (20%UTS)

Peak-to-peak bending amplitude (mm)	Frequency (Hz)							
	10.01				12.29			
	Gauge 1	Gauge 2	Gauge 3	Gauge 4	Gauge 1	Gauge 2	Gauge 3	Gauge 4
0.1	4.8788	4.8359	1.9693	1.8218	5.4212	5.4713	1.7652	1.8233
0.2	9.1871	9.1867	1.7543	1.9833	9.7385	9.5590	1.8679	2.2192
0.3	13.6040	13.4977	1.8884	2.1696	14.4443	13.9908	2.1923	2.3416
0.4	18.1678	17.9645	1.9393	2.4571	18.6358	18.1047	2.3767	2.8087
0.5	22.2598	21.9871	2.0708	2.7517	23.7213	23.0680	2.4742	3.6429
0.6	26.8158	26.3982	2.2704	3.0982	28.6221	27.6529	2.8119	4.0915
0.7	30.9498	30.4065	2.5836	3.4891	33.0309	32.0812	3.0558	4.5281
0.8	35.3551	34.6529	2.9421	3.8509	37.7496	36.6642	3.4923	5.1750
0.9	39.2895	38.4948	3.1436	4.3245	42.2302	40.8939	3.3624	5.3412
1.0	43.6212	42.7616	3.4493	4.7231	47.6384	46.1689	3.8412	6.0006

Table H.16: Bending strain (με) of the line post insulator with ACSR Tern conductor (25%UTS)

Peak-to-peak bending amplitude (mm)	Frequency (Hz)							
	11.54				13.15			
	Gauge 1	Gauge 2	Gauge 3	Gauge 4	Gauge 1	Gauge 2	Gauge 3	Gauge 4
0.1	7.4301	7.5457	2.1567	2.1545	6.0058	6.2256	3.1450	3.1125
0.2	13.8546	13.2277	3.2063	3.5490	12.8793	12.4411	2.6516	2.9558
0.3	21.4561	21.0662	5.3112	5.8195	18.1576	17.4186	3.2058	3.7696
0.4	27.7457	26.9779	7.5802	8.3177	24.4696	23.1751	3.8914	4.8683
0.5	33.5698	32.3963	9.7859	10.7602	30.5808	29.9143	4.5739	5.7780
0.6	40.6401	39.4327	13.3389	14.6494	36.8626	35.8184	5.5139	6.9141
0.7	47.0373	45.6913	16.3672	17.9957	43.3097	41.8444	6.4469	8.1202
0.8	53.3778	51.6421	20.0185	21.9913	49.5658	48.0499	7.6168	9.5014
0.9	60.7581	58.9474	25.2419	27.5004	56.0678	54.7274	8.7245	10.8829
1.0	69.2022	67.0769	30.9803	33.7663	61.8878	59.8581	9.8028	12.0914

Table H.17: Bending strain (με) of the line post insulator with ACSR Tern conductor (30%UTS)

Peak-to-peak bending amplitude (mm)	Frequency (Hz)							
	10.10				13.40			
	Gauge 1	Gauge 2	Gauge 3	Gauge 4	Gauge 1	Gauge 2	Gauge 3	Gauge 4
0.1	4.7522	4.6149	1.6667	1.4109	5.1465	5.1739	1.6543	1.4677
0.2	8.6743	8.1560	1.8049	1.5092	9.1480	8.8272	1.7055	1.6944
0.3	12.5433	11.6611	1.9612	1.5234	13.6546	12.9018	1.7188	1.7394
0.4	16.4803	15.1093	2.0543	1.5364	17.7790	16.9323	1.7658	1.9205
0.5	20.4225	19.1544	2.0845	1.5351	22.3527	21.4922	1.6977	2.2810
0.6	24.3226	22.6566	2.4042	1.7296	26.7336	25.5628	1.7529	2.4717
0.7	28.2678	26.5975	2.2863	1.6750	31.0498	29.6638	1.7131	2.6882
0.8	32.3373	30.3055	2.4236	1.6708	35.4779	34.1392	1.7288	2.9522
0.9	36.4641	34.1223	2.6941	1.7726	39.9097	38.4198	1.8232	3.1207
1.0	40.2483	37.7031	2.7024	1.7951	43.9724	42.0890	1.8957	3.3697